Study of Different Nanomaterials (Alumina & MWCNTs) and their Size Effect on the Stability and Properties of Nanofluids for Energy Applications

Submitted

by

D.Srinivas Rao
Reg.No. 09ETPM05

in partial fulfillment of the requirement for the award of degree of

Doctor of Philosophy
In
Materials Engineering

Supervisor

Dr. Raj Kishora Dash

2016

School of Engineering Sciences & Technology,
University of Hyderabad,
Hyderabad, India – 500046

School of Engineering Sciences & Technology,
University of Hyderabad,

Hyderabad, India – 500046

Certificate

This is to certify that the research work entitled **"Study of different nanomaterials (Alumina & MWCNTs) and their size effect on the stability and properties of nanofluids for energy applications"** has been carried out by **Mr. D.Srinivas Rao**, Ph.D student (Reg.No. 09ETPM05), School of Engineering Sciences and Technology, University of Hyderabad, under my guidance and submitted in partial fulfillment of the requirements for the award of the degree of **Doctor of Philosophy, in Materials Engineering** of **School of Engineering Sciences & Technology, University of Hyderabad, Hyderabad (India).**

Further it is certified to the best of my knowledge that the matter embodied in this work has not been submitted previously in part or in full to this or any other University of Institute for the award of any other degree or equivalent.

Sign of Head of the School.

Prof. M. GhanashyamKrishna
Dean, SEST, UoH,

Sign. Of Supervisor

Dr. Raj Kishora Dash,
SEST, UoH

School Of Engineering Sciences & Technology.
University of Hyderabad,
Hyderabad, India – 500046

Declaration

.

I, **D.Srinivas Rao (Reg. No. 09ETPM05)** declare that the foregoing thesis entitled **"Study of different nanomaterials (Alumina &MWCNTs) and their size effect on the stability and properties of nanofluids for energy applications",** submitted in partial fulfillment of the requirements for the award of **Doctor of Philosophy (Materials Engineering)** in the **School of Engineering Sciences and Technology (SEST), University of Hyderabad** is completely my work except for those referenced. This work was done under the supervision of **Dr. Raj Kishora Dash**. This report is a record of the bonafide research work carried out by me and the results incorporated in it have not been reproduced / copied from any source. This work has not been submitted to any other University of Institute for the award of any other degree or equivalent.

D.Srinivas Rao
Ph.D Student, Reg.No. 09ETPM05
School of Engineering Sciences & Technology
University of Hyderabad,
Hyderabad – 500046. (INDIA)

Acknowledgement

I feel privileged to place before you my research work entitled ***"Study of different nanomaterials(Alumina & MWCNTs) and their size effect on the stability and properties of nanofluids for energy applications".*** For the overall completion of this research work I owe its success to numerous diligent personalities.

First and foremost, I wish to place my sincere gratitude to my young, dynamic and inspiring supervisor **Dr. Raj Kishora Dash**, Assistant Professor, School of Engineering Sciences & Technology, who has provided considerable wealth of resources, opportunities and guidance during my study of nanofluids. His support has been an essential contributing factor towards the completion of this manuscript.

My sincere thanks to my committee members **Prof. Rajender Singh** , School of Physics, and **Prof. M. Ghanashyam Krishna**, Dean, School of Engineering Sciences & Technology, for their kind co-operation and guiding spirit in completion of this research work.

I am would also like to take this opportunity to thank University Grants Commission, New Delhi, India for the financial support received, through **Rajiv Gandhi National Fellowship**.

I also thank all the **lab assistants** for XRD, TEM, FESEM, UV-Vis and AFM Characterizations for their friendship and technical support received.

I would also use this opportunity to convey my thanks to all my **group members and fellow students** for their co-operation and help received.

Last but not the least, I would like to thank **my parents and family** for providing an abundance of love, encouragement and support along my lengthy and sometimes wandering path throughout the years of my pursuit of the doctoral degree.

Finally, I also extend my deep sense of gratitude and thanks to all the **teaching and non-teaching staff** for their guidance, and kind co-operation in completion of this research work. My stay at University of Hyderabad has been made so unforgettable and enjoyable either directly or indirectly by all the people I have worked with through these years.

D. Srinivas Rao.

CONTENTS

Annexure-I

List of Tables:

Annexure-II

List of Figures

Fig.3.3: Transesterification Process of Jatropha raw oil

Fig.3.4: Digital images of the synthesis of Jatropha oil (A) Set-up of Transesterification Process (b) separating flask containing Jatropha biodiesel with Glycerene as the by-product.

Fig.3.5: Flow chart of various parameters considered for nanofluids preparations.

Fig 3.6: Comparision of plots on dispersion stability of Al_2O_3 NPs (~13nm and ~28nm size) by using (A) different surfactants (B) surfactant (Span^{80} and Tween^{80}).

Fig3.7 Photographic images of alumina NFs (~13nm) : (a) as-prepared samples (B) 0 .05, (C) 0.1, (D) 0.2 and (E) 0.4%VF along with neat JBD (A) and neat Diesel (F) (b) stored samples of 0.1VF for (A)1Year, (B) 6Mon (C) 7Mon and (D) 2Years respectively.

Fig3.8 Photographic images of alumina NFs (~28nm) : (a) as-prepared samples (B) 0 .05, (C) 0.1, (D) 0.2 and (E) 0.4%VF along with neat JBD (A) and neat Diesel (F) (b) stored samples of 0.1%VF for (A) 1, (B) 2 (C) 6 and (D) 7Months respectively.

Fig3.9 Photographic image of MWCNTs dispersed nanofluids having 0.001%VF after 24 hours with different surfactants or acids treatment (A) Pure biodiesel (B) Span^{80} and Tween^{80} (C) CTAB (D) SDS (E) PVP surfactants and Functionalized with (F) conc. acids (G) SOA with 2H (H) SOA with 4H (I) Oleic acid

Fig 3.10Photographic image of as-prepared samples of MWCNTs dispersed nanofluids (as-prepared samples with (B)0.001, (C)0.005, (D)0.01, (E)0.0.02, (F)0.1%VF) with (A) neat biodiesel.

Fig.4.1: TEM image of Al_2O_3NP As-Prepared (a) ~13nm size 0.1%VF (b) ~13nm size 0.2%VF (c) ~28nm size 0.1VF.

Fig.4.2 TEM image of Al_2O_3NP ~13nm 0.1%VF (a)2Week old (b)1Month old (c) 2Month old (d) 1year old (e) 0.2VF 1year old samples

Fig.4.3(A) UV-Vis spectroscopy plots of Al_2O_3 NPs (~13nm and ~28nm) for 0.1 and 0.2%VF.

Fig.4.4 UV-Vis spectroscopy of Al_2O_3 nanofluids with different storage times (A) ~13nm (B) ~28nm sizes.

Fig 4.4(C) Absorbance vs stability durations for alumina nanofluids (i) ~13nm (ii) ~28nm

Fig 4.5 Effect of alumina NPs sizes on the absorption peak of 0.1%VF and 0.2%VF alumina nanofluids.

Fig.4.6(A): UV-Vis Spectroscopy of aluminaNPs(~13nm) having 0.1 and 0.2 %VF at different storage time.

Fig.5.5: Plots of Al_2O_3 Nanofluids (~28nm size) for as-prepared samples having varying concentrations of 0.05, 0.1, 0.2 and 0.4%VF (A) Viscosity and Shear Stress (B) Viscosity and Temperature.

Fig.5.6: Plots of Al_2O_3 Nanofluids (~13nm size) for different storage samples having 0.1%VF (A) Viscosity and Shear Stress (B) Viscosity and Temperature

Fig5.7 (A)Viscosity vs storage time of Al_2O_3 nanofluids (~13nm, 0.1VF).

Fig.5.7(B)Viscoisty vs Al_2O_3 NPs size for as-prepared samples.

Fig.5.8: Plots of MWCNTs Nanofluids for as-prepared samples having 0.001, 0.005 %VF as-prepared and 10days old samples showing (A) Viscosity and Shear Stress (B) Viscosity and Temperature

Fig5.9 Viscosity vs storage time of MWCNTs at (A) Shear stress of 0.125Pa. (B) 40^oC

Fig.5.10 Plots of Al_2O_3 (~13nm) and MWCNTs with as-prepared and longer stability time samples (A)Viscosity Vs Temperature (B) Viscosity Vs Shear Stress

Fig.6.1: Regions in an insulated hotwire immersed in a fluid

Fig.6.2: Wheatstone bridge circuit for THW experimental set-up

Fig.6.3 Block diagram of a THW method set-up

Fig 6.4 (A) Experimental set-up (B) Data logger Readings (C) Wheat-stone bridge circuit (D) Multi-meter connections to circuit

Fig.6.5: Series connection of resistors (R1 = Platinum wire and R2 = 3.331Ω)

Fig 6.6 Plots of Del(Tw) vs ln(Del Time) to obtain slope of the graphs for thermal conductivity calculations (A) DI Water (B) Neat Jatropha biodiesel.

Fig 6.7 Plots of Del(Tw) vs ln(Del Time) to obtain slope of the graphs for thermal conductivity calculations of Al_2O_3 NF 0.1%VF (A) ~13nm as-prepared (B) ~13nm 2Months old (C) ~13nm 8Months old (D) ~13nm 14Months old (E) ~13nm 27 Months old (F) ~28nm as-prep sample respectively.

Fig 6.8: Thermal Conductivity versus Stability Time of alumina nanofluids (~13nm) 0.1%VF for different stability time.

Fig 6.9 Plots of Del(Tw) vs ln(Del Time) to obtain slope of the graphs for thermal conductivity calculations of MWCNTs nanofluids : (A) 0.001%VF as-prepared (B) 0.001%VF 10days old (C) 0.005%VF as-prepared (D) 0.005%VF 10days old samples respectively

Fig.7.1: Schematic of the experimental set-up for evaporation rate test

Fig.7.2: Experimental set-up for the evaporation rate test of the nanofluids

Fig.7.3: Plots of evaporation rate vs temp for as-prepared ~13nm and 28nm alumina nanofluid and different storage time ~13nm alumina nanofluids for temperature range

Fig 7.4 (A).Evaporation rate vs storage time of Al_2O_3 NF ~13nm size at 300, 450 and 600^oC.

Fig(B)Evaporation rate of both sizes of Al_2O_3 NPs (~13 and ~28nm) at 300, 450 and 600^oC

Fig.7.5: Comparing bar graph of alumina and MWCNTs nanofluids for as-prepared and their longer storage time samples only

Fig7.6 Evaporation rate vs storage time of MWCNTs at 300, 450 and 600^oC

Fig.7.5: Evaporation Rate Vs Temperature of as-prepared and longer stability time samples of Al_2O_3 (~13nm) and MWCNTs along with neat Jatropha biodiesel and commercial diesel.

Annexure-III

Notations & Abbreviations

~: average

Al_2O_3 NPs: alumina nanoparticles

MWCNTs: multi-walled carbon nanotubes

JBD: jatropha bio-diesel

JME : Jatropha methyl ester

%VF: percentage volume fraction

μ: Dynamic Viscosity

γ: Shear rate

τ: Shear stress

υ: Kinematic Viscosity

R_o: Resistance of platinum wire

R_3: Resistance of potentiometer

I: current

λ: Thermal Conductivity, watts/m/^{o}k

t: Time in sec.

q: Rate of Heat Transfer, watts

ΔṬ : Temperature difference

Ṿ: Voltage, volts,

I: Current, ampere

R: Resistance, ohm

L:length of the Platinum wire, m

T: time the current flows through the platinum wire, sec

CTAB: Cetyltrimethyl ammonium bromide

SOA: Sodium Oleate

ρ_{Al2O3} = Density of Al_2O_3, gm/cc

$Vol._{Surf}$ = Volume of the surfactant, cc

$Vol._{BD}$ = Volume of the Biodiesel, cc

W_{Al2O3} = Weight of Al_2O_3, mg

THW: Transient hot-wire

3ω: Three omega

DF: Diesel Fuel

BD: Biodiesel

DI water: De-ionised water

TEM: Transmission Electron Microscopy

FESEM: Field emission scanning electron microscopy

UV-Vis spectroscopy: Ultra violet and visible spectroscopy

FT-IR: Fourier Transform infra red

Abstract

The increasing industrialization and motorization of world has led to a steep rise of fossil fuel, however, the limited reserves of fossil fuel and environmental degradation due to air pollution caused by the diesel engine have forced for searching for alternative fuels. These forecasts have triggered for searching of alternative sources to replace the fossil fuels which must be technically feasible, economically competitive, environmentally acceptable and readily available. Various fuels have been considered as substitutes for the petroleum fuels used in automobiles. The most prominent of these are ethanol, methanol, NH_3, H_2 and natural or produced gases, biogas, edible oils and non-edible oils. The suitability and feasibility of each of these fuels are studied out throughout the world for efficiently using in the I.C engines. Out of the current progress, vegetable oils are showing excellent fuel properties and possible potential candidate for these purposes. Some of the prominent non-edible vegetable oils which can be considered as biodiesel fuels are: Jatropha,(JME), Karanja, Polanga, Neem, soyabean oil. However, the direct utilization of vegetable oil in a diesel engine is more challenges due to several problems, such as high viscosity, poor atomization and incomplete combustion which gives difficulties with fuel injection and with cold flow pumping. These unsaturated oils are less chemically stable, which affect storage and promotes difficulties on the injection components and pistons. Therefore, to overcome all these issues nanomaterials or nanotechnology are utilized as recently reported by several researcher since they are showing unique properties and nanoscale phenomena which in turns can improve the performance of such biodiesel for commercial applications.

Few of the nanomaterials, such as alumina, carbon nanotubes are of high energetic materials. They are believed to possess high heat transfer properties and if uniformly disperse in diesel or biodiesel can be utilized for applications in diesel engines due to improve the combustion rate, viscosity, lower emissions and hence their thermal efficiency can be improved. In this regard, investigations are going on all over the world to explore the benefits of nanomaterials for the diesel engines fuel characteristics. However, not much progress was achieved by so far achieving higher durations stability of such bio-fuel based nanofluids though improvements are reported in term of fuel properties, combustion characteristics and emission or smoke exhaustions. Therefore, a detailed study and investigations on the nanomaterials disperse

in biodiesel is carried out in this thesis work by investigating the effect of nanomaterials sizes such as alumina nanoparticles having two different sizes (~13nm &~28nm) and types i.e. alumina nanoparticles and multi-walled carbon nanotubes(MWCNT) on the stability of the JME based nanofluids and thermos-physical properties such as viscosity, thermal conductivity and evaporation rateThe basefluid used for investigation is Jatropha biodiesel which is obtained by synthesizing the raw jatropha biodiesel by a standard process known as transesterification. The nanofluids are obtained by dispersing the nanomaterials / nanoparticles in the various percentage volume fractions into the basefluid.The first and foremost task in this research work is to achieve stable nanofluids for longer durations and also to optimize the percentage volume fractions of the nanomaterials in the base fluid. For this task, initially, the nanomaterials were characterized by XRD, FESESM, EDS, TEM, Raman spectroscopy and FT IR to know their structural, phase, compositions, size distributions, disorder (MWCNT), and functional group present (MWCNT). The various chemical approaches were carried out to achieve a longer term alumina NPs disperse nanofluids by considering the different chemicals and surfactants, sonication time, percent volume fractions such as 0.1%, 0.2%, 0.3%, 0.4% and 0.5% for two different sizes of alumina nanofluids (~13nm and ~28nm size alumina nanoparticles). Longer duration having more than 1 year stability nanofluids was obtained by using only Span and Tween (1:1) for only 0.1VF and also in case of ~13nm alumina Nps. However, larger size ~28nm alumina nanoparticles dispersed nano fluids for same volume fractions were not stable for few weeks. Hence, nanomaterials size has the predominant effect on the stability of the nanofluids. However, in case of MWCNT dispersed nanofluids, only 10 days stability was observed since it is very difficult to disperse MWCNT in oil based fluids though we adopted several approaches by using covalent and non-covalent methods. Finally, we concluded that by covalent approach few defects can be created at the side walls of the MWCNT and at least few days (max 10days) stability was achieved. Still, more research work is needed by using novel approaches to disperse MWCNT in biodiesel based nanofluids, and due to time and budget constraint we have not studied more details. However, more details studied was carried out to understand the underlying mechanism for alumina NPs dispersed nanofluids stability by using TEM and UV spectroscopy. It was found that the size and shape of the ~13nm nanoparticles modified to cubical and having larger size ~40nm after one year of storage time. Since, still in nano-scale, such alumina Nps are able to disperse uniformly in biodiesel as confirmed from the TEM analysis sustain stability. Viscosity,

Thermal conductivity and evaporation rate of all the alumina nanoparticles and MWCNTS dispersed nanofluids were carried out in final part of this thesis work by considering the nanolfuids those are showing higher stability. It was observed that viscosity, thermal conductivity and evaporation rate all are size and materials dependent. For instance, as the size of the alumina Nps decreases, viscosity of the nanofluids increases, hence there is a direct correlation between the size of the nanomaterials and viscosity of the nanofluids. However, viscosity of nanolfuids is decreasing with increasing the temperature for all the sizes and materials types. It was also noticed that viscosity of the nanofluids constantly increases with the storage time also, may be due to the fact that the disperse NPs size increases over storage time. Also, same trend was observed in case of thermal conductivity of the nanofluids, i.e. thermal conductivity of the nanolfuids increases with increasing the storage time. The evaporation tests results confirmed that at higher temperature ~13nm dispersed nanofluids is very much similar to that of commercial diesel, and for MWCNTS based nanofluids case even better than commercial diesel.

Therefore, our study concluded that the developed longer term more than one year alumina nanoparticle dispersed bio-diesel nanofluids having improved fuel characteristics such as viscosity, thermal conductivity and higher burning rate can be utilized for diesel engine or as an alternative fuel.

D.Srinivas Rao,
Ph.D Student, Reg.No. 09ETPM05,
School of Engineering Sciences & Technology,
University of Hyderabad, Hyderabad (India).

Acknowledgement

PAPER PUBLICATIONS:

- ✓ D. Srinivas Rao, Raj Kishora Dash, "*Effect of Nanomaterials Sizes on the Dispersion Stability of biodiesel based nanofluids*", Adv. Mater. Lett. 2015, 6(3), 247-251 DOI: 10.5185/amlett.2015.5638
- ✓ D. Srinivas Rao and Raj Kishora Dash, "Investigations on Combustion Characteristics of Alumina NP's dispersed Longer Term Stable Biodiesel Nanofluids" Adv. Mater. Lett. 2016, 7(3), 221-225 DOI: 10.5185/amlett.2016.6152
- ❖ Paper entitled, "Investigations on MWCNTs Dispersed nanofluids for long term stability" submitted to J. of nanotechnology.
- ❖ Paper entitled, "Study on thermo-physical properties of MWCNT's Dispersed nanofluids for long term stability" submitted to J. of nanotechnology
- ❖ Paper entitled, "Investigations on Viscosity and Thermal Conductivity of alumina nanoparticles Dispersed nanofluids for long term stability" submitted to Energy.

PAPER PRESENTATIONS AT INTERNATIONAL CONFERENCES:

- ➢ Presented an Oral Presentation of the paper entitled, "*Effect of Nanoparticles Dispersed Biodiesel Stability for Effectively Using as Alternative Fuel Energy*", at International Conference on Nanomaterials and Nanotechnology,(ICNANO2011), Dated:18 - 21 Dec.2011, University of Delhi, New Delhi, INDIA.
- ➢ Presented a Poster Presentation of the paper entitled, "*Effect of Nanoparticles Size and Phase on the Stability of Nanofluids*", at International Conference on Nanoscience and Technology, (ICONSAT2012) Dated: 20 - 23 Jan.2012, Hyderabad, INDIA.
- ➢ Presented an Oral Presentation of the paper entitled, "*Investigations on γ-Al_2O_3 Nanoparticles Dispersed Nanofluids*" at International Conference on Nanotechnology, (ICNT2013) Dated:25th – 26th Oct.2013, Haldia Institute of Technology, Haldia, West Bengal, INDIA.
- ➢ Presented an Oral Presentation of the paper entitled "*Investigations on the Effect of Functionalized Materials on the Stable Nanofluids of γ-Al_2O_3 ,CuO and CNT Nanomaterials Dispersed Biodiesel*" at International Union of Materials Research Society, International Conference in Asia-2013(IUMRS ICA-2013), Dated:16th-20thDec.2013, Indian Institute of Science, Bangalore, INDIA.
- ➢ Presented a Poster Presentation of the paper entitled, "*Nanomaterials and Their Size effects on Ignition Probability of Biodiesel based Nanofluids*", at International Conference on Nanoscience and Engineering Applications, (ICONSEA-2014) Dated:26 - 28 Jun.2014, JNTUH Hyderabad, INDIA.

Chapter 1

Introduction

There are different forms of energy available in nature and are broadly classified as non-renewable energy resources and renewable energy resources. Fossil fuel energy resources like coal, petroleum and natural gas comes under the classification of non-renewable energy resources since, these fossil fuels when once consumed, cannot be re-grown at the same rate of their consumption, while solar energy, geothermal energy, wind energy, green energy, hydro energy etc. are considered as the renewable energy resources as energy resources can be replaced or regenerated by nature within a short period of time. Since energy resources from the fossil fuel are going to be shortage in the near future, alternative energy resources for the transportation sector have become an essential requirement for the coming years. Green energy such as biodiesel, bio-fuel from the various plants (Jatropha, Karanja, Neem, etc.,) are found to be alternative resources of energy for the transportation sectors [1-8]. However, direct utilization of such raw biodiesel as an alternative fuels undergoes various drawbacks such as low calorific value of the fuel, lower burning rate, high viscosity, longer ignition delay, etc. [8-20], and hence, such drawbacks needs to be addressed in order to use such bio-diesel as alternate fuels for future energy transportation sectors. One of the key solution to overcome these issues is to consider the application of nanomaterial or nanotechnology.

It is well known that few of the materials such as aluminum or aluminum oxide are often used for catalytic properties of high energy heat transfer rates as in the case of rockets and jet propulsion engines. Ever since the nanomaterials came into existence, researchers across the globe are exploring on different nanomaterials for various energy related applications because nanomaterials are showing unique properties which are quite different from their micro or bulk counter ones and can be tailored to suit various applications. Also nanomaterials, such as alumina, carbon nanotubes, graphene etc. are of high energetic materials. Hence, it is believed that such nanomaterials can possess high heat transfer properties and when tailored suitably, can be useful for not only in heat transfer applications, but also for several other applications too[21-30]. In the field of optical applications nanomaterials can be used as anti-reflection coatings, or

as light based sensors for cancer diagnosis [31-37]. In case of magnetic applications, nanomaterials are used for increased density storage media or improved detail and contrast in MRI images [38-39]. Similarly in case of thermal applications, nanoparticles could be used to enhance heat transfer from solar collectors to storage tanks [40-50]. They can also be used to improve the efficiency of the coolants in transformers [51-57]. In case of mechanical applications, nanomaterials are used to improve the wear resistance, or for anti-corrosion properties [58-62]. Further the properties of such nanomaterials can be tailored to synthesize new composite materials having improved properties[63-69]. Nanomaterials are also used for energy applications such as materials possessing properties of ultra high performance in case of solar cells, or catalysts for combustion engines to improve efficiency of the engines or could be used for high energy density and more durable batteries etc[70-77]. Thus applications of nanomaterials are innumerous. After the discovery of the nanofluids by **Choi and Eastmann in 1995[78],** has attracted attention of many researchers across the globe to engineer new class of fluids having unique properties as compared to the basefluids. For instance, **Fedele, et al. 2011[79]** investigated the stability of TiO_2, SWCNT and CuO dispersed in DI water by different methods such as ball milling, sonication and high-pressure homogenizations at concentrations of 0.1%wt, 0.01%wt and 1%wt. and concluded that high-pressure homogenization method provided longer stability of 14days for SWCNT and TiO_2 nanoparticles. Several improvement of such nanofluids are reported as compared to the basefluids.

Sajith et.al. 2013[85] used the cerium oxide nanoparticles as additives in biodiesel and investigated on the performance of the diesel engine by using Jatropha biodiesel as a basefluid. The cerium oxide nanoparticles considered were of 10 to 20nmnm size having a density of 7.13g/ml. They considered particle loading of cerium oxide nanoparticles in the range of 20 to 80ppm (by weight). With these parameters, diesel engine performance test were carried out and concluded that though the viscosity and flash point of the Jatropha biodiesel was high on adding cerium oxide nanopateicles compared with that of neat diesel, few of the particluate emissions such as hydrocarbon and NOx was found to be decreased to a considerable amount. Fig 1.1 shows the improvements in the combustion characteristics of biodiesel by adding CeO_2 nanoparticles.

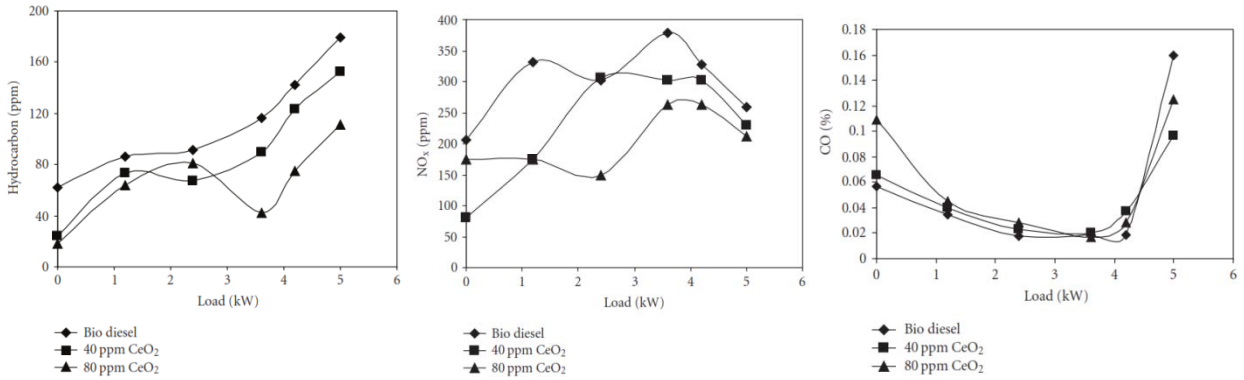

Fig1.1:Variation of hydrocarbon Nox and CO emissions with different dosing levels of fuel CeO_2NPs additive in biodiesel [85]

Jones et al. [87] investigated on the combustion characteristics of nano-metal and metal oxide based nanofluids using ethanol as the basefluid. Aluminum nanoparticles of ~50nm size and alumina nanoparticles of ~36nm sizes were used with various volume fractions such as 1%, 3%, 5%, 7% and 10% for Al while with that of n-al_2O_3 were 0.5%, 1%, 3% and 5% respectively. No surfactants were used in the analysis. It also reported that both aluminum and alumina based nanofluids improved the volumetric heat of combustion. However, none of the changes were observed in higher loading rate for alumina nanoparticles.

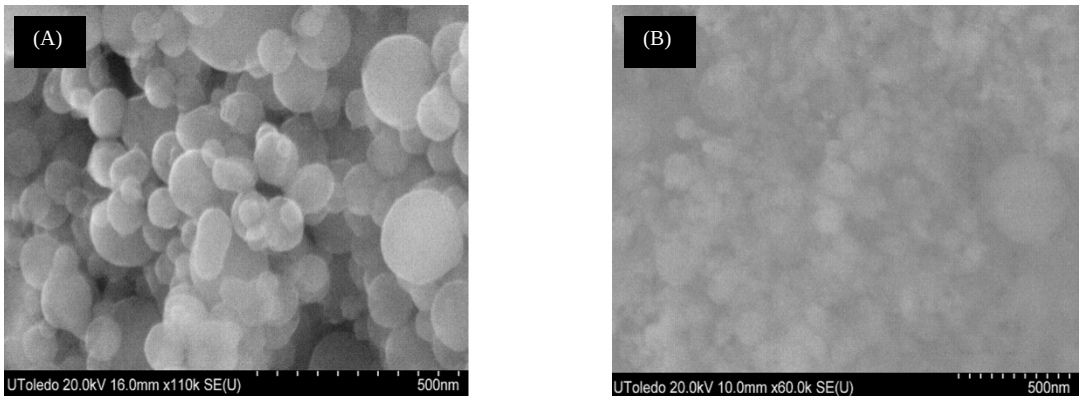

Fig: 1.2 FESEM images of (A) n-Al powder (B) n-Al2O3 powder [87]

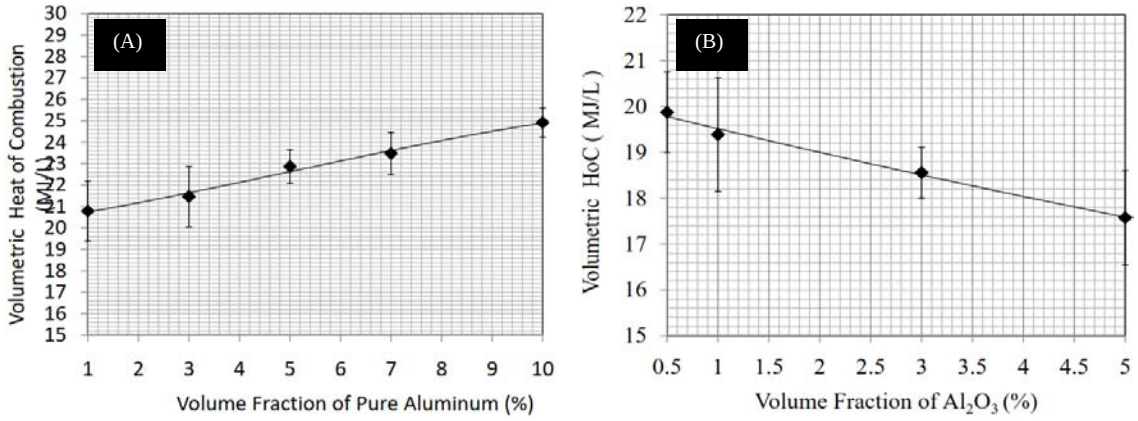

Fig. 1.3 Volumetric heat of combustion, (A) Ethanol with pure aluminium (B) Ethanol with pure aluminium oxide nanoadditives [87]

Ali M.A.Attia et.al. 2014 [90] studied the performance of diesel engine by dispersing alumina nanoparticles into mixture of Jojoba methyl ester and diesel fuel(DF) as the base fluid at different concentrations of 10mg/l to 50mg/l. The basefluid was kept at a constant mixture of 20% JJME and 80% DF for all the variations of alumina NP's. The alumina NP's were added with having a mass fraction of 10mg/l, 20mg/l, 30mg/l, 40mg/l and 50mg/l respectively to the basefluid (which is a mixture of 20%JJME and 80%DF). It was found that the optimum concentration of alumina NP's of 30mg/l gives the best performance of the engine in terms of increase in efficiency of the diesel engine by 7%, reduction of BSFC by 6% and also reduction in emissions of NOx, Co, smoke opacity and UBHC by 70%, 75%, 5% and 55% respectively. The proportion of Jojoba Methyl ester used in their work is shown in Table1.1. Fig.1.5 shows the TEM Characterization of Al_2O_3 NP's.

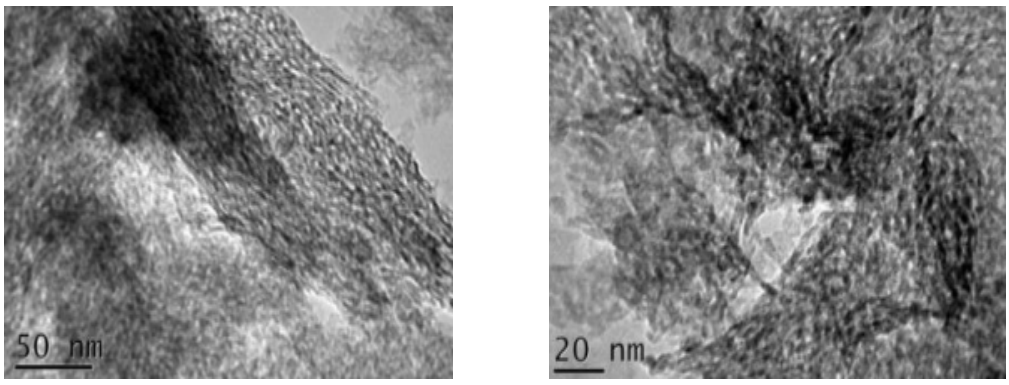

Fig.1.4 TEM image of γ - Al2O3 NP's (~20-50nm) (as-received from suppliers) [90]

Table:1.1 Properties of JJME and Diesel fuel (DF) [90]

Property	Test Method	Diesel	JJME
Calorific value, kJ/Kg	ASTM D-240	45448	44866
Viscosity @40^{o}C, cSt.	ASTM D-445	3.34	11.72
Density @ 15.56^{o}C, g/cm^{3}	ASTM D-1298	0.8427	0.8645
Molecular weight, Kg/Kmol.		191.02	350.73
C,%		86.21	76.01
H,%		11.59	10.05
N,%		1.91	Nil
S,%		0.29	0.3
O_2,%		Nil	13.64

Table:1.2 Details of alumina nanoparticles [90]

Item	Specification
Manufacturer	Nanotech company, Egypt
Chemical name	Gamma Aluminium Oxide (Alumina Al_2O_3) Nano powder, gamma phase, 99.9%
Average particle size	20-50nm
BET surface area)SSA)	>150m^{2}/g
Appearance	White
Melting point	2045 ^{o}C
Density	3.9 g/cm^{3}

Alumina nanoparticles dispersed nanofuels [Table 1.2] were tested on the diesel engine at part load % of the engine for two different engine speeds i.e., at 1300RPM and at 1500RPM respectively, and the engine performance and exhaust emissions were analyzed. Finally these results were compared with that of neat diesel and also with blends of JJME and Diesel fuel without the addition of alumina nanoparticles. Fig.1.6 shows the engine performance in terms of efficiency of the engine for different particle loading of the alumina nanoparticles in the blends of JJME and diesel fuel. The engine performance was measured in terms of the brake specific fuel consumption (BSFC) and also in terms of the efficiency of the engine at two different engine speed such as, at 1500RPM and 1300RPM respectively..

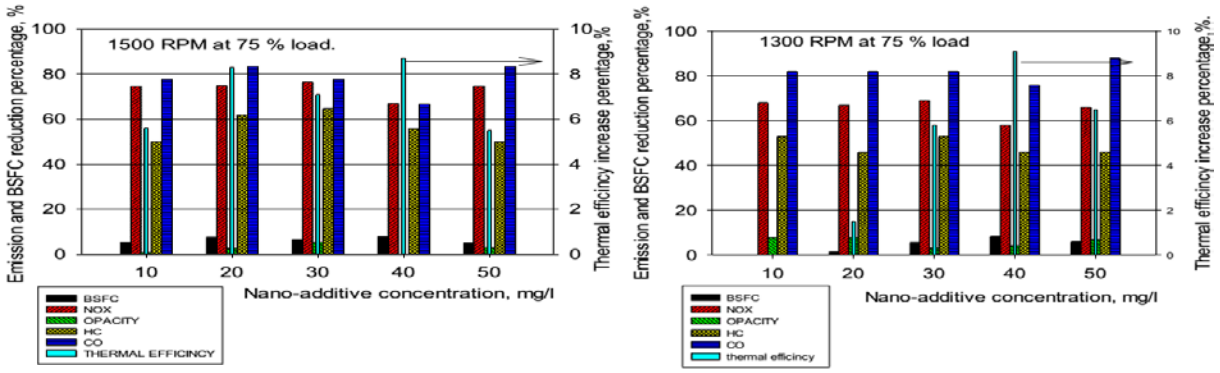

Fig. 1.5 Percentage change in engine performance as a function of nano-additive concentration [90]

It was reported that the efficiency of the engine can be improved significantly with the applications of the alumina nanoparticles for all the loading as compared to that of the diesel fuel without any nanoparticles. Also the smoke opacity of the alumina additive nanofuels was less compared to that of the JJME-diesel blends. The exhaust emissions such as NOx, CO and UBHC though it is high for the JJME-Diesel blends without the nanoparticles, it was reduced when the alumina nanoparticles was dispersed in the JJME-Diesel blends. **Yanan Gan et.al.2011[93]** investigated the combustion properties of boron and iron nanoparticles dispersed in ethanol and n-decane at dilute and dense concentrations. It was reported that the burning behavior in case of dense concentrations was quite different from that of the dilute concentrations of the nanoparticles as shown in the Fig 1.6.

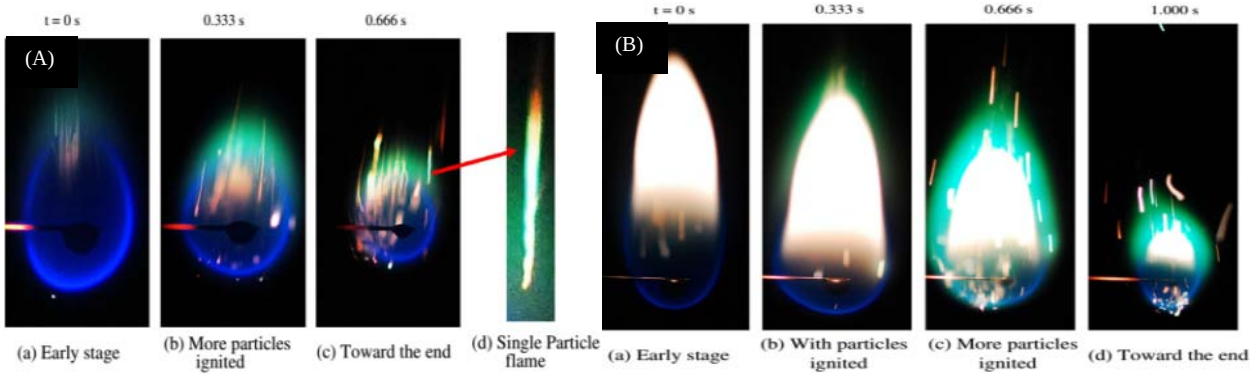

Fig. 1.6 Ignition of Boron NPs in (A) Ethanol based fuel droplet (B) n-decane based fuel droplet [93].

Basha et.al. 2011 [95] carried out the investigations of the nanoparticles as an additive in the Jatropha biodiesel based bio-fuel and tested in diesel engines. Jatropha raw oil was synthesized by the process of transesterification and finally Jatropha Methyl Ester (JME) was used as the basefluid for the dispersion of MWCNTs in different particle-loading conditions. Initially the JME emulsion fuel was prepared along with the surfactants in the proportions of 93% JME, 5% water and 2% surfactants by volume respectively. The dispersions of MWCNTs was carried out with the JME emulsion in the percentages of 25ppm, 50ppm and 100ppm respectively, and then these mixtures of MWCNTs dispersed in the JME emulsion fluids was sonicated in the JME along with the surfactants. Such nanofluids were then tested in the diesel engines for the engine performance along with the exhaust emissions. Table 1.3 shows the various fuel properties of MWCNTS dispersed in JME based nanofluids.

Table:1.3 Fuel Properties of JME and different loading MWCNTs dispersed in JME nanofluids [95].

Properties	JME	JME2S5W	JME2S5W 25CNT	JME2S5W 50CNT	JME2S5W 100CNT
Density @ 15 ^{o}C, kg/m3	895	899.8	897.2	897.8	899.4
Kinematic Viscosity @ 40 ^{o}C, (x10^{-6} m^{2}/s	5.05	5.4	5.43	5.76	5.91
Flash Point ^{o}C	85	140	130	125	122
Net Calorific Value, MJ/kg	38.88	37.05	37.28	37.35	37.85
Cetane No.	53	51	54	55	56

Fig.1.7(A) shows the variations in the performance of diesel engine with using MWCNTs dispersed JME emulsion fuels and Fig.1.7(B) shows the variations of the tested fuel in terms of brake specific fuel consumption. From the Fig.1.7(A), it is clear that the thermal efficiency of the diesel engine was higher for the MWCNTs dispersed JME emulsion fuels when compared with the pure JME as a fuel. And it is also clear that highest efficiency was achieved for the sample containing high concentration of MWCNT than when compared with that of the other concentrations. Fig.1.7(B), shows that the brake specific fuel consumption of JME without the dispersion of MWCNT was the highest and among the different concentrations of the MWCNTs dispersed JME emulsion fuels, the concentrations with 100ppm of MWCNTs emulsified JME fuel has the least bsfc when compared with the rest of the tested samples.

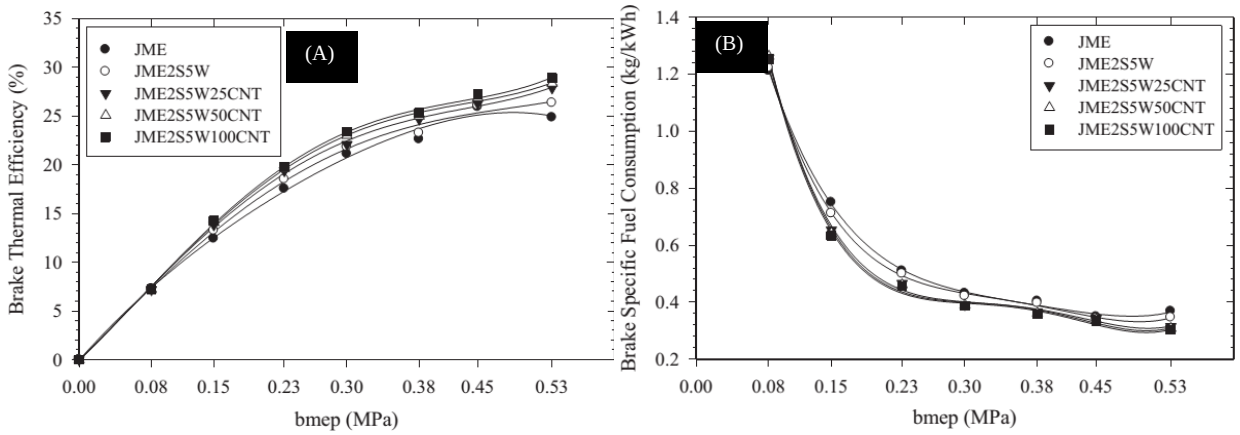

Fig.1.7Variation in (A) Brake Thermal efficiency (B) Brake specific fuel consumption for the tested JME and nanofluels [95]

Fig.1.8(A) shows the exhaust gas temperatures of the JME and MWCNTs dispersed JME emulsion fuels on the diesel engine. It is clear that the exhaust temperatures of the neat JME are higher as compared to the MWCNTs dispersed JME emulsified fuels. Further it is noticed that the test sample having 100ppm of MWCNTs dispersed JME emulsified fuel has the lowest exhaust temperature when compared with the other concentrations. Fig.1.8(B) shows the smoke opacity of the exhaust gases for the tested fuels. It is clear from the Fig.1.8(B) that the smoke opacity was the highest for the JME fuel as compared with the concentrations containing the dispersed MWCNTs in the JME emulsified fuels. Also it is confirmed that the concentration containing 100ppm of MWCNTs dispersed JME emulsified fuel has the lowest smoke when compared with that of the rest of the concentrations.

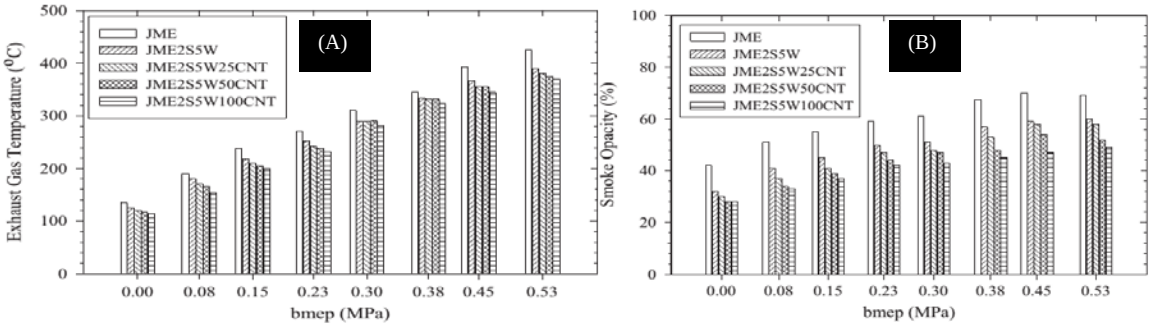

Fig.1.8 JME and MWCNTs dispersed nanofuels on engine performance of (A) Exhaust gas temp. (B) Smoke for the tested fuels [95]

It was also reported that the exhaust emissions of un-burnt hydrocarbons were lowest for the neat JME as compared with the various concentrations of MWCNTs dispersion in the JME emulsified fuels. Similarly, the emissions of CO were the least for the MWCNTs dispersed JME emulsion fuels as compared to that of neat JME bio-diesel. **Himanshu Tyagi et. al. 2008 [97]** conducted the ignition probability tests on hot-pate with diesel as the basefluid by considering aluminum and aluminum oxide nanoparticles having size of ~50nm of aluminum while the aluminum oxide nanoparticles was chosen with two different particle sizes i.e., 15nm and 50nm. The hot-plate ignition tests were conducted for different particles loading of 0.1% and 0.5% and the results were compared with that of neat diesel fuel. The tests were conducted for a temperature range of 680 ^{o}C to 780^{o}C in steps of 20^{o}C. Fig.1.9(A)-(C) show the hot-plate ignition probability results of alumina (~50nm size) and aluminum oxide (~50nm size) and aluminum oxide (~15nm size) having a particles loading by volume fraction of 0%, 0.1% and 0.5% at a temperature of 708^{o}C,

728°C and 748°C respectively. These results were compared with the ignition probability of neat diesel fuel at the same temperature.

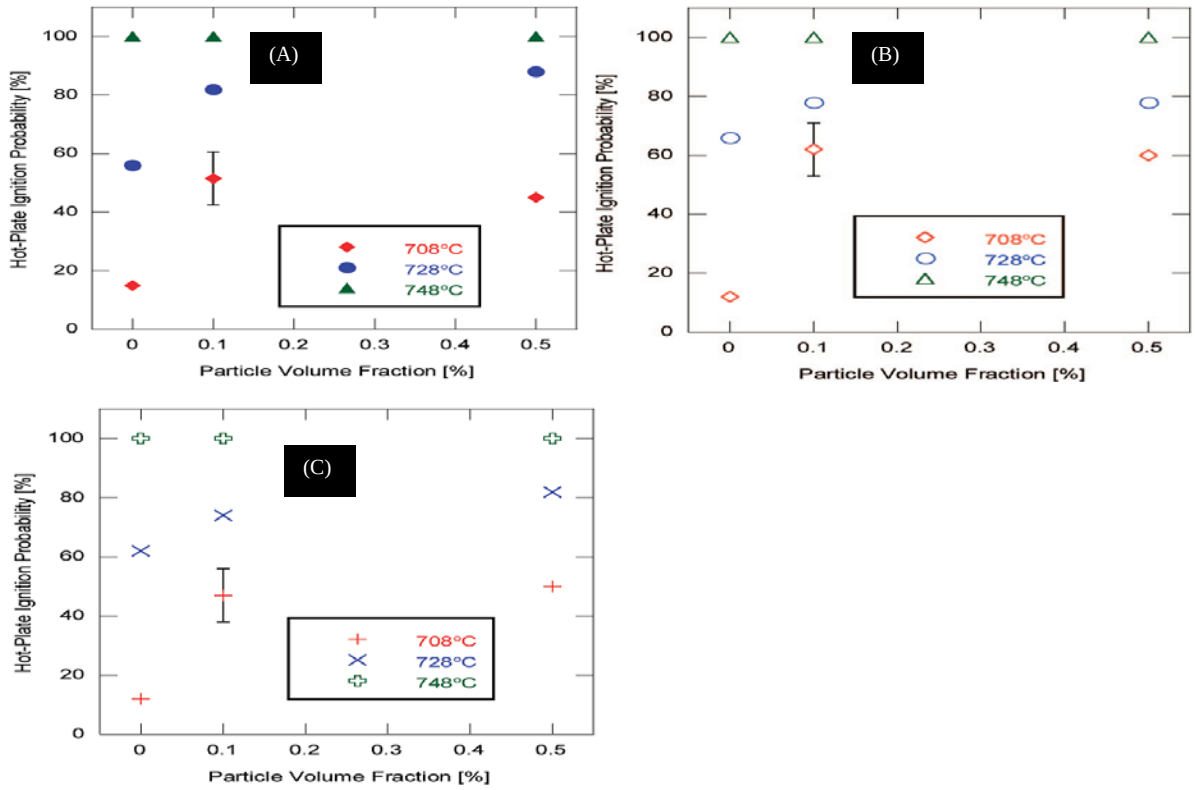

Fig. 1.9 Ignition Probability with (A)Particle VF (%)Al(50nm) + Diesel (B) Al_2O_3(50nm) + Diesel (C) Al_2O_3(50nm) mixtures at hot-plate temperature of 708, 728 & 748 °C [97]

From these experimental results, it was concluded that at higher temperature such as 708 °C, the ignition probability of Al nanoparticles (~50nm) dispersed in diesel at 0.1% volume fraction has much higher which is having 51% when compared to that of neat diesel fuel. The same ignition probability was observed for the 0.5% volume fraction of Al nanoparticles disepersed in diesel when compared with that of neat diesel at the same temperature say 708 °C and also at 728 °C and also at 748 °C respectively the ignition probability of Al nanoparticles dispersed diesel based fuel was found to be 100% higher as compared to that of neat diesel.When materials effects was investigated by comparing the ignition probability of aluminum and aluminum oxide nanoparticles, it was found that a visible "glowing" was seen when aluminum nanoparticles dispersed diesel fuel was ignited while "glowing" was not seen in the case of aluminum oxide dispersed diesel fuel. Hence, it was concluded that the ignition probability of the diesel based both the nanoparticles i.e., aluminum and aluminum oxide nanoparticles irrespective of their

sizes were showing much higher than that when compared to the ignition probability of diesel without any nanoparticles. From these experimental results, it was concluded that when these fuels containing high ignition probability were used in the diesel engines, the efficiency of the diesel engine improved dramatically. **Yanan Gan et.al [98**] investigated the evaporation characteristics of different nanoparticles / nanomaterial by dispersing carbon based nanoparticles i.e., SWCNTs, MWCNTs and aluminum nanoparticles (as shown in Fig 1.10(A)) in ethanol as the basefluid. It was observed that nanofuels containing the carbon nanoparticles i.e., MWCNTs and aluminum nanoparticles were showing much higher evaporation characteristics as compared with that of pure ethanol. It was also revealed that MWCNTs dispersed ethanol based fluids was showing higher evaporation characteristics when compared with aluminium nanoparticles dispersed ethanol based nanofluids. Here the nanofluids were prepared without any surfactant. Polymers were used for the dispersion of MWCNTs which make them hydrophilic in nature. The stability of MWCNTs nanofluids were reported as 24hourswhile the stability of SWCNTs nanofluids could not be achieved even for 5minutes. Fig.1.10(B) indicates the evaporation rate of nanofluids consisting of pure ethanol and also ethanol with aluminum nanoparticles and MWCNTs dispersed nanofluids.

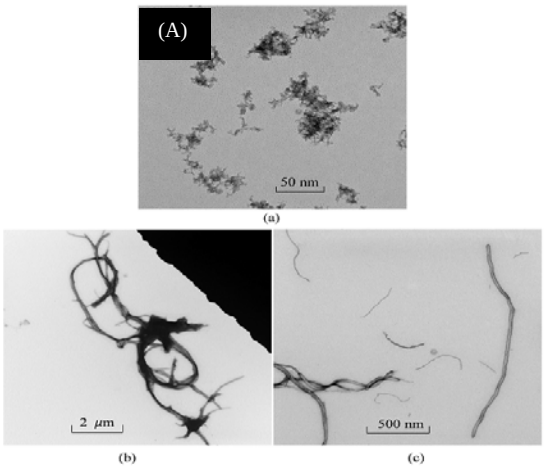

Fig. 1.10(A) TEM images of (a) CNPs (6nm) (b) SWCNTs (diameter, 1-2 nm; length 5-30µm) (c) Dispersible MWCNTs (diameter20nm,Length1-5µm). [98]

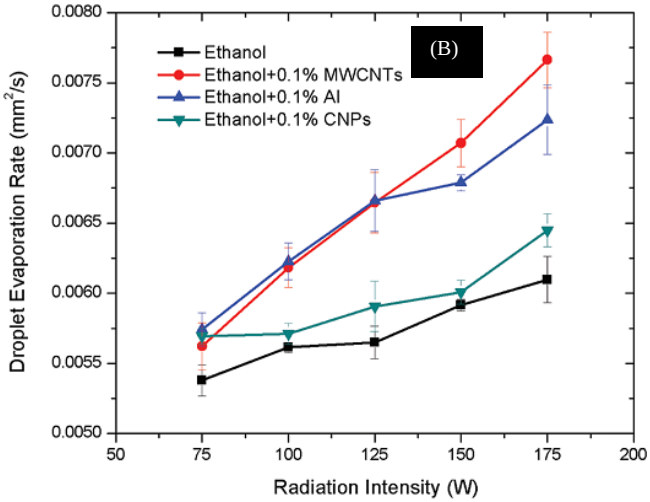

Fig 1.10(B) Plot of Droplet evaporation rate of pure ethanol & nanofluids with addition of Al NPs and dispersible MWCNTs at different radiation levels. [98]

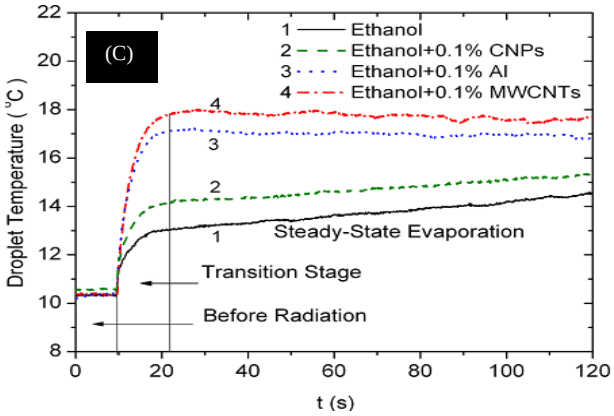

Fig.1.10(C) Droplet temperature history of pure ethanol & nanofluids with addition of Al particles, CNPs& dispersible MWCNTs [98]

.

Fig. 1.10 shows the droplet temperature of ethanol based nanofluids having aluminum nanoparticles, CNPs, and also MWCNTs respectively. It is clear from the slope that Al and MWCNTs dispersed ethanol based nanofluids are more steeper than that of the pure ethanol and CNPs, which indicates that the droplet temperature of MWCNTs and Al is higher than that of ethanol and hence showing higher evaporation rate. **Apichai Jomphoak et.al. [100]** studied the thermal conductivity of alumina nanoparticles dispersed in de-ionised water for different concentrations such as 0.05%, 0.1% and 0.2% using transient planar source (TPS) method. In this method, a thin gold disk was used as a heating filament which acts as electrical resistance thermometer. The set-up was calibrated using DI-Water and then the thermal conductivity of alumina nanofluids with basedfluids as DI-Water was investigated.

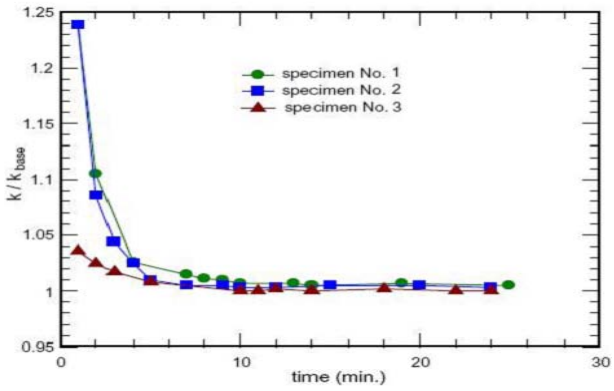

Fig.1.11 Normalized Thermal Conductivity data as a function of measured time [100]

Fig.1.11 shows the ratio of thermal conductivity of alumina nanofluids versus thermal conductivity of its basefluids for three different concentrations. The thermal conductivity of 0.1% volume fraction was the highest with 18.5% enhancement at a time interval of 1 to 2minutes. **Ramaprabhu et.al. 2012 [111]** investigated on thermal conductivity of DI-Water and Ethylene glycol by dispersing ZnO nanoparticles and Al_2O_3 decorated MWCNTs at different concentrations. The surfactant i.e., SDS was added for homogeneity dispersion in the case of ZnO-MWCNTs dispersed nanofluids. Fig.1.12 shows the MWCNTs, ZnO-MWCNTs and Al_2O_3-MWCNT nanomaterials respectively.

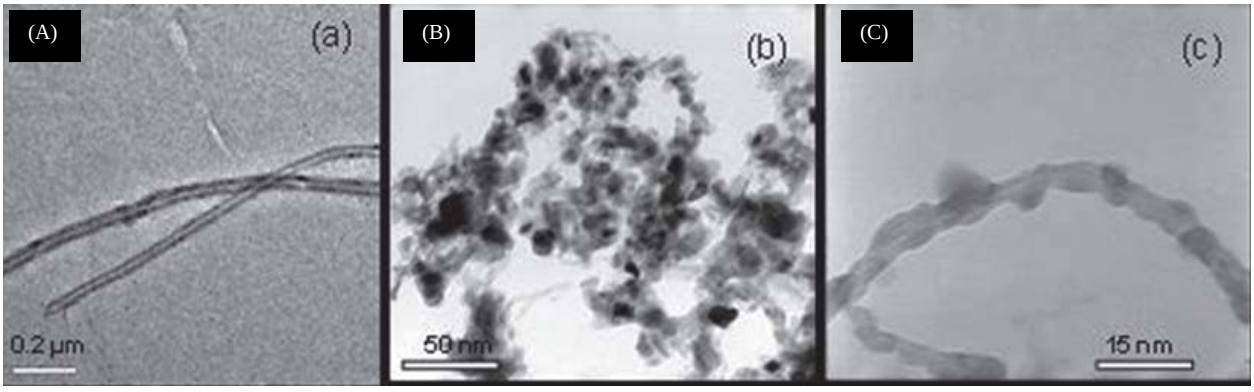

Fig.1.12 TEM images obtained for (a) MWCNT, (b) ZnO-MWCNT and (c) Al_2O_3-MWCNT [111]

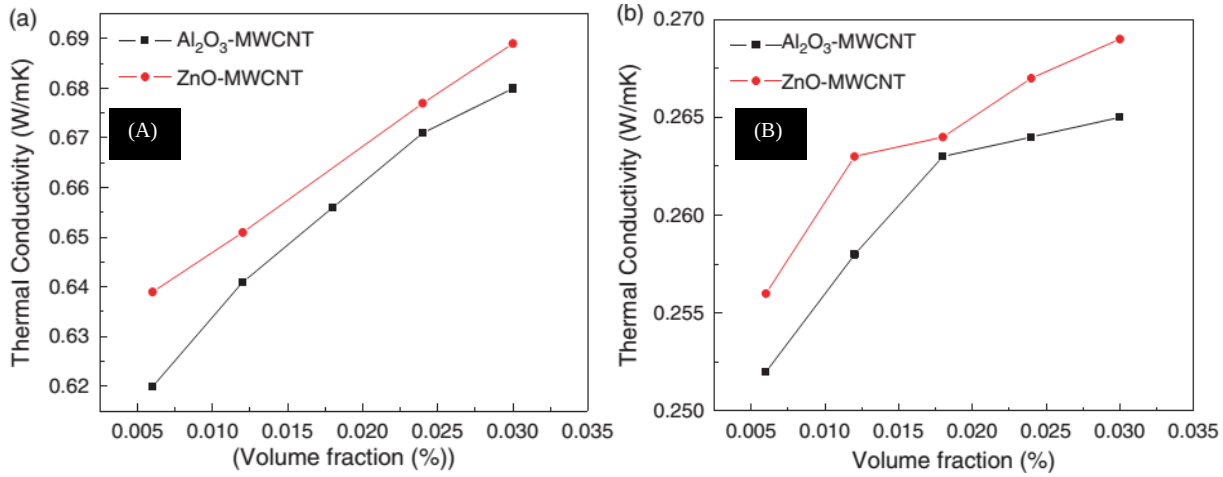

Fig. 1.13 Plots of Thermal conductivity with concentration for ZnO-MWCNT and Al2O3-MWCNT in (A) DI water (B) EG base fluids [111]

Fig.1.13 (a) shows the thermal conductivity of the nanocomposites of ZnO-MWCNT and Al_2O_3-MWCNT using DI-Water as the basefluid whereas Fig.1.13(b) shows the thermal conductivity of ZnO-MWCNT and Al_2O_3-MWCNT using ethylene glycol as the basefluids. The thermal conductivity for pure basefluid (DI-Water) was found to be increased by 11%, with ZnO-

MWCNT and 9.7% for Al2O3-MWCNT. While using EG as the basefluid, the thermal conductivity was found to be 8.5% for ZnO-MWCNT and 6.8% for Al_2O_3-MWCNT. **Kin Yuen LEONG et. al. [113]** carried out their investigations of thermal conductivity for ethylene and DI water based stable nanofluids considering CNTs with surfactants. The stability parameters were studied based on the zeta potential measurement. The surfactants considered were of three types namely, polyvinylpyrrolidone (PVP), gum Arabic (GA) hexadecyl trimethyl ammonium bromide (CTAB). The main objective of these studies was to investigate the effects of different surfactants on the thermal conductivity of MWCNTs when dispersed in Ethylene glycol and comparision of the same with DI-Water. Fig.1.14 shows the FESEM image of MWCNTs (having a diameter of less than 30nm) dispersed in a basefluid which is a mixture of DI-Water (60%) and Ethylene Glycol (40%). Stability studies were done by observation for 4 weeks of time and also by zeta potential methods for the samples without the use of surfactants and also for the samples containing the surfactants. Fig.1.15 shows the MWCNTs dispersed nanofluids with and without surfactants. It is clear from the Fig.1.15that MWCNTs dispersed nanofluids with surfactants of PVP, GA, CTAB were able to modify the surface properties of the MWCNTs from hydrophobic to hydrophilic. Fig.1.16(A) shows the effect of the surfactants on the thermal conductivity measurements of MWCNTs dispersed nanofluids from which it can be seen that the thermal conductivities with respect to the surfactants of PVP, GA and CTAB were having enhancement of 25.7%, 18.4% and 16.0% respectively.

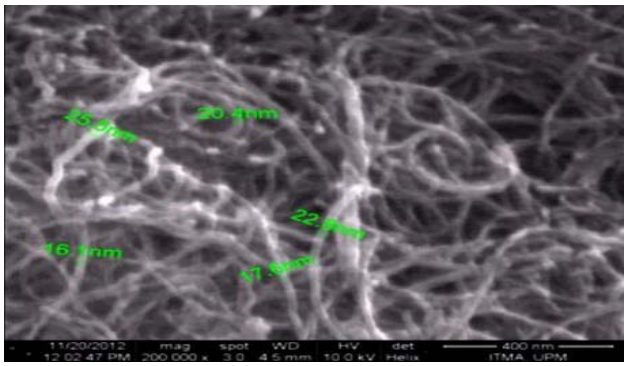

Fig:1.14 FESEM image of MWCNTs [113]

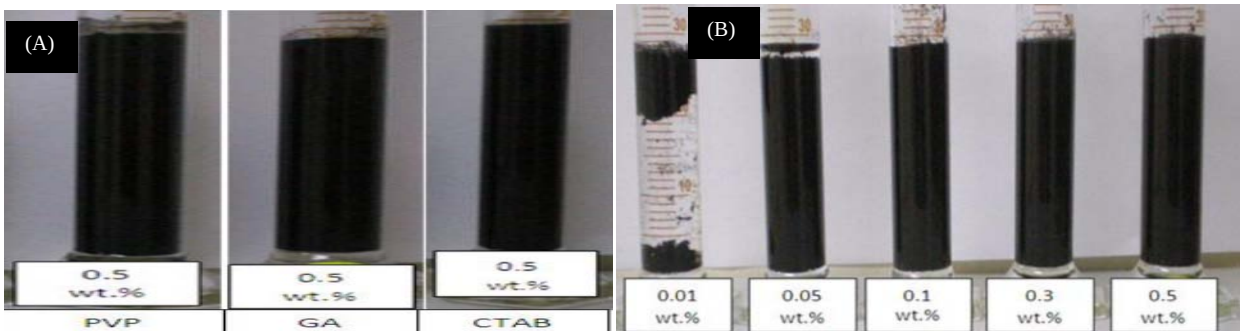

Fig.1.15 Condition of CNT's dispersed nanofluids (A) with surfactant and (B) without surfactant [113]

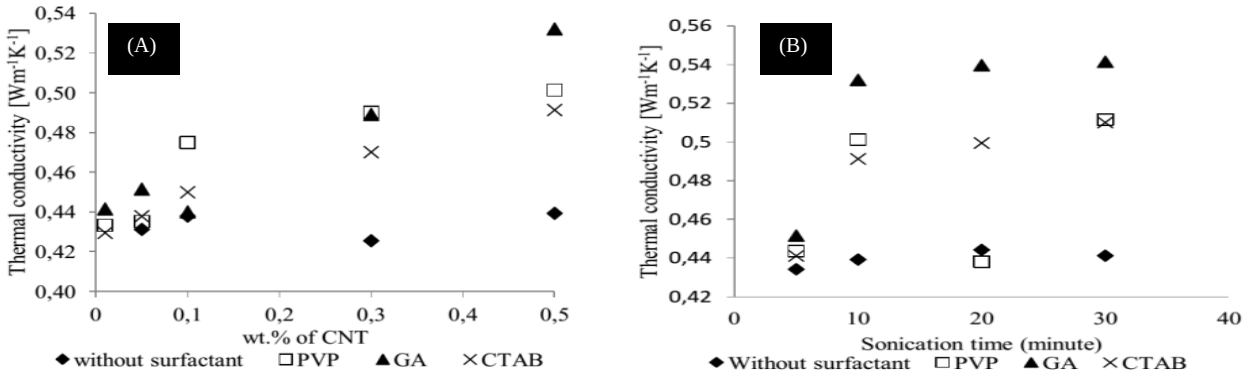

Fig.1.16 Effect of (A) CNT Concentration (B)Sonication time on TC of CNTs based nanofluids with and without surfactants [113]

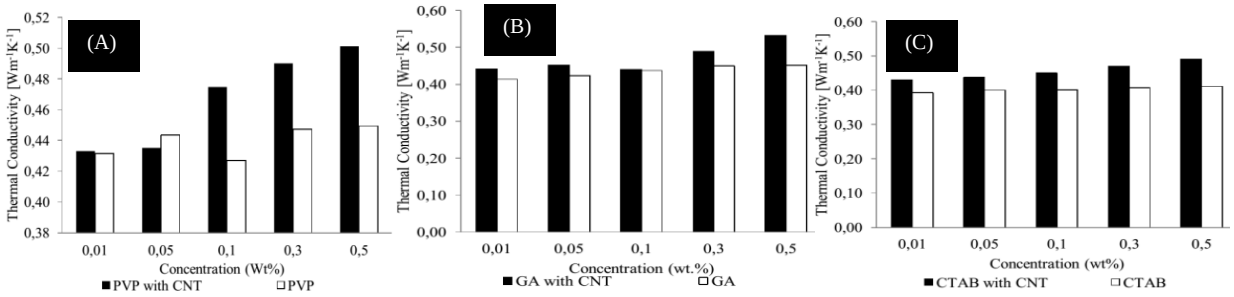

Fig.1.17 . TC of CNT based nanofluids with (A) PVP (B) GA (C) CTAB respectively [113]

Fig.1.17((A)-(C)) show the comparison of thermal conductivities of basefluids with surfactants of PVP and having with and without the dispersion of MWCNTs, basefluids with surfactants of GA and having with and without the MWCNTs dispersion and finally the basefluids having surfactant of CTAB and having with and without the dispersion of MWCNTs respectively. It is found from the Fig. 1.17((A)-(C)) that the thermal conductivity of the nanofluids containing the MWCNTs dispersion was having higher thermal conductivities than those of the samples that were not having the MWCNTs dispersion. And it is seen that thermal conductivities of nanofluids having MWCNTs were increasing as the sonication time was increasing with the use of the surfactant i.e., PVP. **J.K. Lee et.al. 2007 [115]** investigated the thermal conductivities of

stable nanofluids considering 4 different nanoparticles / nanmaterials such as MWCNTs, Fullerene, CuO and SiO_2 with considering 3 different basefluids namely, DI-Water, Ethylene Glycol and Moneral Oil. Table 1.4 shows the properties of these nanomaterials. Fig.1.18 shows the TEM images of these four different nanomaterials such as, (a)MWCNTs, (b) CuO, (c) Fullerene and (d) SiO_2. Stability of the nanofluids was characterized with respect to the UV-Vis spectra of nanomaterials dispersed in mineral oil. The peak positions of MWCNTs and Fullerene was found at 397nm in the UV-Vis spectra measurement when these materials were dispersed in mineral oil.

Table 1.4 Property of different nanomaterials (MWCNTs, Fullerene, CuO, SiO_2) and basefluids [115]

Parameter	MWCNT	Fullerene	CuO	SiO_2	H_2O	Ethylene Glycol	Oil
Density (g/cm^3	2.6	1.6	6.32	2.22	1	1.11	0.915
Thermal Conductivity (W/mK)	~3000	0.4	76.5	1.38	0.613	0.252	0.107
Average size (L)	10-50µm	~10nm	33nm	12nm			
Average size (D)	10-30nm						

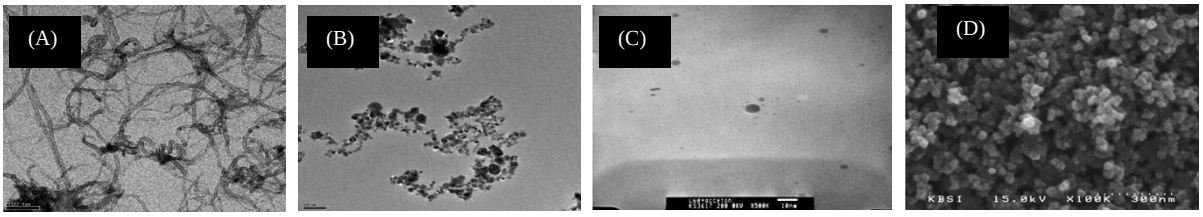

Fig.1.18 SEM images of test particles (a) MWCNT, (b) CuO, (c) Fullerene, (d) SiO_2 [115]

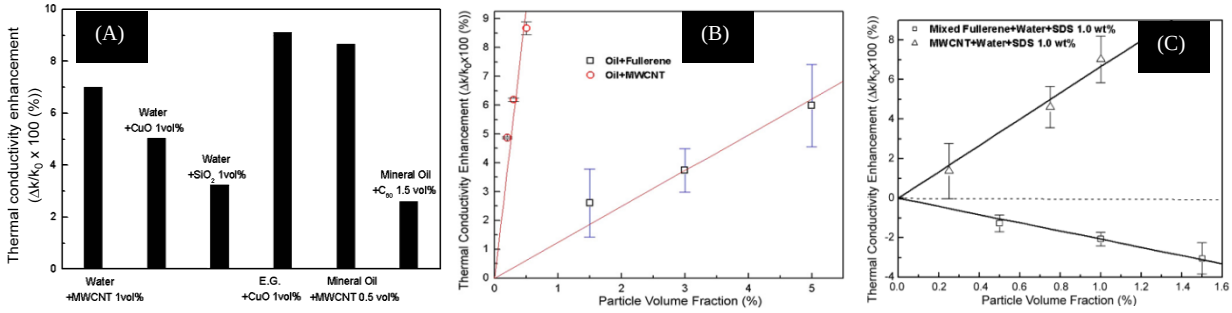

Fig.1.19 TC of (A) nanofluids (B) TC enhancement of oil-based fullerene NFs (C) TC enhancement of water-based MWCNT & Fullerene NFs [115]

Fig.1.19((A)-(C)) show the enhancements in thermal conductivities of different nanomaterials in different basefluids using the transient hot-wire method. Fig.1.19(A) shows the thermal conductivity enhancements of different nanomaterials dispersed in different basefluids, each having a particle loading of 1vol.% .Fig.1.19(B) shows the enhancements in thermal

conductivities for fullerene dispersed mineral oil based nanofluids. It is concluded that at 0.5Vol.%, the thermal conductivity was increased by 8.7% with respect to MWCNT, while fullerene is having an enhancement of 6% for a concentration of 0.5vol%. Fig.1.19(C) shows the enhancement of thermal conductivities of MWCNTs and fullerene having basefluids as DI-Water. From the Fig.1.19(C), it is clear that the thermal conductivities of MWCNTs nanofluids increases with increase in concentration of the nanomaterials while the thermal conductivities of fullerene nanomaterials based nanofluids decreases with increase in volume concentrations. **Yong-Jin Yoon et.al.2014 [116]** investigated the influence of different nanomaterials such as Al_2O_3, CuO, ZnO and MWCNTs on their viscosity and thermal conductivity of DI-Water based nanofluids. The particles sizes of these nanomaterials were 40-50nm, 23-37nm, 40-100nm for Al_2O_3, CuO, ZnO respectively as shown in the Fig 1.20. Investigations regarding the stability these nanofluids reported only 6 hours of duration for these nanoparticles dispersed nanomaterials using DI-Water as the basefluid without the use of any surfactants. The nanofluids of MWCNTs were prepared by considering 3 different surfactants such as gum Arabic, sodium dodecyl sulfate and sodium dodecylbenzene sulfonate out of which Gum Arabic with a volume concentration of 0.1%, was found to be the most effective stabilizing agent for MWCNTs dispersed in water. Fig.1.20((A)-(C)) shows SEM images of Al_2O_3, CuO, ZnO dispersed in DI-Water without the use of any surfactants and it is clear that Al_2O_3NPs were spherical with polydisperse size, CuO NPs formed clusters having different sizes, ZnO NPs were also having polydisperse size at different angles.

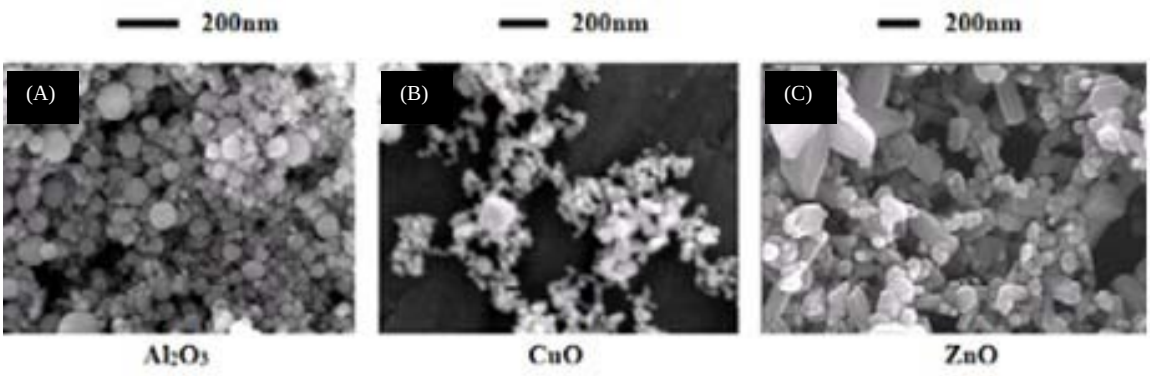

Fig.1.20 SEM images of dried oxide NPs [116]

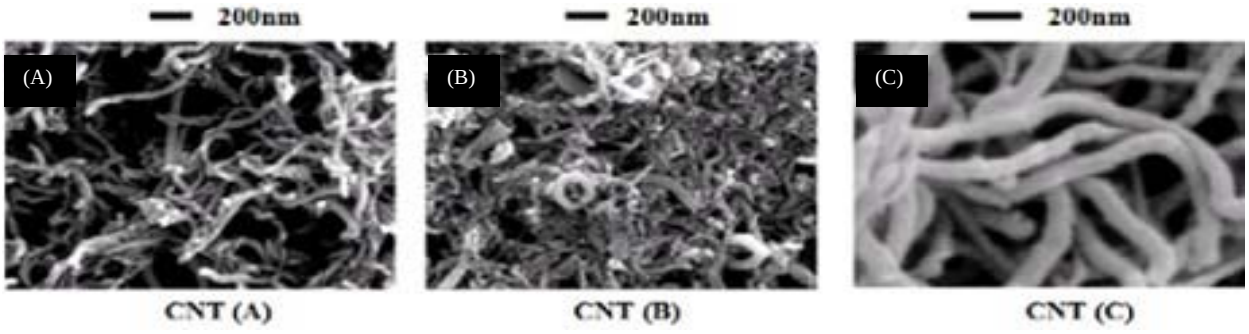

Fig.1.21 SEM images of three different types of CNTs [116]

Fig.1.21 shows the SEM images of MWCNTs for 3 different samples which were obtained by directly loading them in the SEM instrument after they were gold coated in the dry form, without dispersing in any of the basefluids. Fig.1.22 shows the SEM images of agglomerated particles of Al_2O_3 nanofluids and CuO, sonicated for 1 hour of duration. It was found that the aggregate oxides of Al_2O_3NPs were having a size of ~155nm while that of CuO NPs clusters was having size of ~170nm. Fig.1.23 shows the SEM images of CNTs which were sonicated for 1 hour of duration. It was found that the clusters of MWCNT were having individual groupings of sizes ranging from 1µm to 35µm.

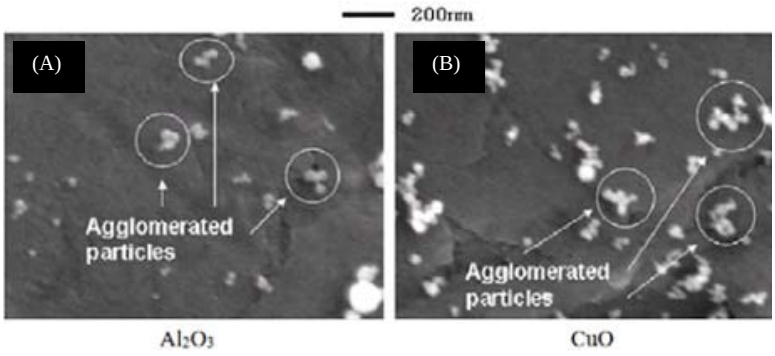

Fig.1.22 SEM images of aggregated oxide NPs [116]

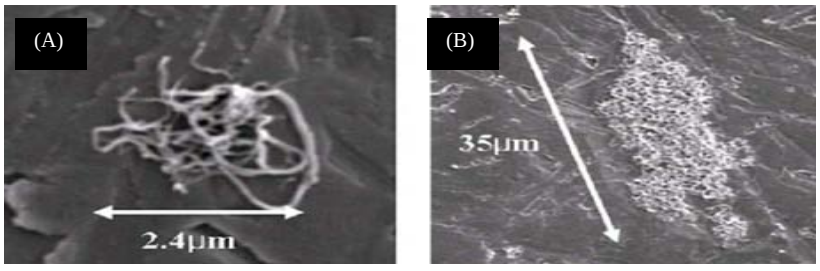

Fig.1.23 SEM images showing individual groups of entangled CNTs [116]

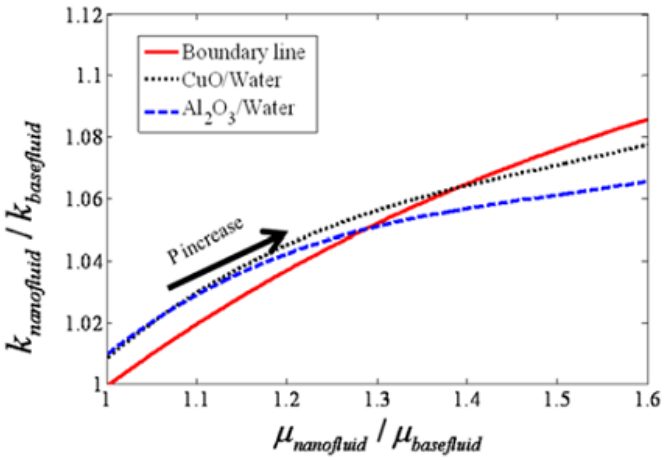

Fig.1.24 TC and Viscosity change of Al_2O_3/water and CuO/water based nanofluids [116]

Fig.1.24 shows the plots of thermal conductivity ratio of Al_2O_3 NPs dispersed in DI water and also that of CuO NPs dispersed in DI water with respect to the boundary line. Thermal conductivity was calculated from the Maxwell's effective medium theory. From the Fig.1.24, it is clear that as the viscosity of the nanofluid increases, the thermal conductivity of both the nanofluids falls below the boundary line which means that the thermal conductivity of the nanofluids were less effective than the thermal conductivity of the basefluid alone. At lower viscosity, the thermal conductivity ratio of both the fluids were above the boundary line which means that the thermal conductivity of both the nanofluids was higher than that of the thermal conductivity of the basefluid alone. **Rad Sadri et. al. 2014 [117]** investigated viscosity and on the thermal conductivity of MWCNTs based nanofluids by varying the ultrasonication time and also by using different surfactants in the basefluids.

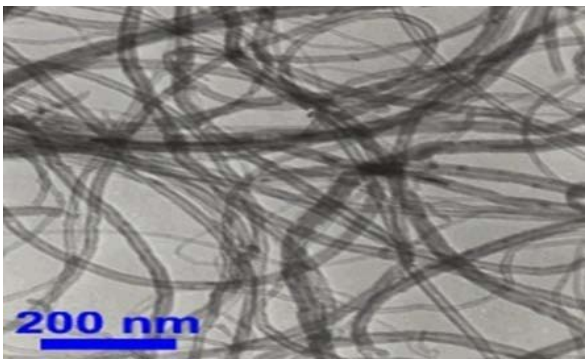

Fig1.25TEM image of multi-walled CNTs (as received) [117]

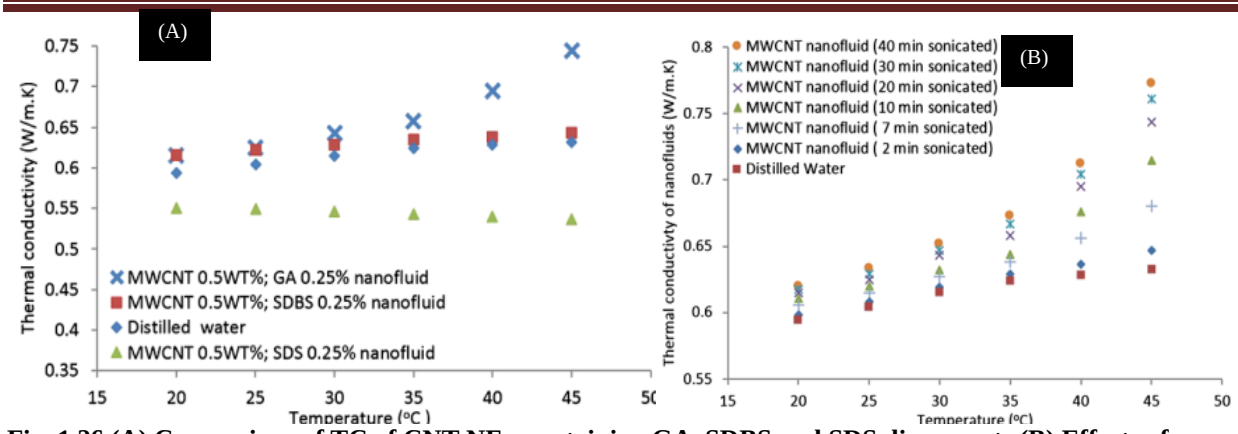

Fig. 1.26 (A) Comparison of TC of CNT NFs containing GA, SDBS and SDS dispersants (B) Effects of ultrasonication time and temperature on TC of NFs [117]

Fig.1.26(A) shows the comparison of thermal conductivity of MWCNTs dispersed in DI-Water containing the three different surfactants namely, GA, SDBS and SDS respectively. For all the samples, thermal conductivity was measured using the KD2 Pro instrument (Decagon, Pullman, WA, USA). The different concentrations and the surfactant content considered were 0.5wt% of MWCNT was dispersed in 60ml of DI-Water containing 0.25% of GA, 0.25 and 0.5% of SDBS and SDS respectively and the results were compared with respect to the DI-Water. From Fig. 1.26(A), it is seen that the nanofluids having the surfactant GA has the highest thermal conductivity than that of the other samples. Also it is found that the sample containing MWCNTs with SDS as the surfactant has thermal conductivity lower than that of the thermal conductivity of DI-Water. It is also found that in all the cases, as the temperature is increasing thermal conductivity also increases. The effect of viscosity with respect to thermal conductivity was measured using the rotational rheometer (Physica, MCR-301, Anton Paar, Graz, Austria). They measured by varying the shear rate was varied at a range of 10 to 140/s and corresponding viscosity readings were obtained from the instrument at three different temperature that is, 15 ^{o}C, 30^{o}C and 45^{o}C respectively. Dynamic viscosity measurements of various samples of MWCNT as a function of shear rate at these different temperatures of 15^{o}C, 30^{o}C and 45^{o}C for different sonication times (2min,10min. and 30min.) for DI-Water without the MWCNTs dispersion and also for DI-Water with MWCNTs dispersed containing the GA surfactant was considered. Investigations was also carried out to study the dispersion stability of the MWCNTs for different sonication time using GA as the surfactant by sedimentation method. It was found that as the sonication time increases, the agglomerated clusters of MWCNTs start to segregate into broken

fragments in the basefluid with the surfactant GA. As a result of that, the lengths of these segregated MWCNTs get reduced.

Hence, there are several reported contributions towards the improvement of engine performance, ignition probability, thermal conductivity, etc. by dispersing the nanoparticles and nanomaterials in the bio-fuel or diesel. Few of them worked on aluminum nanomaterials in diesel fuel at lower engine speeds and concluded that the exhaust emissions and fuel consumption were lower when compared to that of the pure diesel fuel. **Nasrin, et.al [120]** reported on the magnetic nanofluid fuels by dispersing Fe_3O_4 in diesel fuel and concluded that even at very less concentrations of nanomaterials, the performance of the diesel engine can be improved with the reduction of harmful pollutants like NOx and SO2. **Karthikeyan et.al. 2014 [122]** investigated the emissions of diesel engine by using Zinc Oxide nanoparticles dispersed Promolion Stearin Biodiesel as an alternate fuel and reported in favor of zinc oxide dispersed biodiesel based nanlfuels for reduction in emissions of diesel engine. **Shafii et.al. 2011 [125]** investigated the diesel engine emissions by using the blends of ferrofluids in the diesel fuel as alternate fuels. **Ribeiro et.al. 2007 [127]** concluded that the transition elemnets such as Ce, Fe, Cu, Sr, and Pt, nanoparticles if used as additives, lower the NOx temperature substantially by large extent.

Therefore, from the reported literatures, it is concluded that for different characteristics of the bio-diesel/ bio-fuel such as ignition probability, dispersion stability, viscosity of the nanofluids, emissions of the nanofluids, and finally the thermal conductivity of the nanofluids are strongly depended on the size of different types of the nanomaterials, synthesis parameters and the surfactants used. It was found that many researchers often reported on improving the efficiency of the diesel engines by using various types of nanomaterials in either diesel or biodiesel mainly focusing on the combustion properties of the bio-fuels. However, not much progress has been reported to utilize such biodiesel / bio-fuels in diesel engines because of certain issues such as formation of agglomerations of the nanoparticles in the basefluids, unable to obtain longer stable nanofluids, lack of data regarding the use of nanofluids as an alternate fuels, effect of nanomaterials size and shape on the biodiesel, etc. Because the main issues associated with the dispersion of nanoparticles or nanomaterials to achieve long term stable dispersion of nanoparticles or nanomaterials in the biodiesel since nanoparticles tends to get agglomerated and

do not show the properties of diesel / bio-fuel over a certain period of time and also they tend to block the fuel passage in the combustion chamber due to the formation of aggregated clusters. Therefore, this thesis deals with the investigation of long term stable biodiesel based nanofluids for using in the diesel engines by considering different types of nanomaterials and their size effects on the stability and properties (viscosity of the nanofluids, ignition probability and thermal conductivity) of the nanofluids of the bio-diesel based nanofluids for future applications as alternate fuels.

Objective:

The main objective of this thesis research work is to study the effects of two types of nanomaterials and their sizes (alumina (Al_2O_3) and Multi-walled carbon nanotubes (MWCNTs)) on the dispersion stability to achieve long term stability and thermo-physical properties to improve the fuel properties of the bio-diesel so that it can be suitable for energy sector applications. Two different materials such as alumina nanomaterials and multiwalled carbon nanotubes were considered in this work. Jatropha biodiesel (JME) was considered as the basefluids. Scope of this research work involves to investigate the longer term stable biodiesel based nanofluids and effect of nanomaterials and their sizes on the thermo-physical and fuel properties to diesel engines, and also to sustain their long term stable nanofluids having lower viscosity and higher thermal conductivity properties for potential use as alternate fuel energy.

Description of the Thesis work:

In this thesis work, Chapter 2 deals with the characterization of the two different types of the nanomaterials Al_2O_3 NPs and MWCNTs by XRD, EDX, FESEM, TEM and Raman for their structure, composition and morphology analysis. Chapter 3 deals with the preparation of nanofluids from biodiesel by Transesterification process and followed by dispersion process of the nanoparticle / nanomaterials blended biodiesel for different percentage volume fractions for the above mentioned alumina NP's and MWCNT's. Chapter 4 involves the study of stability and formation of aggregates with storage time of the nanofluids of alumina NPs and MWCNTs dispersed in the biodiesel by FESEM, TEM and UV-Vis spectroscopy. Chapter 5 deals with the investigation of nanomaterials sizes and types on the viscosity of the biodiesel based nanofluids

Chapter 6 deals with the investigation of size effect of Al_2O_3 NPs and nanomaterials on thermal conductivity of biodiesel based nanofluids. Chapter 7 deals with the investigation of size effect of Al_2O_3 NPs and nanomaterials effect on the evaporation rate of the biodiesel based nanofluids. And finally, Chapter 8 deals with the conclusions of the thesis with future scope on this research work.

Chapter 2.

Characterization of Nanomaterials

2.1 Introduction

This chapter deals with the characterization of two different types of nanomaterials such as alumina NP having two different sizes (Sigma Aldrich, USA) and high aspect ratio MWCNTs (Reinstae, India) by using XRD, FESEM, TEM, Raman and FT-IR for structural, Morphological, disorder and composition analysis. The first part of this chapter deals with the characterization of Al2O3 NPs having two different sizes, purchased from Sigma Aldrich, USA). The high aspect ratio MWCNTs purchased from Reinstate, India are discussed in the latter part of this chapter.

2.2 Characterization of Alumina nanoparticles (NPs-1 & NPs-2):

2.2.1 X-Ray Diffraction:

X-ray powder diffraction patterns of the alumina nanoparticles were recorded on a Bruker D8 Advance X-ray diffractometer equipped with graphite monochromatized Cu Kα (λ=0.1540 nm), with an accelerating voltage of 40 KV. Data was collected using a scanning rate of 0.02° s^{-1} in

ranges from 10° to 90°. The Fig 2.1((A) and (B)) show the XRD spectrum of alumina nanoparticles of two different sizes (NP-1 & NP-2). The average crystallite size is determined by using the Scherrer formula:

$$a = 0.9\lambda / \beta\cos\theta,$$

Where "a" is the particle size, "λ" is the X-ray wavelength, "β" is the full width of the half maxima (in radians) of the X-ray peak, and "θ" is the Bragg angle.

XRD pattern (as shown in Fig 2.1(A) and (B)) of the Al_2O_3 nanoparticles (NPs-1) confirms that the Al_2O_3 nanoparticles are highly crystalline. Crystalline planes corresponding to the peaks for δ and γ of Al_2O_3 nanoparticles of NPs-1 have been indexed. 2θ = 32.12, 34.4, 36.5, 38.6, 45.4, 56.7, 67.5 and 76.08 are δ- phase have planes (021), (117), (122), (124), (122), (1,2,11), (040) and (2,3,11) respectively. These are identified with JCPDS NO 00-046-1131 Al_2O_3 -δ - Al_2O_3 and 2θ = 39.5, 60.85, 66.9 and 84.8 are γ- phase have planes (222), (511), (440) and (444) respectively. These are identified with JCPDS NO 00-010-0425 Al_2O_3 – γ - Al_2O_3.

Table .2.1 Calculation of interplanar distance (d) and crystallite size for sample NP-1

2θ	Phase	Inter planar distance(d) Å	Crystallite size(D) nm
32.5	γ	2.7	3.9
60.85	γ	1.5	3.7
34.44	δ	2.6	7.7

Average crystallite size (γ) = 3.8nm

Average crystallite size (δ) = 6.5nm

Table .2.2 Calculation of interplanar distance (d) and crystallite size for sample NP-2

2θ	Phase	Inter planar distance(d) Å	Crystallite size(D) nm
39. 4	γ	2.3	4.3
66.7	γ	1.4	3.78
32.7	δ	2.75	6 .3
45.2	δ	1.98	6.87

Average crystallite size (γ) = 4.04nm

Average crystallite size (δ) = 6.6nm

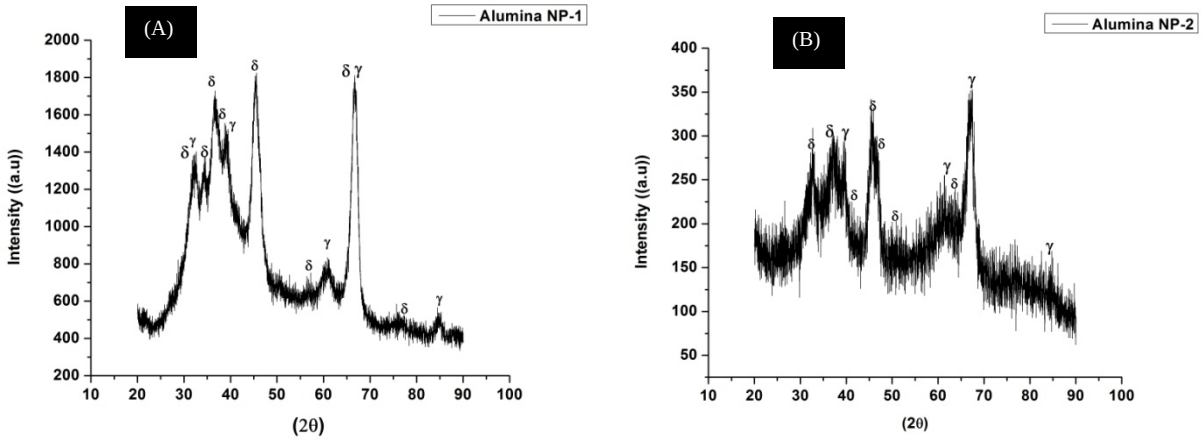

Fig.2.1 XRD patterns of (A) alumina NPs-1 (B) alumina NPs-2

In (b) 2θ = 32.6, 36.9, 39.3, 45.03, 46.5, 50.9, and 60.8 are δ – phase have planes (022), (217),(026), (220), (222),(2,0,10) and (2,2,13) respectively. These are identified with JCPDS NO 00-046-1131 Al2 O_3 -δ - Al_2 O_3 and also (217) and (2,2, 13) planes for taken JCPDS NO 00-047-1770 Al_2 O_3 - δ - Al_2 O_3 and 2θ =39.3, 60.8, 67.03 and 84.7 are γ-phase have planes (222), (511), (440) and (444) respectively. These are identified with the JCPDS No. 00-010-0425.

Hence, the crystallite size of Alumina nanoparticles samples NP-1& NP-2 at room temperature are 3.8nm(avg), 4.04nm(avg) for γ – phase and 6.5nm(avg),6.6nm(avg) for δ-phase respectively.

2.2.2 FESEM and EDX analysis of alumina NPs:

FESEM analysis was performed by using the CARL ZEISS which consists of GEMINI column (primary electron source) and the EDS attachment manufactured by OXFORD instruments. It consists of four detectors namely, In-Lens, Secondary Electron Detector, Energy and angle Selective Back-Scatter (ESB) and Angular Selective Back Scatter (ASB). Field Emission Scanning Electron Microscope (FESEM) images the sample surface by scanning it with high-energy beam of electrons in a raster scan pattern. The electrons interact with the atoms thus producing signals that contain information of samples topography, and composition. When an electron beam hits the sample surface, produces secondary electrons from the sample which would be collected by a secondary detector or a backscatter detector. These electros from the backscatter detector are then converted to a voltage and then gets amplified. This amplified

voltage is then applied to the grid of the cathode ray tube and changes the intensity of the spot of light. The image formed consists of innumerous spots of varying intensity on the screen of cathode ray tube (CRT), which corresponds to the topography of the sample. The types of signals produced by an scanning electron microscope consists of secondary electrons, back-scattered electrons (BSE), characteristic x-rays, cathodoluminescence, specimen electrons and transmitted electrons. The signals result from interactions of the electron beam with atoms at or near the surface of the sample. The secondary electron imaging produce a very high-resolution images of a sample surface.

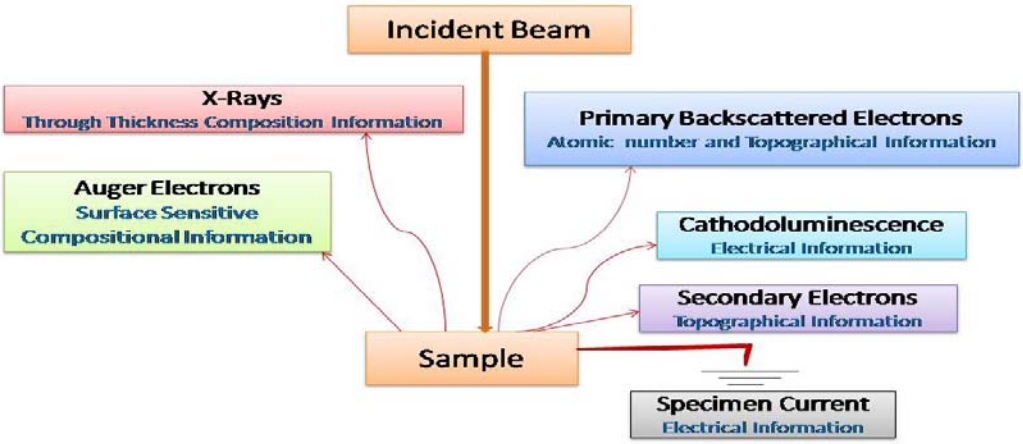

Fig.2.2: Electron –Specimen interactions when loaded in FESEM microscope.

Sample Preparation for FESEM analysis:

A small quantity of alumina NPs of both the sizes (NPs-1 and NPs-2) were dispersed in the DI water and sonicated for about 30 minutes and then a drop of the DI Water based alumina nanofluids was casted on a pre-cleaned silicon substrate of 15cm x15cm dimensions followed by gently warming so as to evaporate the water content and then the substrate was loaded into the FESEM tool with EDX attachment. Prior to the loading the sample into the FESEM, the sample was gold coated by low vacuum sputter coating with about ~5-10nm thick to make the specimen to be electrically conductive so as to prevent the accumulation of electrostatic charge at the surface. Fig.2.3(A) and (B) show the FESEM images of both sizes of alumina nanoparticles

displaying the morphological and compositional analysis. From the Fig 2.3((A) and (B)), it is clear that the morphology of both the sizes of alumina nanoparticles are nearly spherical in the shape and having average ~13nm and ~28nm in sizes respectively. Fig 2.4 (A) and (B) show the Energy Dispersive Spectroscopy images of both sizes of alumina nanoparticles (NP-1 and NP-2) dispersed in DIwater showing the presence of aluminum and oxygen elements only which confirms the purity of the samples considered for this research work.

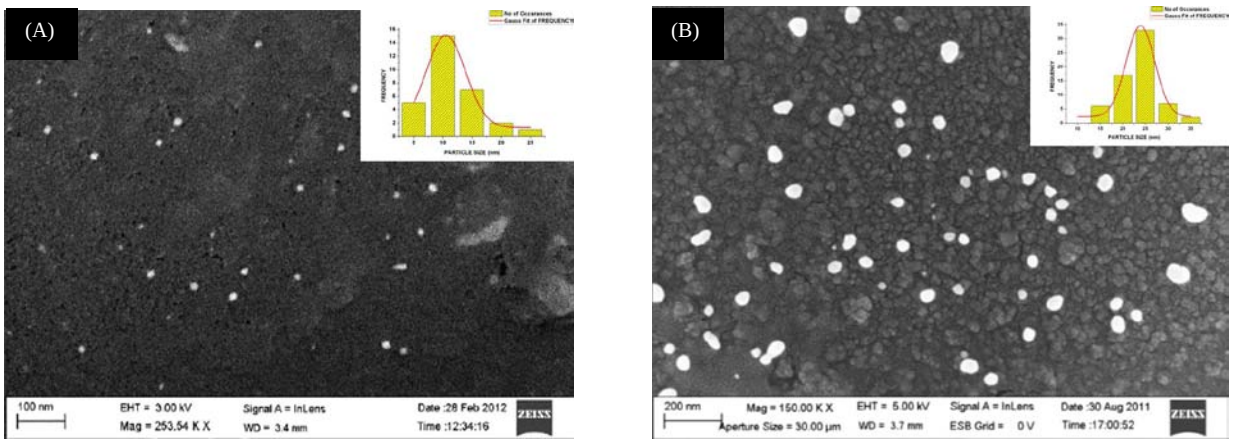

Fig.2.3 FESEM Image of (A)Alumina NP-1 (B) Alumina NP-2 , dispersed in DI Water

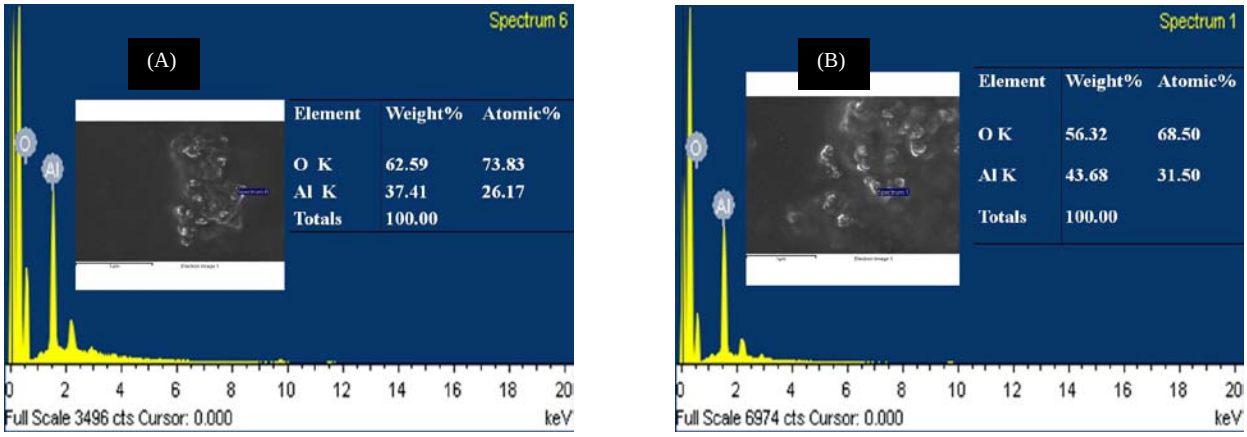

Fig.2.4 EDX spectrum of (A) alumina NP-1 (B) alumina NP-2

2.3 Characterization of MWCNTs

2.3.1 X-ray diffraction analysis of MWCNTs

X-ray powder diffraction pattern of MWCNTs were recorded on Bruker D8 Advance X-ray diffraction. Same parameter as mentioned on 2.2.1. Fig.2.5 shows the XRD spectrum of

MWCNTs. It exhibits a sharp (002) Bragg reflections at about 2θ = 30.135 and it shows the ordered arrangement of concentric cylinders of graphitic carbon (Ref: JCPDS File No: 01-075-1621). From XRD analysis it concludes that the MWCNTs belongs to ***Hexagonal crystal structure*** with the lattice parameter of a = 2.47 Å, b= 2.47 Å, c = 6.79 Å, and angles α = β = 90º and γ = 120º.

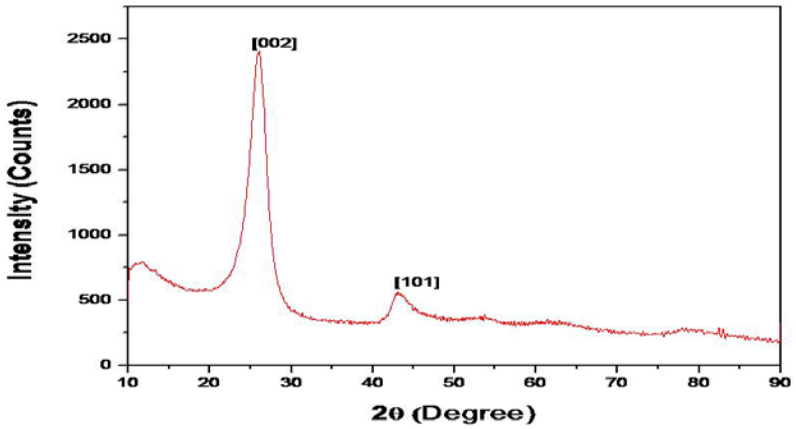

Fig.2.5 XRD pattern of MWCNTs

2.3.2 FESEM and EDX Characterization of MWCNTs

For FESEM analysis, DI water based MWCNT nanofluids was prepared by using 1 volume percentage of MWCNTs with 1:1 ratio of SDS were sonicated for 30 minutes. Then a drop was casted on a pre-cleaned silicon wafer and it was dried by using hotplate at 50^0C for 15minutes for complete evaporation of the liquid. Fig.2.6(A) shows the FESEM image of the multi-walled carbon nanotubes (MWCNTs) and it confirmsthe presence of multi-walled carbon nanotubes having an average diameter of 16.5nm and having length ~10 μm . Fig.2.6(B) shows the compositional analysis of the presence of the elements carbon and silicon which confirms the purity of the samples considered for this research work.

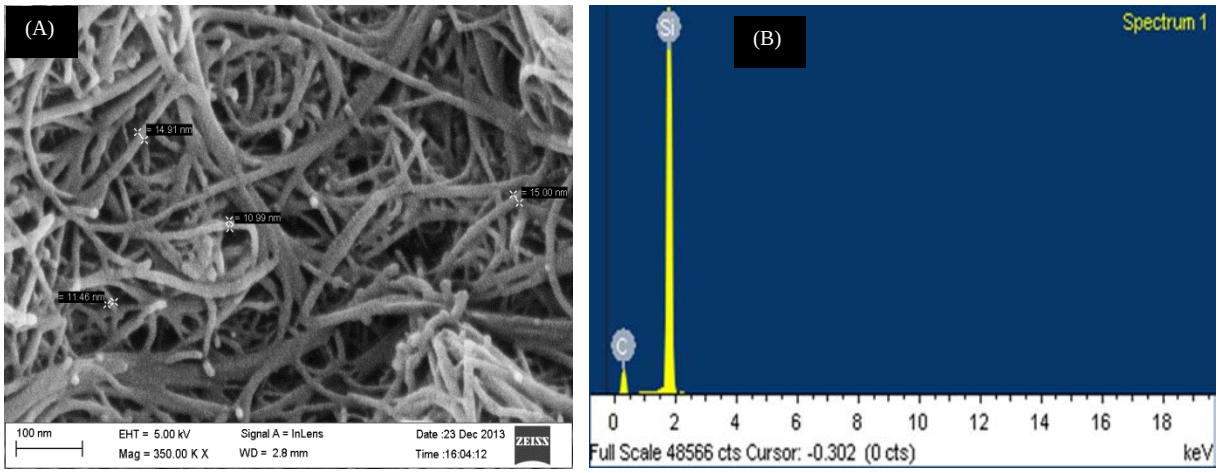

Fig.2.6 (A) FESEM image showing MWCNT's dispersed in DI Water (B) EDX image of carbon nanotubes

2.3.3 TEM analysis of MWCNTs

DI water based MWCNTs nanofluids was prepared by using 1 volume percentage of MWCNTs with 1:1 ratio of SDS and sonicating for 30 minutes. A drop was casted on the carbon coated copper grids and dried at ambient condition. Fig 2.7 shows the TEM images of MWCNTs in colloidal dispersion of the fluid with a small aggregation in varying dimensions. The centre diameter of the MWCNTs and the concentric arrangements of the nanotubes are clearly evident.The outer diameter of the MWCNTs is about 16 nm and the inner diameter is 2.4nm and the individual internal walls of smaller diameter nanotubes are discernable. The number of walls are approximately 3-15 as confirmed from TEM analysis.

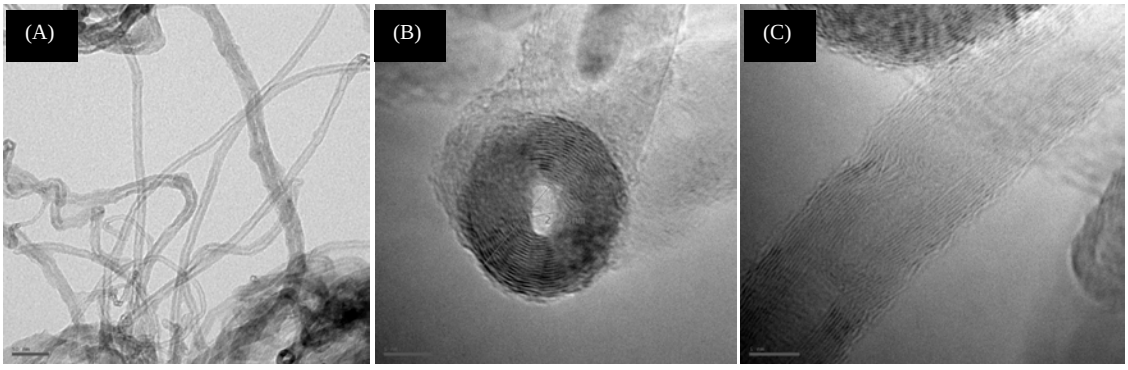

Fig 2.7: TEM Micrograph of DI water based MWCNT NFs with SDS

2.3.4 FI-IR spectroscopy analysis of MWCNTs

Fourier transform infrared spectroscopy (FTIR) was performed for functionalized MWCNTs, to identify the functional groups attached on the surface of the MWCNTs surface after functionalization. Fig shows the FTIR spectra of the functionalized MWCNTs in the range of 500 to 4500 cm^{-1}. It is found from the Fig. That after functionalization of MWCNTs, peaks were found on the side walls at around 1630 cm-1. The peak at 3006 cm^{-1} corresponds to the stretching of C-H bonds. The peak at 2926 and 2848 cm^{-1} is associated with the anti-symmetric and symmetric stretching of CH_2 bonds from n-alkanes groups.

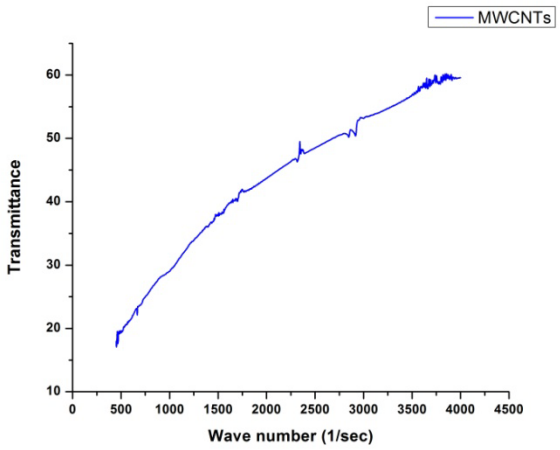

Fig 2.8 FT-IR spectra of MWCNTs

The C=O stretching band observed at 1747 cm^{-1} & 1243 cm^{-1} and CH_2 deformation band observed at1467 cm^{-1}. 1358 cm^{-1} corresponds to symmetric bending of the methyl groups. The Asymmetric and symmetric stretching of C-O-C groups are noted at 1171 and 1193 cm^{-1}, the higher frequency asymmetric stretching is usually the more intense than symmetric band. The peak 1018 and 722 cm^{-1} belongs to C-O-C symmetric stretching and $-(CH_2)_n-$ rock, it will appear when $n \geq 4$.

2.3.5 Raman spectroscopy analysis of MWCNTs

Raman spectroscopy is used to obtain the information about the purity, defects and tube alignment. The presence or absence of G-band and D-band in the corresponding spectra is used to infer electronic and structural information about the MWCNTs. The G-band's frequency and line shape are comparable to those of the E_{2g} phonon of graphite. The presence of a single-shell

vibration is usually expressed by the presence of a low-frequency radial breathing mode (RBM) and in the splitting of the G-band.

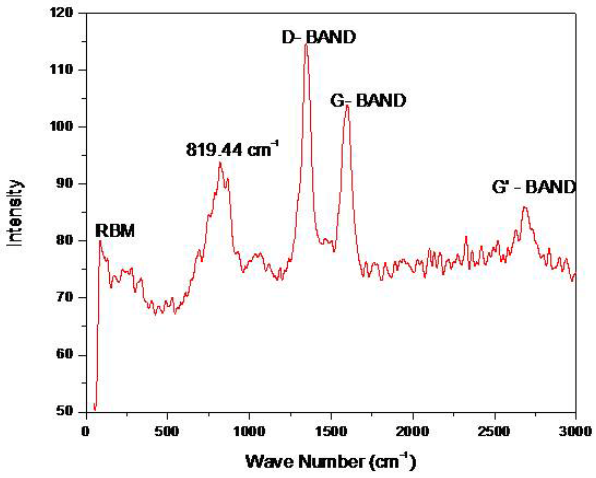

Fig.2.9 Raman Spectra of MWCNTs

Fig 2.9 shows the Raman spectra of MWCNTs having two sharp dominating peaks , G band (Graphite band) and D band (Disorder band). The peak (1345cm^{-1}) of D band corresponds to the amount of amorphous carbon present in the sample while the G band is the tangential shear mode of carbon atoms that corresponds to the stretching mode in the graphite plane present at 1598 cm^{-1}. Radial Breathing Mode (RBM) is confirmation regarding the presence of CNTs in the sample. G' band (2673.17 cm^{-1}) is the intrinsic property of the nanotubes**.**

2.4 Conclusions:

Two different alumina nanoparticles were purchased from Sigma Aldriech, (USA), and their structure, morphology, size and composition were analyzed by using XRD, FESEM, EDX and TEM. It was confirmed that both the alumina nanoparticles were mixture of (δ + θ) phases and were crystalline in nature. Their morphology was spherical in shape having ~13nm and ~28nm sizes. Both the sizes of alumina nanoparticles were having a composition of nearly 37:63 which confirms that the ratio of aluminum to oxygen is nearly stoichometric. That is, no contaminations were present in both the samples.

Multi-Walled carbon nanotubes (MWCNTs) were purchased from Reinste India Pvt.Ltd., India and were analyzed by using XRD, FESEM, TEM, RAMAN and FTIR. It was found that the

purchased MWCNTs were having Hexagonal crystal structure with the lattice parameter of a=2.47Å, b=2.47Å c= 6.79Å and α=β=90 ^{o} and γ=120^{o}. The average length is 5-10μm, and having diameter ~16nm (outer) and 2.5nm (inner). It is also confirmed that 3-15 walls are present in the MWCNTs. These two nanomaterials (~13nm and ~28nm alumina NPs) and MWCNTs are used for synthesis of bio-diesel based nanofluids and described in the next chapter.

Chapter 3

Synthesis of Nanofluids

3.1 Introduction

Dispersions of nanoparticles or nanomaterials (nanorods, CNTs, grapheme) uniformly into the suitable basefluids is termed as the "*Nanofluids*" where the base fluids can be either of the water, alcohols, ethylene glycol, diesel, glycerol, organics, or biodiesel, while the nanoparticles / nanomaterials can be nanoparticles / nanomaterials of any the ceramics or oxide materials, metals, etc. Nanofluids are generally prepared by the one-step or two-step synthesis process. In the two-step process, the dry nanopowder is dispersed in the liquid by using an ultra sonication or mechanical agitator. This method is more economical as compared to one-step method, due to the low cost of nanopowders in the market. There are generally two approaches to synthesis nanomaterials such as top-down and bottom-up approaches as shown in the Fig.3.1. In the top-down approach, the bulk materials are broken down and brought to the micron and submicron scale by means of different physical methods such as hammering, sintering, etc. In bottom-up approach, the nanoparticles are produced by different chemical methods like in-situ techniques

methods, in which, the precursor molecules are built up atom by atom until the atoms assume the form of a nanoparticles.

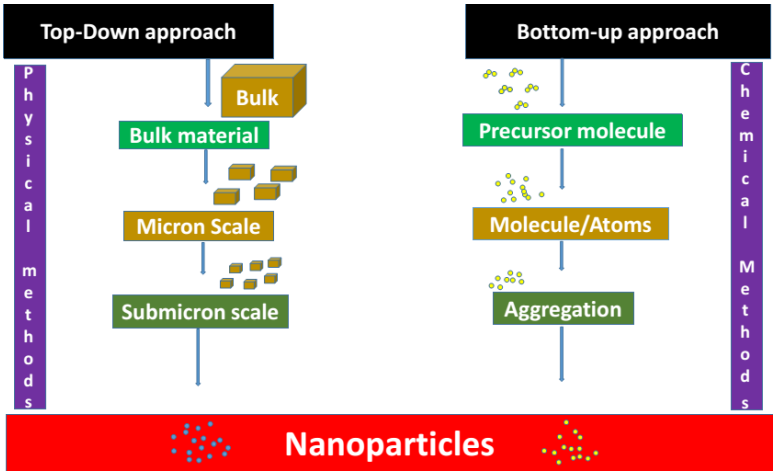

Fig.3.1: Different approaches for synthesis of nanomaterials / nanoparticles

Long term stable suspensions of the nanoparticles / nanomaterials in their basefluids are mostly required to retain the properties of the nanofluids longer durations. Otherwise agglomeration of nanoparticles or nanomaterials can lead to settlement of the micro or even millimeter sizes aggregates and hence the properties of the nanofluids degrade after certain period of storage time. Therefore, stability is very crucial for any of the applications of the nanofluids. It involves various parameters to be taken into consideration. Some of the most important parameters to be considered for the preparation of long term stable nanofluids are nanomaterials sizes, their shape, their phases, their percentage loading, type of the materials, type of the base fluids, type of the surfactants, quantity of the base fluids, etc.

Fig 3.2 shows the different materials and basefluids generally used for synthesis of nanofluids for several applications. In our synthesis process of nanofluids, Jatropha methyl ester (JME) is used as basefluids and alumina nanopartiecles, MWCNTs are used as nanomaterials. However, in this work, Jatropha raw oil was purchased from local dealer and JME was synthesized by using Transesterification process. Since the viscosity of Jatropha raw oil was 52cst, 2-stageTransesteriafication process was adopted to obtain JME having lower viscosity for use in diesel engine.

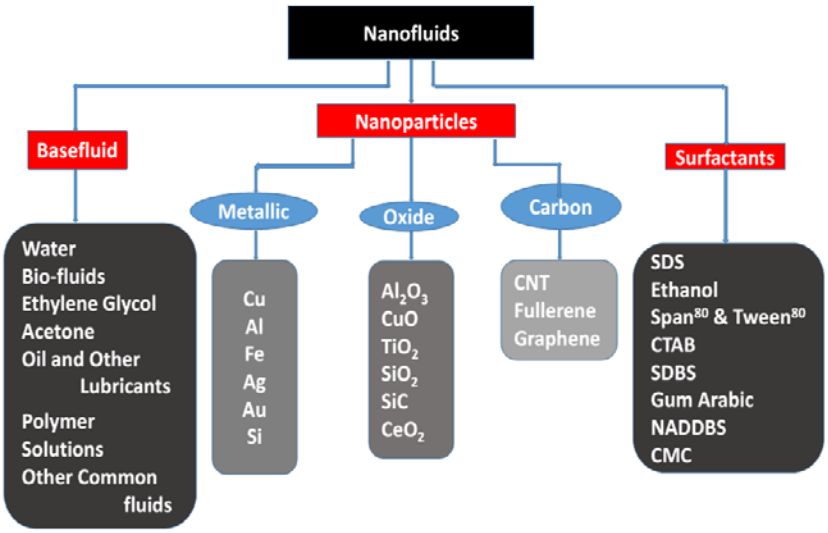

Fig.3.2: Materials and basefluids for preparation of different types of nanofluids

3.2 Preparation of Jatropha Biodiesel from raw oil:

Synthesis of raw jatropha oil was carried out by taking a volume of 500ml for raw oil and then 120 ml of methanol was added and stirred it vigorously for about 20 minutes using a magnetic stirrer. 0.1 ml of Conc. H_2So_4 acid was added to it and again stirred it gently for about 15 minutes. The apparatus was then set for transesterification process by using a refluxing condenser arrangement and allowed it to esterify for about 4h at low supply of electric energy. After heating it for 4 hours, the transesterification set up was removed and the oil mixture was transferred to the separating flask where separation of oil was carried out. Since, now the oil was acidic in nature, it was neutralized by washing it with DI water for nearly three times. This is the first stage of transesterification process. The second stage of transesterification was carried out for the products of first stage transesterified oil by repeating the process as done for the first stage transestrification process using alkaline as a catalyst for about 2h of duration under refluexing condenser. After completing the second stage transesterification, jatropha biodiesel was obtained with glycerin as a by-product which was separated out in separating flask as shown in Fig.3.4. Again the final product (JME) was neutralized by washing it with DI Water for 3 times until the pH of Jatropha biodiesel becomes neutral. Now the viscosity was found to be reduced to 5cst which could be now considered as biodiesel for diesel engines fuel properties. The chemical equation of the transesterification process is shown in Eq. 3.1

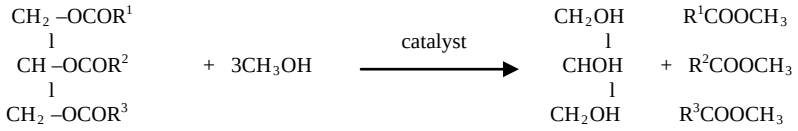

General equation for transesterification of triglycerides.---------3.1

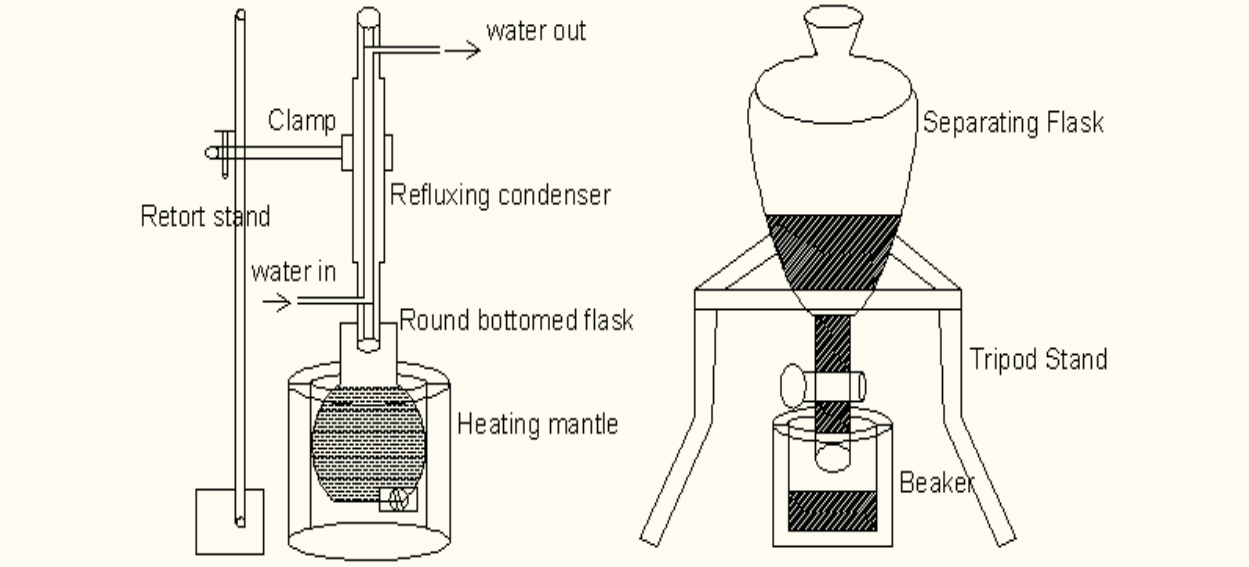

Fig.3.3: Transesterification Process of Jatropha raw oil

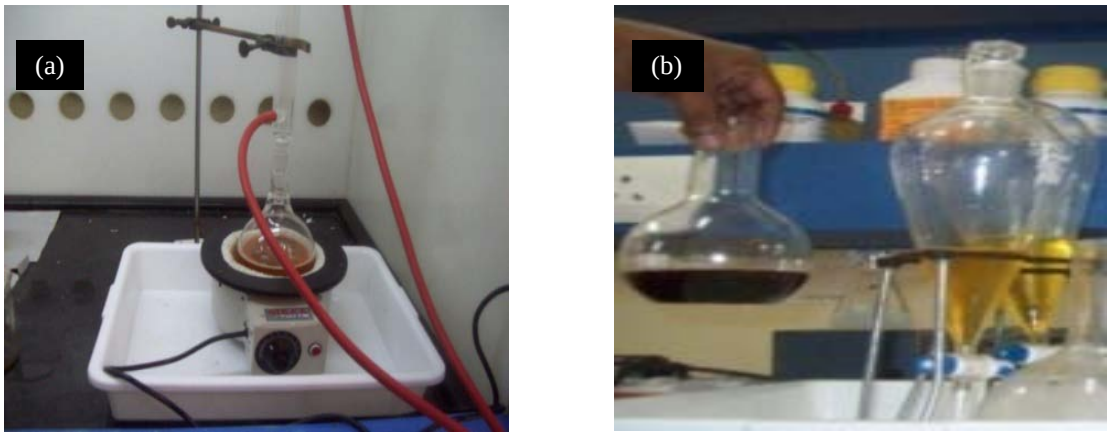

Fig.3.4: Digital images of the synthesis of Jatropha oil (A) Set-up of Transesterification Process (b) separating flask containing Jatropha biodiesel with Glycerene as the by-product.

3.3 Synthesis of Alumina NPs based Nanofluids

Alumina nanoparticles having two sizes (~13nm and ~28nm) were dispersed in synthesized Jatropha biodiesel (basefluid) by using ultrasonication (Model BRANSON 3510). Fig.3.5 shows the flow diagram of the various parameters taken into consideration for preparing nanofluids

(both alumina NPs and MWCNTs). For this Jatropha biodiesel based alumina nanofluids were synthesized by varying the sonication times 15, 30, 45, and finally for 60minutes.

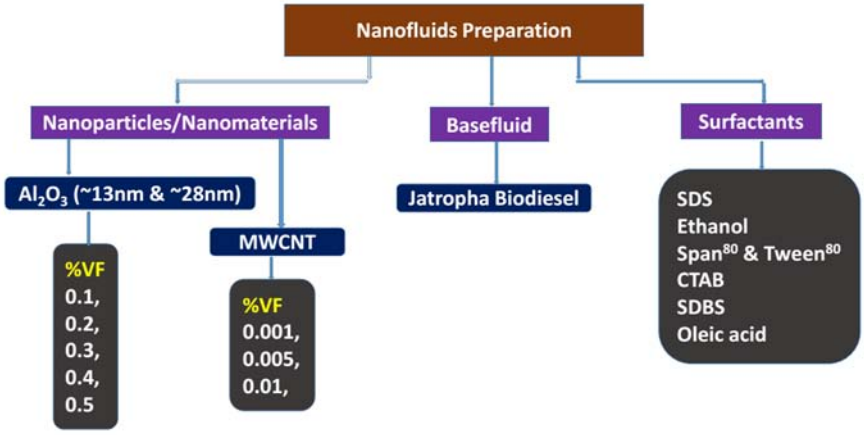

Fig.3.5: Flow chart of various parameters considered for nanofluids preparations.

But it was found that none of the sonication times yielded stable alumina nanofluids and within half-an hour, alumina NPs started to settle down. The procedure was repeated for many times by changing the percentage volume fractions of the alumina nanoparticles into the basefluid(JBD). On finding that different composition of the JBD based alumina nanofluids was not giving considerable results, the same procedure was repeated by adding different surfactants like methanol, ethanol, iso-propyl alcohol, acetone etc. and again kept for observation. Broadly, the investigations of obtaining stable nanofluids were carried out by considering various percentage of volume fractions by addition of different surfactants as listed in Table 3.1, 3.2, 3.3, 3.4 and 3.5.

i. Low Concentrations of Alumina nanoparticles (2.5mg, 5mg, and 10mg) with ultra-sonication time of 30min. and 60min. without using any surfactants. (Biodiesel only).

ii. Low Concentrations of Alumina nanoparticles using different surfactants in theBasefluid (Biodiesel + Surfactants (Ethanol, Acetone, Iso-Propyl alcohol, Carbonol)).

iii. Low Concentrations of Alumina nanoparticles using ethanol as the surfactant(Biodiesel + Ethanol) and varying the ultra-sonication time.

iv. Low Concentrations of Alumina nanoparticles with Diesel as the Base fluid and varying the ultra-sonication time.

v. Low Concentrations of Alumina nanoparticles with Jatropha Biodiesel as the basefluid and using Span^{80} and Tween^{80} as the surfactants.

vi. Hgh Concentrations of Alumina nanoparticles with Jatropha Biodiesel as the basefluid and using Span^{80} and Tween^{80} as the surfactants.

Formula for calculating the percentage Volume Fraction (%VF) is shown below

$$\% \text{ Volume Fraction} = \frac{(V_{Al2O3})*100}{\{(V_{Al2O3}) + Vol._{BD} + Vol._{Surf}\}}$$

$$= \frac{(W_{Al2O3}/\rho_{Al2O3})*100}{\{(W_{Al2O3}/\rho_{Al2O3}) + Vol._{BD} + Vol._{Surf}\}}$$

Where ρ_{Al2O3} = Density of Al_2O_3, gm/cc

ρ_{Al2O3} = 3.6g/cc (Alumina NP of ($\gamma + \delta$) Phase)

$Vol._{Surf}$ = Volume of the surfactant, cc

$Vol._{BD}$ = Volume of the Biodiesel, cc

W_{Al2O3} = Weight of Al_2O_3, mg

Table-3.1: Alumina nanoparticles with Basefluid (Biodiesel + Surfactants (Ethanol, Acetone, Iso-Propyl alcohol, Carbonol))

Sl.No.	Base fluid (JME+ Surfactants) , (ml.)	Al_2O_3 Nano Particles (mg.)	Ultra Sonication Time. (min.)	Remarks
1.	JME-(5) + Ethanol-(2)	2.5	30	Good Dispersion for 48 hours.
2	JME- (5) + Acetone-(2ml)	2.5	30	Good Dispersion, but settled down within 30 minutes.
3	JME-(5) + Iso-PropylAlcohol-(2)	2.5	30	Good Dispersion, but settled down within 30 minutes.
4.	JME-(5) + Carbinol-(2)	2.5	30	Good Dispersion, but settled down within 30 minutes.

Table-3.2: Alumina nanoparticles with Base fluid (Biodiesel + Ethanol)

Sl.No.	Base fluid (JME + Ethanol), (ml.)	Al_2O_3 Nano Particles, (mg)	UltraSonication Time. (min.)	Remarks
1.	(20) + (5)	2.5	30	Good Dispersion for 4 days
2.	(20) + (5)	2.5	45	Good Dispersion for 24 hours.
3.	(20) + (5)	2.5	60	Good Dispersion for 24 hours.
4.	(20) + (5)	5	30	Good Dispersion for 4 days
5.	(20) + (5)	5	45	Good dispersion for 24 hours
6.	(20) + (5)	5	60	Good dispersion for 24 hours

7.	(20) + (5)	10	30	Good dispersion for 45 minutes
8.	(20) + (5)	10	45	Good dispersion for 45 minutes
9.	(20) + (5)	10	60	Good dispersion for 45 minutes
10.	(20) + (1)	5	30	No Dispersion

Table-3.3: Alumina nanoparticles with Base fluid (Diesel only)

Sl.No.	Base fluid (Diesel), (ml.)	Al_2O_3 Nano Particles, (mg)	UltraSonication Time. (min.)	Remarks
1.	(20) + (5)	2.5	15	Good Dispersion for 2days
2.	(20) + (5)	2.5	30	Good Dispersion for 2 hours.
3.	(20) + (5)	5	15	No Dispersion
4.	(20) + (5)	5	30	Good Dispersion for 2 Hours
5.	(20) + (5)	7.5	15	No dispersion
6.	(20) + (5)	7.5	30	No Dispersion
7.	(20) + (5)	10	15	No Dispersion
8.	(20) + (5)	10	30	No Dispersion

Table-3.4: Alumina nanoparticles with Base fluid (Diesel + Ethanol).

Sl.No.	Base Fluid (Diesel + Ethanol), (ml.)	Al_2O_3 Nano Particles, (mg.)	UltraSonication Time, (min.)	Remarks.
1.	(20) + (5)	2.5	30	Good Dispersion for 10 hours.
2.	(20) + (5)	5	30	Good Dispersion for 10 hours.
3.	(20) + (5)	7.5	30	Good Dispersion for 2 hours.
4.	(20) + (5)	10	30	Good Dispersion for 30 minutes.

Table-3.5:Alumina nanoparticles (~13nm) with Basefluid(Jatropha Biodiesel + Span^{80} and Tween^{80} in the 1:1 ratio).

Sl.No.	Base Fluid (JBD + Span^{80} and Tween^{80} (1:1), (ml.)	Al_2O_3 NPs, ~13nm (%VF.)	Ultra Sonication Time, (min.)	Remarks.
1.	(20) + (2.5+2.5)	0.05	30	Good Dispersion for 14 months
2.	(20) + (2.5+2.5)	0.1	30	Good Dispersion for 14 months
3.	(20) + (2.5+2.5)	0.2	30	Good Dispersion for 7 months
4.	(20) + (2.5+2.5)	0.4	30	Sedimentation after 30 min.

Table 3.1–3.5 show the visual observations of various alumina NP based nanofluids by using different approaches. It was found that the use of surfactants span^{80} & Tween^{80} in equal proportion (1:1) showed better stable nanofluids for low percentage of volume fractions. Hence, different higher concentrations such as 0.05%, 0.1%, 0.2%, and 0.4% are considered by using the same procedure for preparing the nanofluids followed by their characterization on regular intervals using different characterization tools such as FESEM, TEM, UV-Vis spectroscopy, which are discussed in more details in chapter4.

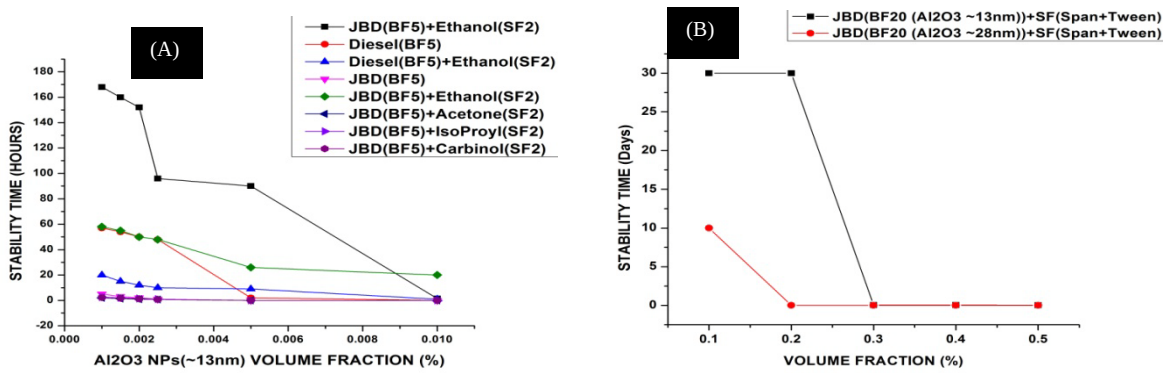

Fig 3.6: Comparision of plots on dispersion stability of Al_2O_3 NPs (~13nm and ~28nm size) by using (A) different surfactants (B) surfactant (Span^{80} and Tween^{80})

From Table 3.5 the optimized parameters for alumina NPs based nanofluids for ~14months are 0.1%VF having ~13nm sizes with 1:1 ratio of span^{80} and tween^{80} as surfactants, while the sample having 0.2%VF of alumina NPs dispersed Jatropha biodiesel based nanofluids has a stability durations of 7 months duration. However, alumina nanofluids having average size ~13nm having 0.4%VF was not stable even for more than an hour. Similar observations were found for alumina NPs having an average size ~28nm also. Therefore, the remaining synthesis of Al_2O_3 NPs dispersed nanofluids are carried out by using Span^{80} and Tween^{80} (1:1) for achieving higher duration stability.

Fig 3.7(a) shows the photographic image of alumina nanofluids (~13nm) for as-prepared samples having different percentage volume fractions that is, 0 .05, 0.1, 0.2 and 0.4%VF along with neat Jatropha biodiesel and neat diesel. From the Fig 3.7(a), it can be easily distinguished between the samples having lesser percentages of volume fractions and samples having higher percentages of volume fractions in terms of intensity of color variations. Fig 3.7(b) shows the photographic image of ~13nm size alumina nanofluids having 0.1%VF for different storage time such as 1Year, 6months, 7months and 2years old samples. It is clear from the Fig.3.7(b) that though the intensity of color is less as compared to the samples of Fig 3.7(a), still considerable percentage of alumina nanoparticles are dispersed even after 1 year of duration. Therefore, 0.1%VF ~13nm Al_2O_3 NPs dispersed in biodiesel is showing better stable nanofluids as compared to higher volume fractions samples.

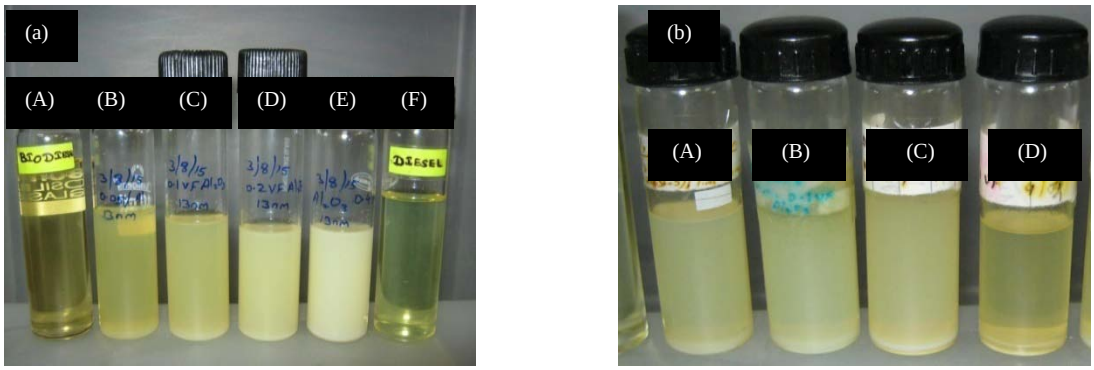

Fig3.7 Photographic images of alumina NFs (~13nm) : (a) as-prepared samples (B) 0 .05, (C) 0.1, (D) 0.2 and (E) 0.4%VF along with neat JBD (A) and neat Diesel (F) (b) stored samples of 0.1VF for (A)1Year, (B) 6Mon (C) 7Mon and (D) 2Years respectively.

Similarly, Fig 3.8((a) and (b)) show the alumina nanofluids of average size ~28nm size having different percentage volume fractions for as-prepared samples stored samples respectively. Here also, distinctions can seen from the color variations regarding the samples having varying percentage volume fractions of alumina nanoparticles ~28nm size. Comparing the Figs 3.8((a) and (b)), it can be clearly distinguished that all the samples of alumina nanoparticles of average size ~28nm were agglomerated at the bottom of the sample tubes (as seen from Fig 3.8(b)) and hence, they are considered as unstable nanofluids. Therefore, from the visual inspections, it is concluded that ~13nm Al2O3 NPs having 0.1VF is more stable upto 1year, however longer size ~28nm alumina NPs dispersed nanofluids are not showing stability of more than two weeks. Also higher volume fractions is not favorable for longer duration stable nanofluids. More details on stability analysis by UV-Vis spectroscopy and TEM are described in next chapter.

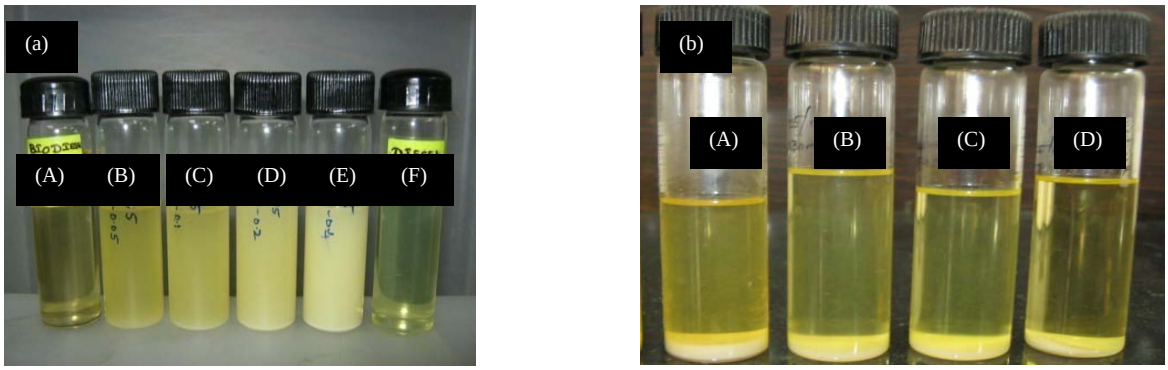

Fig3.8 Photographic images of alumina NFs (~28nm) : (a) as-prepared samples (B) 0 .05, (C) 0.1, (D) 0.2 and (E) 0.4%VF along with neat JBD (A) and neat Diesel (F) (b) stored samples of 0.1%VF for (A) 1, (B) 2 (C) 6 and (D) 7Months respectively.

3.4 Synthesis of MWCNTs based Nanofluids

There are generally two approaches to dispersed MWCNTs in basefluis. One is known as Co-valent approach and the second one is non-covalent approach [ ]. Firstly the non-covalent was carried out by dispersing the MWCNT in the Jatropha biodiesel (basefluids) using the different surfactants such as SDS, PVP, CTAB, Span^{80} and Tween^{80} for different volume fractions. However, the But the resultant nanofluids in such process were not stable even for a day due to their poor suspension stability as shown in Fig.3.9 (B, C, D, E).

Table: 3.6 MWCNTs dispersions in biodiesel by using different surfactants (non-covalent approach)

Basefluids	SDS	PVP	EG	Span^{80} and Tween^{80}	CTAB
Jatropha methyl ester (JBD)	MWCNTs were agglomerated and got settled within 1hour	MWCNTs were not stable for more than 2 hours	MWCNTs settled down within 30minutes	MWCNTs settled down within few hours	MWCNTs were stable for 30min. and agglomerated within 2days

Table 3.6 summaries the stability of MWCNTs based nanofluids synthesized by using non-covalent approach. Since none of the nanofluids are stable, the second approach, i.e., the covalent approach was adopted. In this method, surface modification are generally carried out by treating the MWCNTs in acids (i.e., sodium oleate, H_2SO_4 and HNO_3).

3.4.1 *Convalent approach by using mixture of H_2SO_4 and HNO_3 acids:*

In this approach, 100mg of MWCNTs were taken and 50mL HNO_3 was added to it. The sample was refluxed for 4 hours at 100°C. Furthermore, the sample was given multiple washings via centrifugation at 5000 rpm for 15mints and dried over night at 80°C. In the next step, 1:1ratio ofHNO_3 and H_2SO_4 (30mL each) was slowly added to the above dried sample, and it was refluxed for 2 hours at 30 to 40°C. In order to give the sample multiple washings, centrifugation was done at 5000rpm for 15min. The functionalized sample was dried overnight in an oven at 120°C. Then functionalized MWCNTs were dispersed in the biodiesel by using the ultra sonicatorfor 30minutes (30kHz). and it was shown in Fig 3.9(F). It was observed from Fig 3.9(F) that nanofluids are not stable and settled down within24 hours.

3.4.2 *Covalent approach by using Sodium Oleate (SOA)*:

In this approach, 100mg of MWCNTs were refluxed (60 to 80^{o} C) with 25mL of H_2O_2 for 5 hours. Then the resulting product was water washed and prepared sodium oleate solution [1:1 ratio of NaOH and oleic acid was dissolved in 50mL of ethanol. This reaction mixture was stirred for 5 to 15 hours at room temperature (50wt% or 25mL)] was added. And the mixture was heated (80 to 95^{o}C) with vigorous stirring (1500rpm) for 2 hours and also for 4hours. After the reaction, the resultant was neutralized by adding 1N HCl and then filtrated. The final product was washed with DI water and ethanol several time till pH =7. Finally, it was dried at 120^{0}C for 24hours on a hotplate. Then resultant functionalized MWCNTs were sonicated with biodiesel for stability analysis. It is observed that this process of preparation of nanofluids was stable upto few days as shown in Fig 3.9(G and (H).

3.4.3 Covalent approach by using oleic acid

In this approach, 200µL of oleic acid was added in 20mL of biodiesel in a 40mL beaker and then sonicated for 30minutes (30kHz). Then, 4mg of MWCNTs was added to the solutions and again it was sonicated (at 30kHz) for 30minutes. The prepared nanofluid was kept in a glass tubes idle without any disturbance to analysis the stability. It was preliminary observed that oleic acid treated nanofluids was showing better stability even after 24 hours of preparation as compared to the other methods of preparation as shown in Fig.3.12(I).

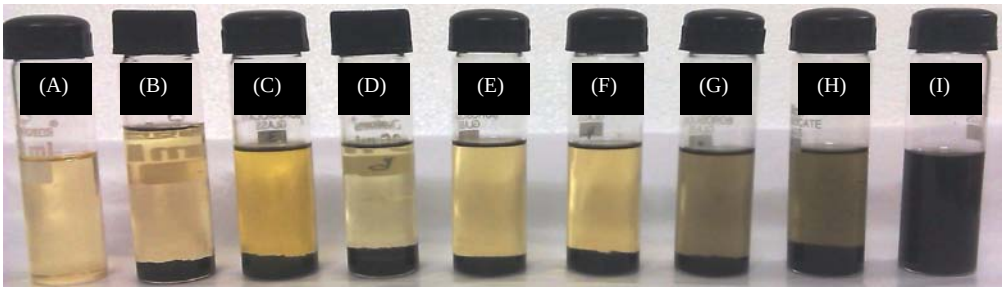

Fig3.9 Photographic image of MWCNTs dispersed nanofluids having 0.001%VF after 24 hours with different surfactants or acids treatment (A) Pure biodiesel (B) Span^{80} and Tween^{80} (C) CTAB (D) SDS (E) PVP surfactants and Functionalized with (F) conc. acids (G) SOA with 2H (H) SOA with 4H (I) Oleic acid

Since, only oleic acid treated MWCNTs in biodiesel based nanofluids was showing better stability as compared to the other methods of preparation of biodiesel nanofluids, only this method was further considered for the more details dispersion stability analysis by preparing

different volume percentages (0.001%, 0.005%, and 0.01%) with different ultrasonication time (i.e.1, 2 and 4 hours) for two different concentrations of oleic acid (200µL and 400µL.

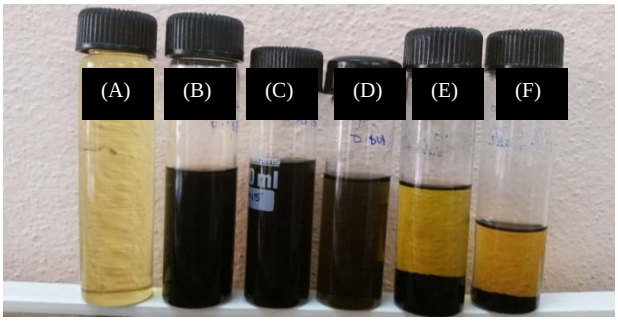

Fig 3.10Photographic image of as-prepared samples of MWCNTs dispersed nanofluids (as-prepared samples with (B)0.001, (C)0.005, (D)0.01, (E)0.0.02, (F)0.1%VF) with (A) neat biodiesel.

Fig.3.10 shows the photographic image of MWCNTs dispersed nanofluids having different percentage volume fractions such as 0.001%VF, 0.005%VF, 0.01%VF, 0.02%VF and 0.1%VF respectively. From the Fig.3.10 it is confirmed that MWCNTs were dispersed without any agglomerations for the samples of 0.001%VF, 0.005%VF and 0.01%VF, while higher percentage volume fractions of MWCNTs were not having good dispersions even for as-prepared samples. It is concluded from the sedimentation method that only 0.001%VF and 0.005%VF are showing stability upto 10days while other percentage volume fractions are not showing stability even for 10days. Therefore, all the MWCNTs are synthesized only by considering these two volume fractions for further studies.

3.5 Conclusions

Bio-diesel based nanofluids were synthesized by dispersing different nanomaterials (Alumina and MWCNTs) in the Jatropha biodiesel (JME). Two different nanomaterials such as Al_2O_3 (average sizes of ~13nm and ~28nm) and MWCNTs are considered for this work

Different sets of alumina (~13nm and ~28nm sizes) and MWCNTs dispersed nanofluids were prepared by using different approaches such as using the surfactants and applying different functionalization methods. Out of all the approaches, Span^{80} and Tween^{80} surfactants based alumina nanoparticles based nanofluids showed higher stablility which was observed by sedimentation method. Also, different percentage volume fractions such as 0.05, 0.1, 0.2, and 0.4

nanofluids were synthesized by using span^{80} and Tween^{80} surfactants in equal proportions (1:1) for both ~13nm and ~28nm sizes alumina nanoparticles dispersed nanofluids. It was confirmed that ~13nm size alumina nanoparticles dispersed 0.1vf nanofluids are showing better stability as compared to ~28nm size alumina nanoparticles dispersed nanofluids. Hence, in the subsequent chapter, more detailed study was carried out regarding the long term stability of alumina nanoparticles dispersed nanofluids by using different analysis. For preparation of MWCNTs suspended in biodiesel based nanofluids, two approaches such as non-covalent (SDS, PVP, CTAB, Span^{80} and Tween^{80}) and covalent approach (Oleic Acid, H_2SO_4 and HNO_3) were carried out for different volume percentage and sonication time. Out of all the surfactants and surface modification process, Oleic acid showed better dispersions of MWCNTs in bio-diesel. Hence, we investigate the properties of such nanofluid to compare with alumina based nanofluids. Though more research work is still required to adopt several new novel methods to achieve longer term stable MWCNTs dispersed in bio-diesel nanofluids, our MWCNTs based bio-diesel nanofluids were stable upto 10days which is not reported before.

Chapter 4

Nanomaterial and Their Size Effect on the Stability of Nanofluids

4.1 INTRODUCTION

It is very well known fact that the nanoparticles or nanomaterials dispersed in the basefluids settles down rapidly and then nanofluids do not retain any more the properties as required for the applications. Such drawbacks are needed to address before using such nanofluids for several potential applications. It is also known that the stability of the nanofluids strongly depends on the nature of base liquid, nature of surfactant, type of nanoparticles, and the mode of aggregation of nanoparticles. An agglomerated nanofluid when used as a fuel in diesel engine may cause operational problems similar to those encountered with micro-sized particulate suspensions due to the sedimentation and clogging of the nanoparticles / nanomaterials in the engine. Hence, it is very much essential to address the issue of agglomerations of nanomaterials in their basefluids so that the nanofluids retain their properties for longer durations. In this regard, many of the researchers had investigated on the issues of stability of nanofluids in different basefluids by different approaches such as addition of different surfactants, surface modification techniques, etc.

Therefore, this chapter presents the study of stability of the Al_2O_3 NPs (both sizes, ~13nm and ~28nm) and MWCNTs based bio-diesel bnanofluids (as already discussed in chapter-3) in more detail by using UV-Spectroscopy for analytical analysis and by using TEM for morphological analysis by considering different factors such as volume fractions, nanoparticles sizes and the types of the nanomaterials.

4.2 Alumina NP Size and Conc. Effect on Stability of nanofluids:

The stability analysis of the alumina nanofluids with different storage time were performed by using TEM, and UV-Vis spectroscopy. It was discussed in the chapter-3 that the dispersion of stability of ~13nm size alumina nanofluids and ~28 nm size alumina nanofluids are different. It is also confirmed that the ~28nm alumina nanoparticles based nanofluids were not stable even for few days which may be due to the settlement of the aggregates nanoparticles as result of gravity whereas, the ~13nm size alumina nanoparticles based nanofluids were stable even for more than one year for the 0.1% volume fraction. However, for all the other volume fractions ~13nm size alumina nanofluids are not showing better stability and were seen to be settled down in few weeks. Further, the stability of all the 0.1 volume fractions ~13nm sizes alumina nanofluids were carried out by using the Transmission Electron microscopy (TEM) for the agglomeration and morphology analysis of the nanoparticles in the biodiesel with storage time and UV-Vis spectroscopy to observe the stability from the absorbance peak ratio of as-prepared and older sample with storage time. All the as-prepared nanofluids were kept idel in a stand without disturbing them and periodically analyzed by using both TEM and UV-vis spectroscopy for the dispersion stability.

4.2.1 TEM analysis:

First of all, one droplet of as-prepared and 1 year old alumina nanofluids (~13nm having 0.1%vf) were casted on the carbon coated Cu- grids and then heated on a hot plate for 10 minutes to evaporate the biodiesel and for TEM analysis. Fig 4.1((A) and (B)) show the TEM images of the alumina NPs dispersed in 0.1%VF (~13nm) nanofluids and Fig 4.1(B) shows the alumina NPs morphology of 0.2%VF(~13nm) based nanofluids. Fig 4.1(C) shows the TEM image of the alumina NPs dispersed in 0.1%VF (~28nm) nanofluids. It is concluded that the alumina NPs are dispersed uniformly in 0.1%VF (~13nm) nanofluids as compared to 0.2%VF(~13nm) nanofluids.

Also agglomeration of alumina NPs having clusters are noticed as shown in Fig 4.1(B). In the case of morphology of alumina NPs in 0.1%VF (~28nm) nanofluids, it is agglomerated having very larger size as shown in Fig 4.1(C). Therefore, larger aggregates are settled down very rapidly in the case of ~28nm alumina NPs dispersed nanofluids and hence, are showing stability of not more than one day.

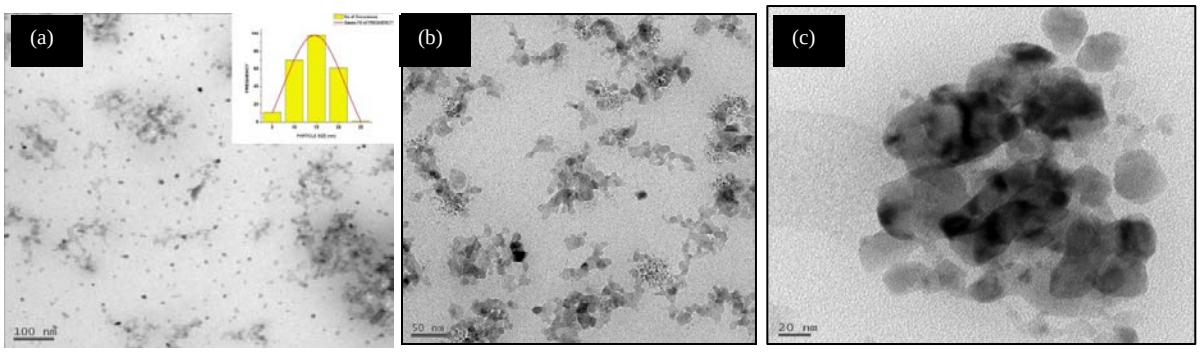

Fig.4.1: TEM image of Al_2O_3NP As-Prepared (a) ~13nm size 0.1%VF (b) ~13nm size 0.2%VF (c) ~28nm size 0.1VF

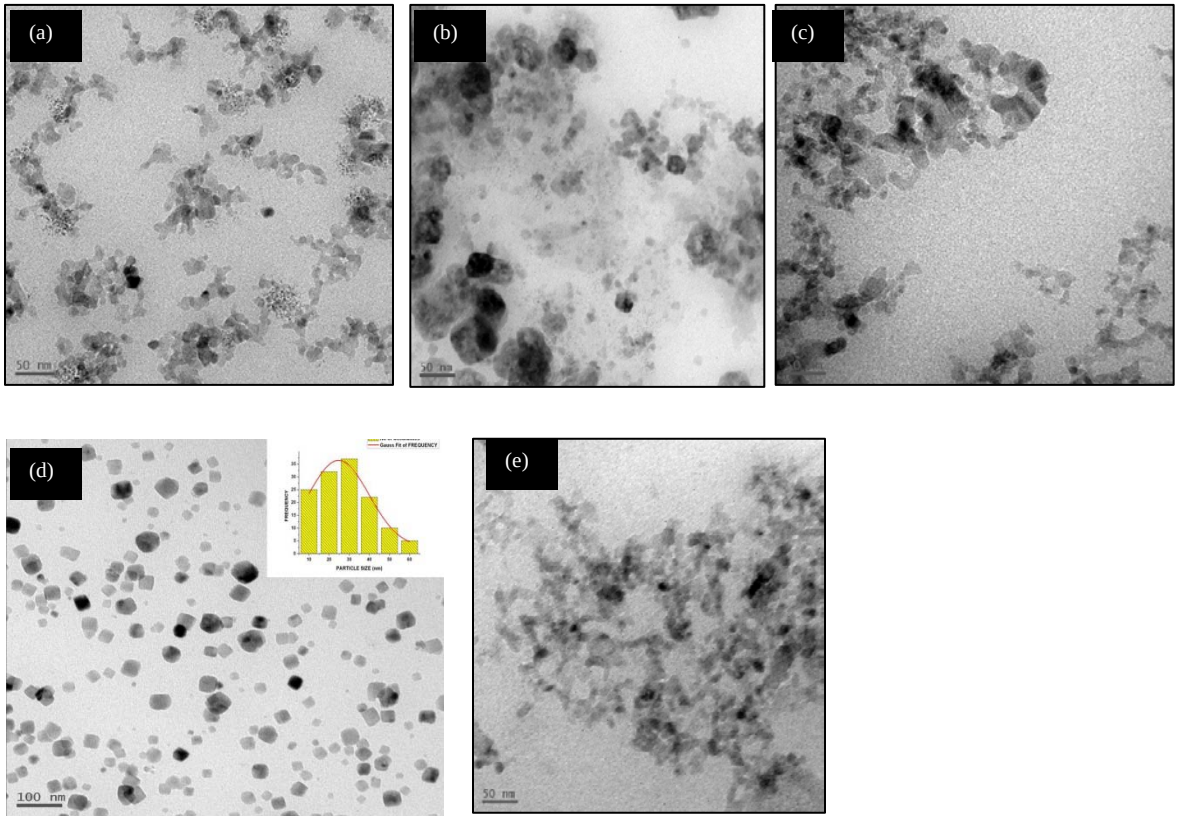

Fig.4.2 TEM image of Al_2O_3NP ~13nm 0.1%VF (a)2Week old (b)1Month old (c) 2Month old (d) 1year old (e) 0.2VF 1year old samples

Fig 4.2 ((A)-(D)) show the TEM images of alumina NPs dispersed in 0.1%(~13nm) nanofluids for 2weeks, 1month, 2months and 1Year older samples respectively. As seen in the TEM micrographs, initially alumina nanoparticles start to agglomerate and form aggregated after 2weeks storage time and keeps on increasing the aggregate sizes after 1month and 2months. However, after 1year storage time, alumina nanoparticles are dispersed uniformly in the nanofluids (as shown in the Fig 4.2(D). However, the alumina nanoparticles those are initially ~13nm in sizes and shperical in morphology change drastically to ~30-40nm in sizes and morphology change to cubical in shape. Since, ~30-40nm sizes alumina nanoparticles are still in nanomaters scale, they are dispersed very uniformly in the nanofluids (Fig 4.2 (D)). Therefore, 0.1%VF (~13nm) alumina NPs nanofluids is still showing stability after one year of storage time. Fig 4.2(e) shows the TEM image of alumina NPs dispersed in 0.2%VF)~13nm) nanofluids. In this case, it is seen that alumina NPs are agglomerated and form a network nanostructure in larger scale after one year of storage time.

Therefore, 0.2%VF (~13nm) alumina nanofluids are not stable upto one year of storage time. The analytical analysis was also carried out by using UV-Vis spectroscopy and is discussed in next sction.

4.2.2 UV-vis Spectral Analysis:

It is a very reliable method to evaluate the stability of nanofluids since there is a linear relationship between the suspended nanoparticles and absorbance of the suspended nanoparticles. All the prepared alumina nanofluids were periodically analyzed by UV-Vis Spectroscopy analysis by using the standard sizes of cuvette (path length of cuvette is 10). Initially, the baseline was fixed considering the Jatropha Biodiesel as the reference sample as well as the specimen sample. After fixing the baseline, Jatropha Biodiesel was taken as the reference sample and the alumina nanofluids was considered as the specimen sample and the data were obtained for the different stability time of alumina nanofluids.

Fig.4.3 shows the UV-Vis spectra of the 0.1%VF of both ~13nm and ~28nm alumina nanofluids along with 0.2%VF of ~13nm alumina nanofluids. On comparing, it is clear from the Fig 4.3(A) that the absorption peak of ~13nm size Al_2O_3 NPs dispersed nanofluids having 0.1%VF is

slightly lower than that of 0.2%VF. This is due to the higher percentage volume fraction of alumina NPs present in the 0.2%VF sample. It is also seen from Fig 4.3(A) that alumina NPs having ~28nm sizes nanofluids has the highest absorption peak than the other two samples, which indicates that the absorption of alumina NPs increases as the size of the nanoparticles increases which is also reported earlier in the case of alumina in DI water based nanofluids [ ].

Fig.4.4(A) shows the UV-Vis spectra of alumina NP-13nm nanofluids having 0.1%VF with various storage time starting from as-prepared samples to 14months old samples. It is seen from Fig 4.4(A) that as-prepared saples has the highest absorption and the percent of absorption peak decreases upto 5 months then for the sample having storage time more than 6months, the absorption peak increases with reduction in its area. This is due to the reason that since, all the alumina nanoparticles may not be of the same sizes. Hence one settlement of the bigger nanoparticles or initial aggregates sizes of the alumina NPs increases and hence, higher absorption peak is seen. Also due to the settling down of larger size alumina nanoparticles, there would be reduction in the percentage of alumina nanoparticles and hence, absorption peak decreases as the percentage of nanoparticles reduced. But, during this period, there would be increase in the size of the alumina nanoparticles which were still in the suspensions state, due to which, absorption peak increases as the sedimentation time increases.

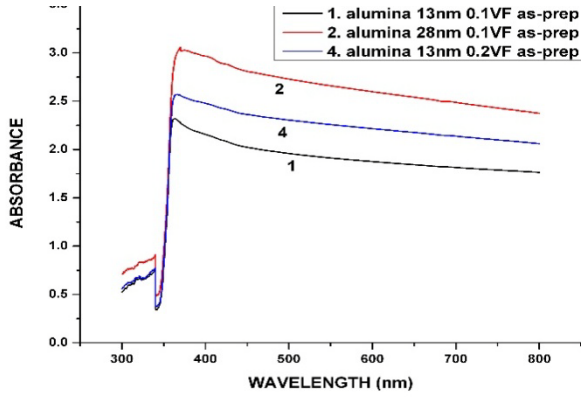

Fig.4.3(A) UV-Vis spectroscopy plots of Al_2O_3 NPs (~13nm and ~28nm) for 0.1 and 0.2%VF.

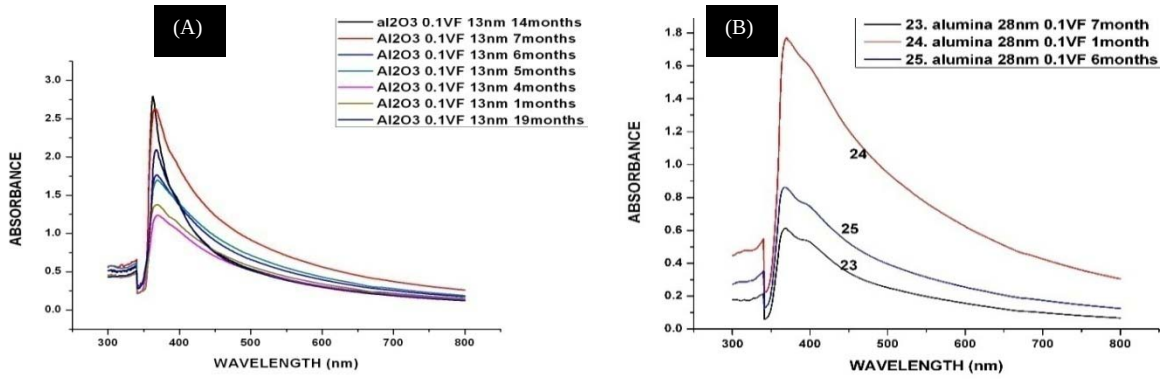

Fig.4.4 UV-Vis spectroscopy of Al_2O_3 nanofluids with different storage times (A) ~13nm (B) ~28nm sizes.

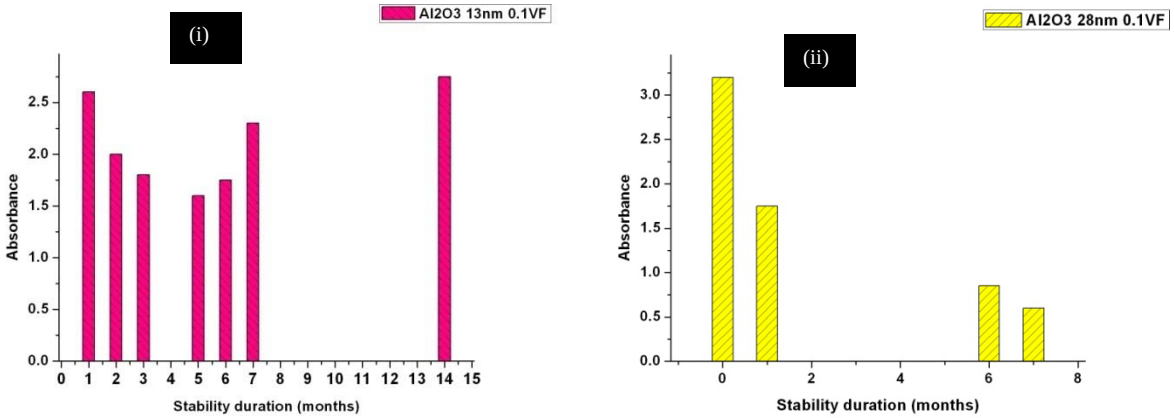

Fig 4.4(C) Absorbance vs stability durations for alumina nanofluids (i) ~13nm (ii) ~28nm

Fig 4.4(B) shows the UV-Vis spectra of alumina nanoparticles dispersed nanofluids of ~28nm size having a percentage volume fraction of 0.1% for different sedimentation times. It is seen from the Fig 4.4(B) that the peaks of stored samples decreases when compared with that of the subsequent samples respectively which is an indication that as the storage time of the nanoparticles increases, the considerable quantity of percentage of nanoparticles gets agglomerated at the bottom of the stored bottle. But the rate of settling down of alumina nanoparticles having average size ~28nm is quite higher than that of alumina nanoparticles having average size of ~13nm. Therefore, the absorption peak drastically decreases as the storage time increases. Hence, from UV-Vis analysis, it is concluded that 0.1%VF (~13nm) alumina nanofluids are showing higher stability in longer storage time as compared to other volume fractions and also as compared to ~28nm alumina NPs dispersed nanofluids.

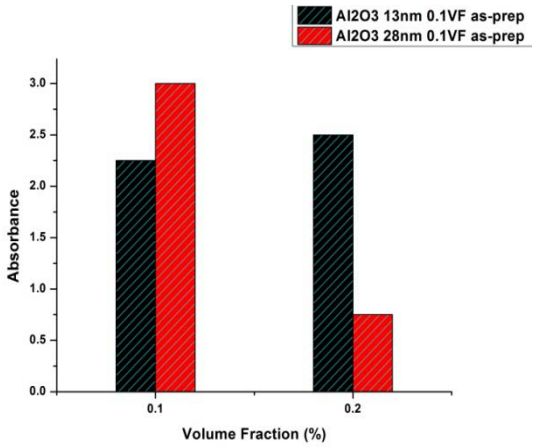

Fig 4.5 Effect of alumina NPs sizes on the absorption peak of 0.1%VF and 0.2%VF alumina nanofluids.

Fig 4.5 shows the plots of absorbance versus percentage volume fractions (%VF) of alumina nanoparticles having two different sizes that is, ~13nm and ~28nm sizes respectively. It is seen from the Fig 4.5 that for a volume fraction of 0.1%, alumina nanoparticles dispersed nanofluids of average size ~28nm has higher absorbance than that of alumina nanoparticles dispersed nanofluids having an average size of ~13nm for both being as-prepared samples respectively. But in the case of 0.2%VF alumina nanofluids of ~13nm size has higher absorbance than that of alumina nanofluids having an average size of ~28nm. This is due to the fact that alumina nanoparticles of average size ~28nm are poorly dispersed in the basefluid, as compared to that of alumina nanoparticles of average size ~13nm of same percentage volume fractions. Therefore, not only ~28nm sizes 0.1%VF is not stable, higher volume fractions are stable for ~28nm alumina nanofluids.also not stable

Fig 4.6 shows the UV-Vis spectra of the ~13nm alumina nanofluids for two volume fractions (0.1%VF and 0.2%VF) for two different storage time. From 4.6, it is confirmed that upon certain duration of time, the peak value of absorbance decreases as the storage time increases but after reaching the threshold time, the peak value of absorbance increases along with the increase in the storage time. This may be due to the reason that once the threshold duration of storage time is reached, there would be a change in the size and morphology of the alumina nanopaticles, that is alumina nanoparticles would increase in size and also the morphology of the alumina nanopaticles changed to cubical shape as seen in the TEM images of Fig 4.3(D). Fig 4.6(B) shows the plot of absorption of alumina nanoparticles of ~13nm size having 0.1%VF and

0.2%VF for different storage time duration ranging from as-prepared samples to a maximum period of 18 months durations. Comparing these two different percentage volume fractions of alumina nanoparticles, it is clear that in both the cases, the amount of absorption value decreases upto a threshold time limit of 6 to 7 months after which there would be increase in the absorption values as the storage time increases.

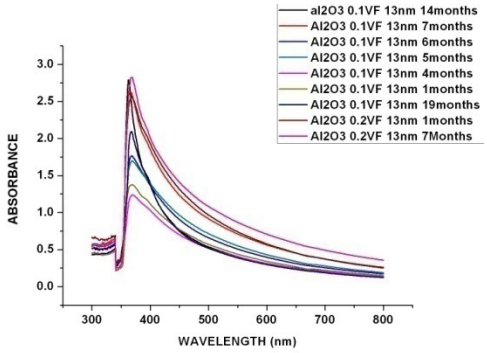

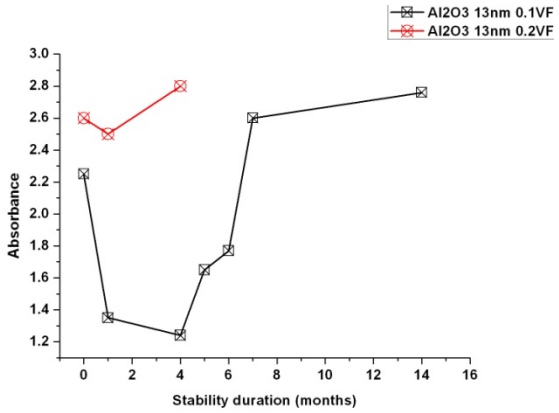

Fig.4.6(A): UV-Vis Spectroscopy of aluminaNPs(~13nm) having 0.1 and 0.2 %VF at different storage time

Fig.4.6(B): Effect of %VF on aluminaNPs (~13nm) having 0.1 and 0.2%VF at different storage time.

4.3 MWCNTs Effect on Stability of nanofluids

Multi walled carbon nanotubes (MWCNTs) were purchased from Reinste Pvt. Ltd. The CNT nanofluids were prepared in different volume percentage starting from 0.005, 0.001, 0.01 and 0.1 by two step process. In all the nanofluids preparation process, the volume of methyl esters biodiesel was kept constant (20mL) to investigate the effect of MWCNTs concentrations on the stability. For each sample, the sonication was done starting initially for 30 minutes and then the prepared samples were kept idle in a glass tube without causing any disturbance to investigate on the dispersion stability. It was found that the MWCNTs were settling down within 5 to 10 minutes and few times MWCNTs were not being fully dispersed with the biodiesel during the ultrasonication process itself. To attain the stability of the nanofluids two different approaches are followed to modify the surface of the MWCNTs: 1) non-covalent approach, 2) covalent approach. The surface modification technique with treating in Oleic acid improved the stability of the MWCNTs dispersions in the Jatropha biodiesel (as discussed in chapter-3).

4.3.1 TEM analysis

Fig. 4.7 shows the TEM images of the oleic acid treated MWCNT in nanofluids as-prepared and 14 days older sample respectively. It was seen from Fig. 4.7 that, there is not much change in the morphology of both the samples i.e. as prepared and the older sample but small aggregations are observed in case of the 14days older sample. However, surface modification or defects are still present in both the samples i.e. MWCNT walls. It is concluded that oleic acid can be used as the agent for the surface modifications of the MWCNT and to achieve the long term stability of the biodiesel based nanolfuids. Similar effect was also observed for different quantity of Oleic acid for the same percentage volume fractions of 0.01 MWCNTs as seen in Fig 4.8.

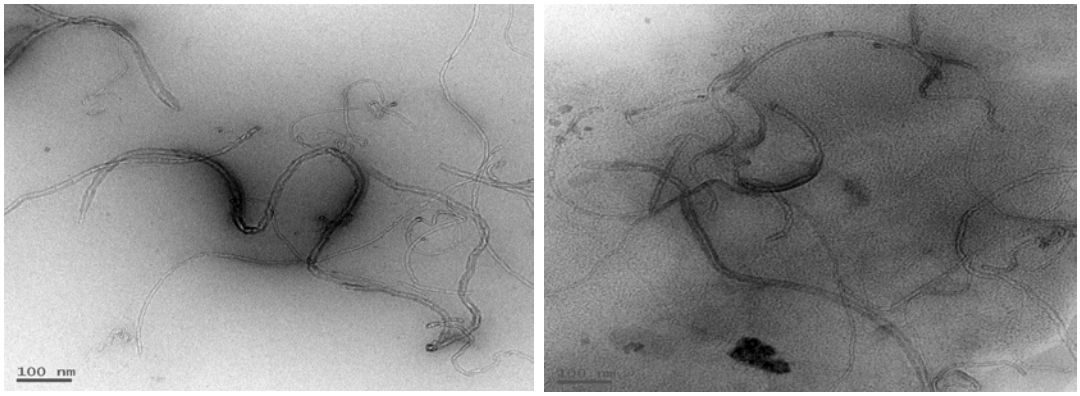

Fig.4.7 TEM micrographs of MWCNT-NFs (0.001%VF) with Oleic acid (a) As Prepared (b) 14Days Old Nanofluids

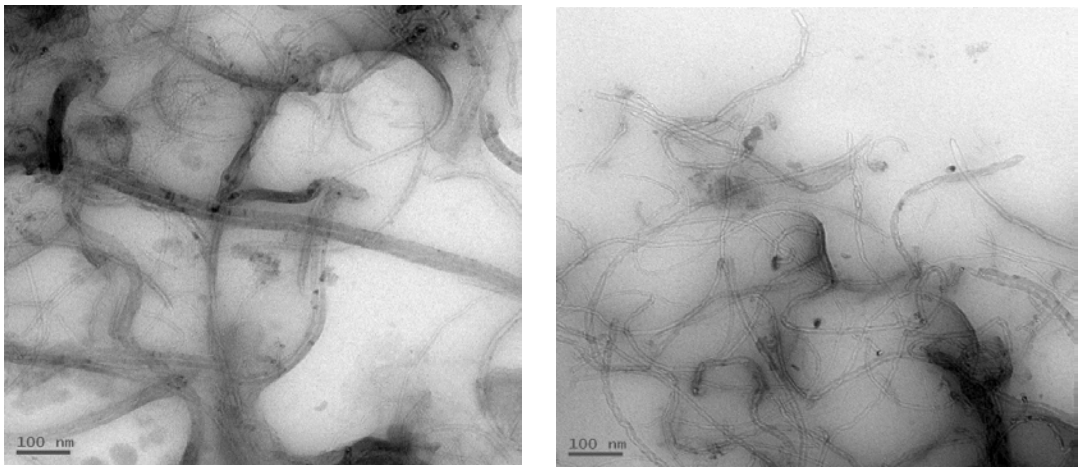

Fig.4.8 TEM micrographs of 28days old, (2hours sonicated 0.001% V.F) with (a) 200 µl OA and (b) 400 µl OA nanofluids

4.3.2 FT-IR spectroscopy analysis

Fig 4.9 shows the FT-IR spectrum of MWCNTs dispersed nanofluids using surface modification technique of Oleic acid for different sedimentation time. The peak at 3006 cm^{-1} was assigned to the stretching of C-H bonds. The peak at 2926 and 2848 cm^{-1} is associated with the anti-symmetric and symmetric stretching of CH_2 bonds from n-alkanes groups. The C=O stretching band observed at 1747 cm^{-1}& 1243 cm^{-1} and CH_2 deformation band observed at1467 cm^{-1}. 1358 cm^{-1} corresponds to symmetric bending of the methyl groups. The asymmetric and symmetric stretching of C-O-C groups are noted at 1171 and 1193 cm^{-1}, the higher frequency asymmetric stretching is usually the more intense than symmetric band. The peak 1018 and 722 cm^{-1} belongs to C-O-C symmetric stretching and -$(CH_2)_n$- rock, it will appear when $n \geq 4$

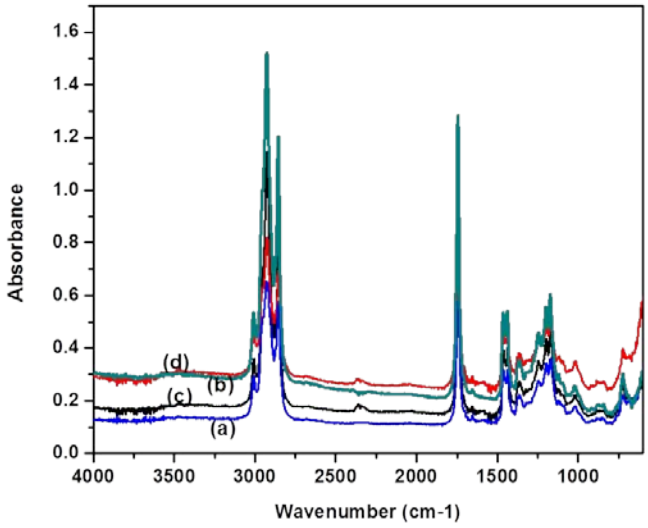

Fig 4.9. FT-IR spectra of (a) Pure Biodiesel (b) Biodiesel with OA (c) 3days old 1Vol.% NFs and (d) 30 days old 1Vol.% nanofluids

4.3.3 Raman spectroscopy analysis

Raman spectra of pure biodiesel and nanofluids are shown in Fig 4.10. There is not any frequency shift in the nanofluids spectra with difference in intensity variations. This is because of the bandwidth which is its characteristics of more than one compound, and then the intensity is the contribution of all compounds present in the sample. i.e., there is a local concentration of the component responsible for Raman modes. On comparing pure biodiesel and nanofluids, it is

found that the intensity of the nanofluids are very less than the pure one this is may be because of MWCNTs are dominating the biodiesel.

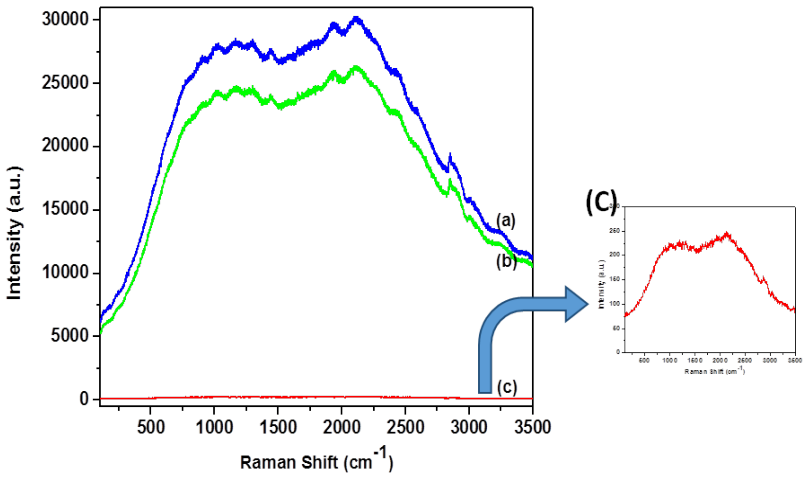

Fig 4.10 Raman Spectra for (a) Pure Biodiesel (b) Biodiesel with Oleic acid and (c) 1Vol. % of NFs

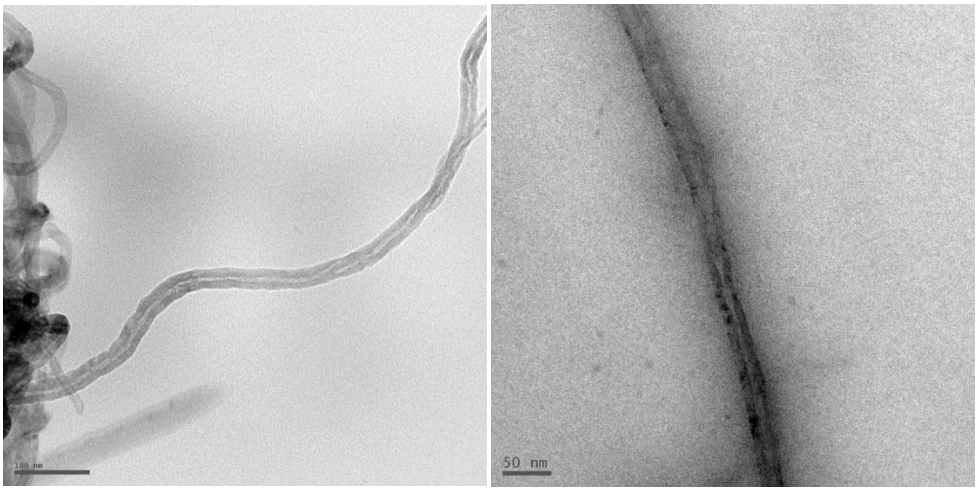

Fig 4.11. TEM micrograph of MWCNTs (a) without oleic acid (b) with oleic acid

Fig 4.11 shows the TEM micrographs for the comparison of MWCNTs dispersions of without using Oleic acid and with using Oleic acid. It is seen that, there was not any functional groups present in the sample even after the addition of Oleic acid and also the preparation of nanofluids, which shows that the Oleic Acid does not vary the biodiesel properties and would not attach any

functional groups with the MWCNTs walls. It may create some defects on the side walls of the MWCNTs which may be helpful to disperse the MWCNTs with the biodiesel.

4.3.4 UV Spectroscopy analysis

UV spectroscopy used to quantitatively characterize the stability of MWCNTs dispersion in the basefluids. Fig 4.12 shows the UV spectrum of different volume percentage of MWCNTs suspension with different ultra-sonication time such as 1hour, 2hours and 4hours. In this investigations, the stability period and oleic acid concentration are kept constant to find suitable volume fraction and suitable ultrasonication time period. That is, MWCNTs are well dispersed by ultrasonication which is an external mechanical energy that helps the nanomaterials to overcome the attractive Vander Waals forces. So if the ultrasonication time period is increased, it should give greater stability. But here, in all volume percentage, very long time sonicated sample gives less stability, that is, 2hours ultrasonicated sample gives more stability than 4 hours ultrasonicated sample. And also lower volume percentage has high stability than very higher volume percentage, i.e.0.5 and 1 volume percentage gives higher stability than 1.5 and 2 volume percentage in all period of ultrasonication shown in Fig 4.12. Fig 4.13(a) shows the different oleic acid concentration with maintaining all the parameters constant i.e., volume percentage, and ultrasonication time were kept constant to find the optimization of oleic acid concentration. It shows the 200µl has higher stability than other.

Fig 4.14 shows the UV spectra for different stability with Optimized condition i.e., percentage volume fraction, ultrasonication time period and oleic acid concentration were fixed to observe the stability of nanofluids for different reaction time. It is found that as-prepared sample has higher absorption intensities, indicating more nanomaterials were dispersed in the basefluids. After 14 days the absorption intensities were slightly reduced. This could be due to the difference in reaction time as some of nanomaterials would have been settled. But in 28 days old sample it can seen that there is another peak found which is having slightly low intensity of absorption. This may be the due to the reason that the tube like structure was decomposed by the domination

of basefluids and also the surface modified agents. In the 35 days old sample, MWCNTs were no longer in the suspensions state and hence, the MWCNTs dispersed nanofluids loses its stability properties.

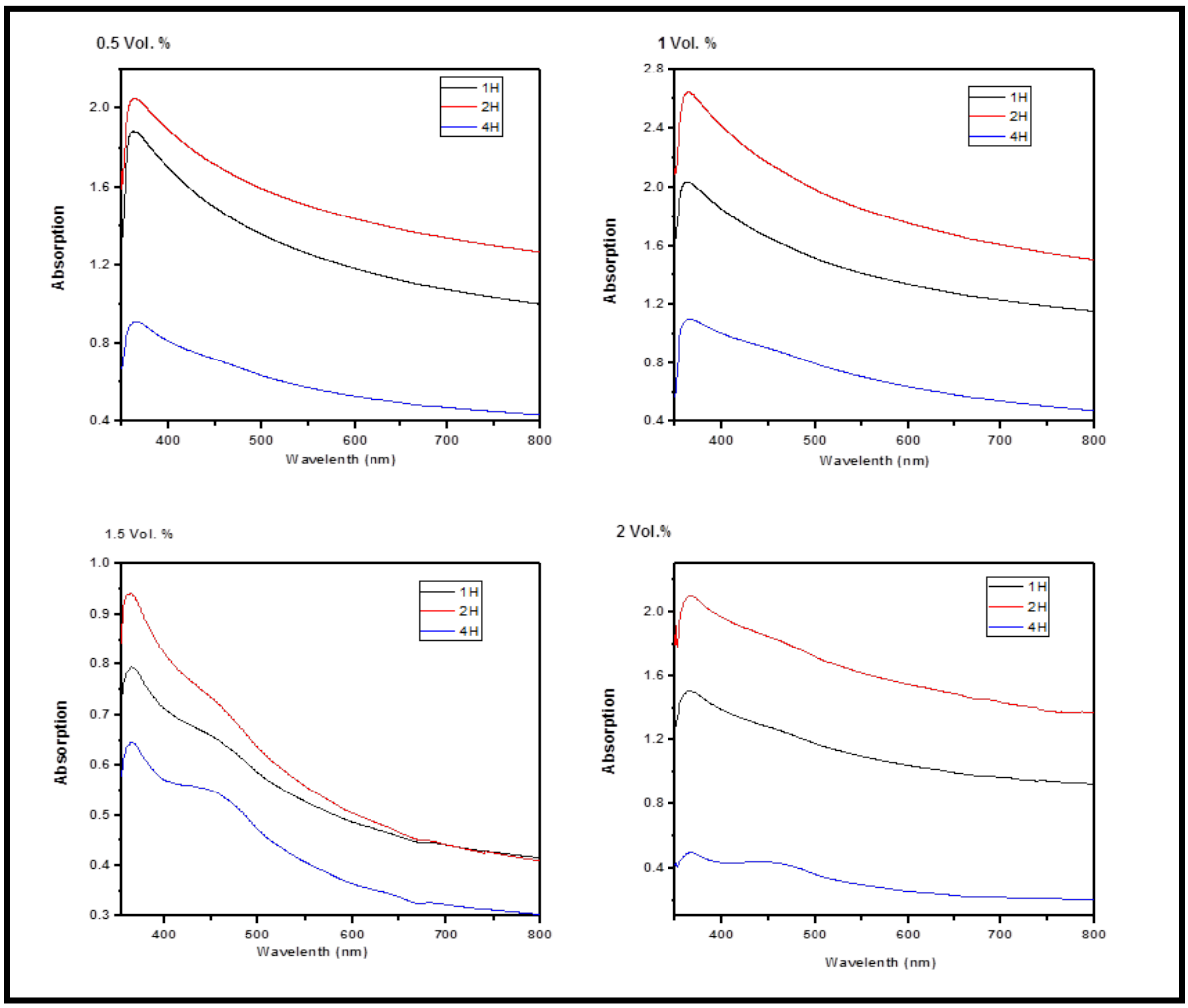

Fig 4.12 UV spectrum for different volume percentage and different sonication time for Biodiesel based MWCNT-NFs

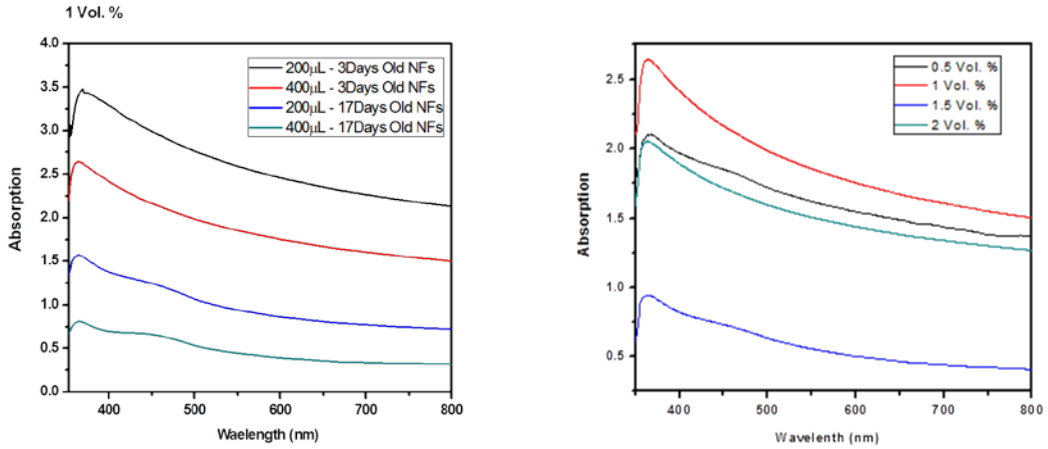

Fig 4.13 UV spectrum for Optimized condition for good suspension stability of MWCNT nanofluids with (a) Variable Oleic acid Concentration (b) Variable Volume percentage

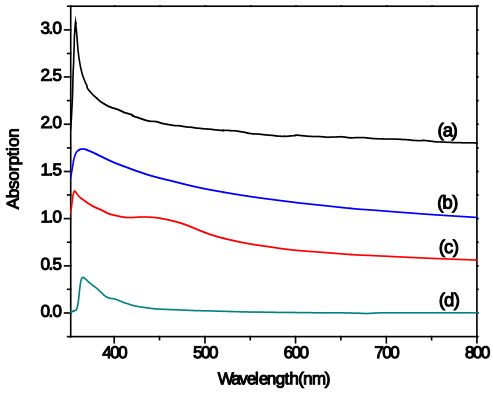

Fig 4.14. UV–Vis spectra for different stability period with Optimized condition (a) As prepared (b) 14 days old sample (c) 28days old sample (d) 35 days old sample

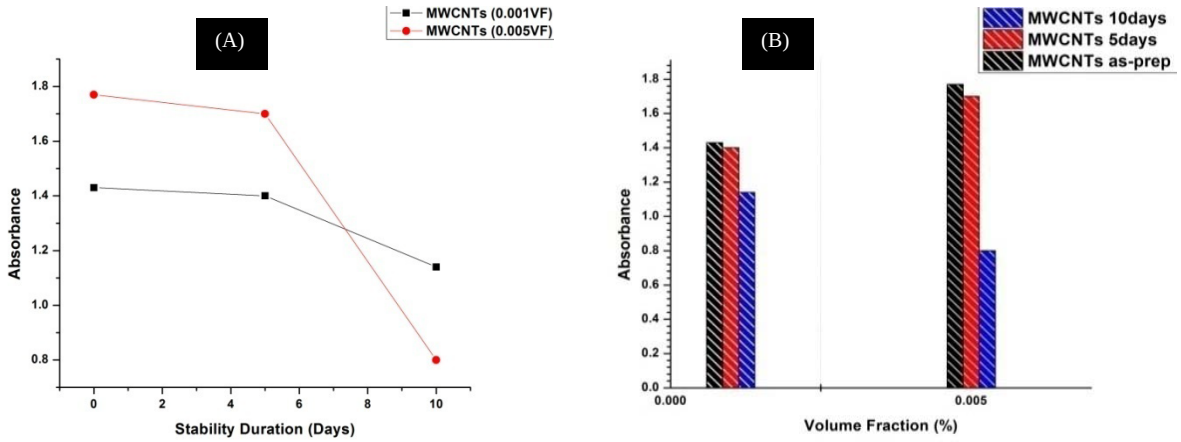

Fig.4.15: Plots of absorbance with (A) storage time for 0.001 and 0.005%VF MWCNTs nanofluids (B) Volume fraction for as-prepared, 5days and 10days older samples.

Fig 4.15((A) and (B)) shows the absorption of 0.001%VF and 0.005%VF of MWCNTs nanofluids with storage time. It is clear (from the Fig 4.15(A)) that the absorption peak value decreases gradually upto 5days of storage time while after 5 days of storage time, it rapidly decreases and more rapidly for 0.005%VF as compared to 0.001%VF nanofluids. Fig 4.15(B) shows the absorption of MWCNTs nanofluids having 0.001%VF and 0.005%VF for as-prepared samples, samples of 5 days old and 10days old. From the bar graph of Fig.4.15(B), it is seen that as the storage time increases, there is a decrease in the absorption peaks of both the samples (0.001%VF and 0.005%VF). But the decrease is more in the case of sample having 0.005%VF when compared with the sample having 0.001%VF respectively. Therefore, 0.001%VF MWCNTs (treated with oleic acid) based bio-diesel nanofluids are more stable for almost 2weeks. However, all other covalent and non-covalent approaches of MWCNTs nanofluids are not showing stability for higher volume fractions.

4.4 Material Effect (alumina and MWCNTs) on Stability of nanofluids:

Fig 4.16((A) and (B)) shows the comparison of absorbance for the different percentage volume fractions of alumina nanoparticles having average size of ~13nm and multi-walled carbon nanotubes for as-prepared samples and also for 10 days old samples respectively. Comparing both the figures (Fig.4.16(A) and (B)), it is clear that regarding the alumina nanoparticles, the difference between the absorbance peaks for as-prepared samples of 0.1%VF and 0.2%VF is high during the as-prepared stage while the same differences in peaks of 0.1%VF and 0.2%VF have narrow gap with lower absorbance peak values which implies that considerable amount of nanoparticles might have agglomerated and settled down at the bottom of the sample tubes. Regarding the MWCNTs, also the same trend was noticed for 0.001%VF and 0.005%VF respectively in both the cases, that is in the case of as-prepared samples and also in the case of 10days old samples except for the 0.01%VF which does not show any peak after 10days (as shown in the Fig 4.16(B).

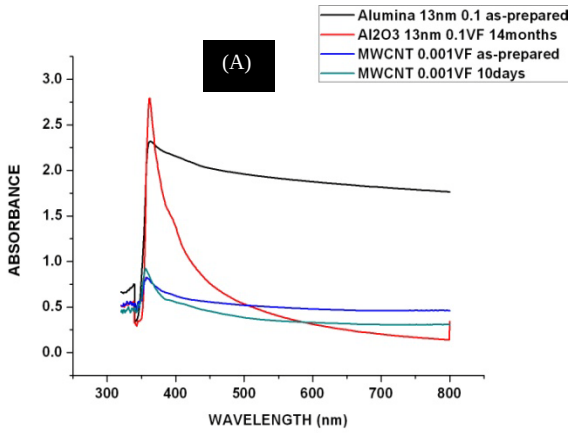

Fig.4.16 (A) : UV-Vis Spectroscopy of different material for higher stability storage time.

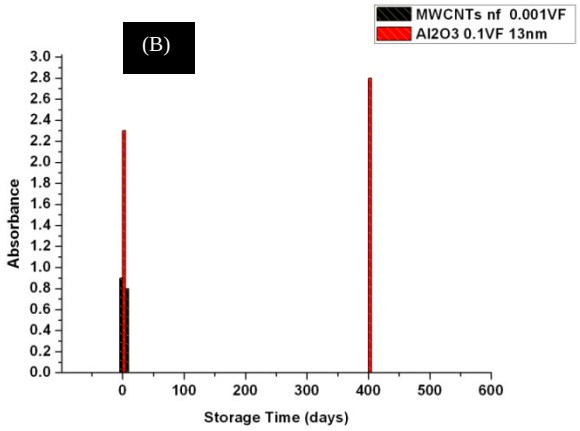

Fig.4.16(B) : Absorbance for alumina and MWCNTs for older samples

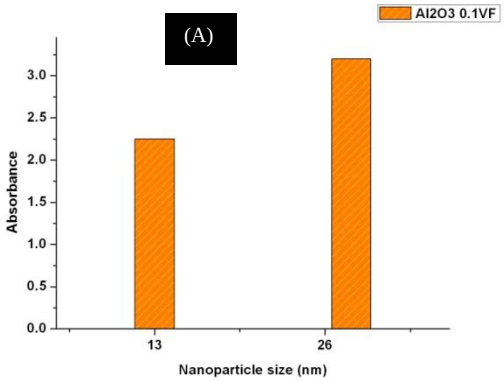

Fig.4.17 : Effect of size variations on 0.1%VF of aluminaNPs (as-prepared)

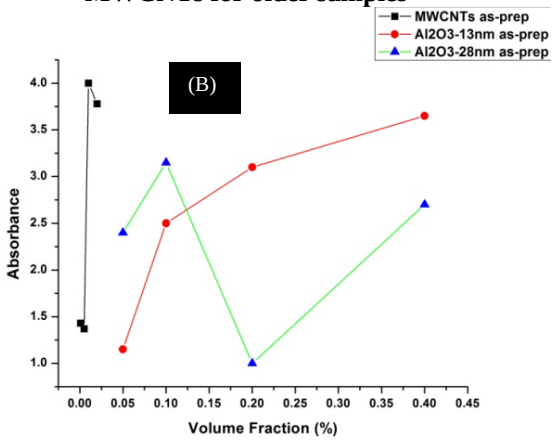

Fig.4.18: Effect of material variations on different loading.

Fig 4.17 shows the plot of absorption with percentage volume fractions of as-prepared samples of 2 different materials that is multi-walled carbon nanotubes and alumina nanoparticles. The percentage volume factions of MWCNTs were 0.001%VF, 0.005%VF, 0.01%VF and 0.02%VF respectively, which were compared individually with two different sizes of alumina nanoparticles (~13nm and ~28nm sizes) having percentage volume fractions of 0.05%VF, 0.1%VF, 0.2%VF and 0.4%VF respectively. It is seen from the Fig 4.17 that the percentage of absorption for MWCNTs and alumina nanoparticles of ~13nm size is increasing as the concentration increases but the same trend is not seen in the case of alumina nanoparticles of average size ~28nm respectively. Fig 4.18 shows the comparison of MWCNTs having percentage volume fractions of 0.001 and 0.005 which were stable for 10 days with the stable alumina nanofluids of average size ~13nm having percentage volume fractions of 0.1 and 0.2 for

10 days old samples respectively. Hence, the properties of alumina and MWCNTs with respect to viscosity, thermal conductivity and evaporation rate are discussed in the subsequent chapters.

4.5 Conclusions

In this chapter, the effects of nature of alumina nanoparticles and MWCNTs and also the size effects of alumina nanoparticles was investigated for their longer term stable properties when dispersed in jatropha biodiesel. For this purpose, alumina nanomaterials sizes of ~13nm and ~28nm and MWCNTs having length ~10µm, no. of walls 3-15 were considered. Different volume fractions(VF) such as 0.05%, 0.1%, 0.2%, and 0.4% were prepared by using two different sizes of alumina nanoparticles(~13nm and ~28nm). Since, the higher concentrations of alumina nanofluids were not possible with the basefluids alone, the surfactants namely, $Span^{80}$ and $Tween^{80}$were used in the ratio of 1:1 for Al_2O_3 nanofluids for better and longer term dispersion stability. The results showed that the Nanofluids with smaller average size alumina nanoparticles having 0.1% volume fraction (1:1 $Span^{80}$ and $Tween^{80}$) were showing longer stability more than one year as compared to the larger (two times) size nanoparticles having 0.1% volume fraction (1:1 $Span^{80}$ and $Tween^{80}$) since smaller nanoparticles having the larger solid/liquid interface as compared to the larger nanoparticles. Stability of alumina nanoparticles (~13nm and ~28nm) based nanofluids was investigated periodically by TEM, FESEM, and UV-Vis spectroscopy for different concentrations. Also multi walled carbon nanotubes (MWCNTs) having different volume fractions was also investigated for their stability in the Jatropha biodiesel by considering the covalent and non-covalent approaches. It was seen that all the surfactants such as $Span^{80}$ and $Tween^{80}$, SDS, PVP, CTAB and the surface modifications by treating with sodium oleate, sulphuric and nitric acids, MWCNT biodiesel based nanofluids were showing very poor dispersion stability.

Chapter 5

Nanomaterials and Their Size Effect on the Viscosity of the Nanofluids

5.1 Introduction

Alternate fuels such as biodiesel or nanoparticles / nanomaterials dispersed biodiesel based nanofluids should satisfy some of the basic requirements such as flash point, fire point, viscosity and combustion characteristics prior to its practical applications in the diesel engines. Out of these, viscosity is one of the most important property for the consideration of alternate fuels for diesel engine. As per the American Standards for Testing and Measurements (ASTM), the viscosity of diesel engine fuels should be of less than 4centi-stokes. High viscous fuels may cause problems such as incomplete combustion of the fuel droplets, noise pollution, emissions of harmful pollutants, soot formation, cold starting problems like blocking of the fuel passage in the combustion chamber. In this context, though several research for finding alternate fuels was carried out all over the globe, unless the requirements of viscosity levels are satisfied, it cannot be implemented as an alternate fuel in the existing diesel engines.

Though similar works on the nanoparticles dispersed biofuels based nanofluids were carried out by many researchers across the globe, most of their work was carried out for as-prepared samples or for few days older samples and hence, correspondingly, the viscosity was also limited to the as-prepared samples or few days older samples only. However, measurements of the viscosity for alternate fuels of more than 1week of such nanofluids storage time were not addressed in any of the literatures till date as per our knowledge. Therefore, this chapter deals with the viscosity measurement for different concentrations of alumina and MWCNTs dispersed nanofluids for having long term storage time. The stability of the alumina and MWCNTs nanofluids are mentioned in the previous chapters. Viscosity of all the samples were measured by using a Rheometer as Viscometer for long term durations of the stable nanofuels having different volume concentrations namely, 0.05%VF, 0.1%VF and 0.2%VF for alumina based nanofluids and 0.001%VF, 0.01%VF and 0.1%VF for MWCNTs based nanofluids respectively. These considerations were important from applications point of view also as long term stable nanofuels satisfying the viscosity limitations would help to combat challenges posed by the alternate fuels for diesel engines.

5.2 Viscosity and its types:

Viscosity is the property of fluids offering resistance to the free movement of layers of fluids one above the other by virtue of the various internal forces acting on them. When two layers of a fluid which are separated by a small distance ‘dy’ apart, move one over the other with different velocities x and x+dx, the viscosity along with their relative viscosity causes a shear stress between the two layers of fluids. The upper layer causes a shear stress over the lower layer of the two fluids and simultaneously, the lower layer also causes a shear stress on the upper layer. This shear stress is proportional to the rate of change of velocity with respect to velocity gradient.

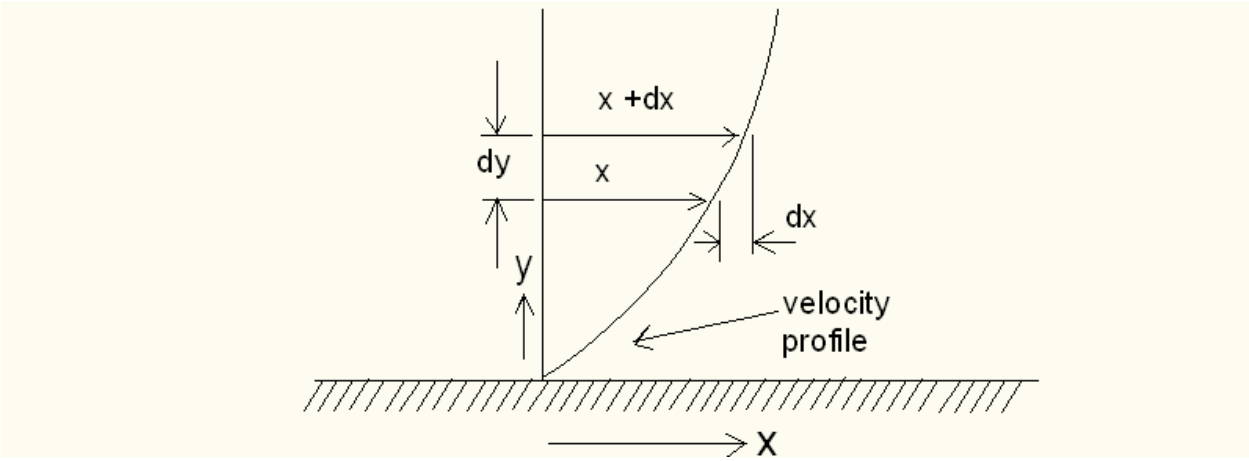

Fig 5.1: Velocity profile with solid boundary

Thus, shear stress $\tau = \mu dx/dy$, Pa s or Ns/m^2

Where τ=shear stress

μ = proportionality constant also known as co-efficient of dynamic viscosity or viscosity,

dx/dy is the rate of shear strain or velocity gradient.

Thus, viscosity $\mu = \tau / (dx/dy)$

Hence, viscosity can also be stated as the shear stress required to produce unit rate of shear strain.

Kinematic viscosity (υ) :

Kinematic viscosity (υ) is the ratio of dynamic viscosity to that of the density of the fluid.

That is, Kinematic Viscosity, $\upsilon = \mu / \rho$, m^2/s

Newton's Law of Viscosity:

Newton's law of viscosity states that the shear stress (τ) on a fluid element layer is directly proportional to the rate of shear strain. The constant of proportionality is called the co-efficient of viscosity, and is expressed as:

$$\tau = \mu dx/dy$$

Fluids which obey the above relation are known as Newtonian fluids and the fluids which do not obey the above relation are the Non-newtonian fluids.

Types of fluids:

Fluids are broadly classified as follows:

- Ideal fluid: A fluid that is incompressible and has no viscosity is known as ideal fluid.
- Real Fluid: A fluid having viscosity is known as real fluid.
- Newtonian fluid: A real fluid having the shear stress proportional to the rate of shear strain or the velocity gradient is known as Newtonian fluid.
- Non-Newtonian Fluid: A real fluid in which the shear stress is not proportional to the rate of shear strain or the velocity gradient is known as Non-Newtonian Fluid.
- Ideal Plastic fluid: A fluid having shear stress more than the yield value and shear stress is proportional to the rate of shear strain or the velocity gradient is known as ideal plastic fluid.

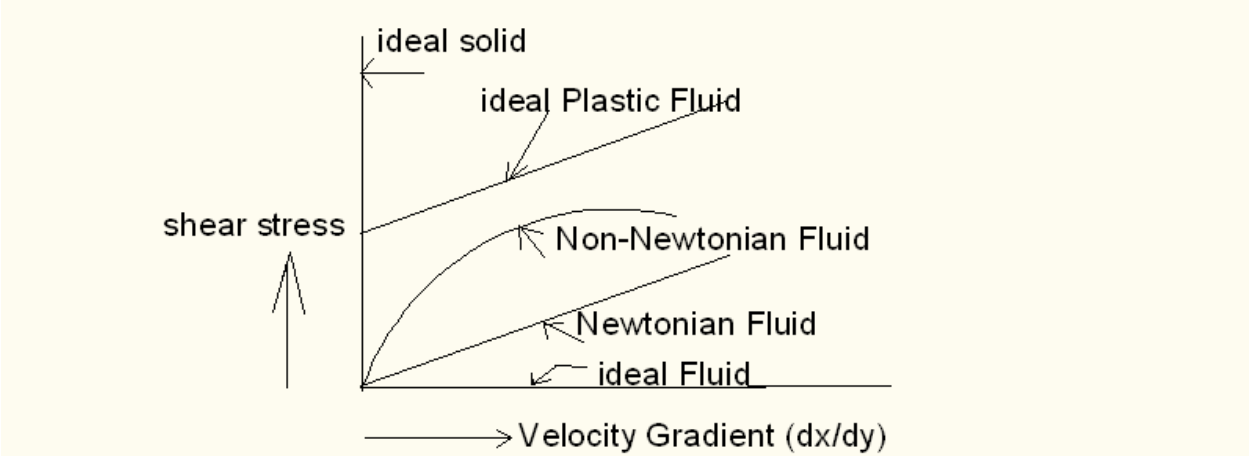

Fig 5.2:Different types of fluids

A **Rheometer** is a laboratory device used to measure the way in which a liquid, suspension or slurry flows in response to applied forces. It is used for those fluids which cannot be defined by a single value of viscosity and therefore require more parameters to be set and measured than is the case for a *viscometer*. Viscosity is a measure of the resistance of a fluid which is being deformed by the shear stress. Stress is the measure of internal force applied to an object. Shear stress is the stress which is applied parallel to the face of an object or material. More specifically, rheometers measure the forces (like shear associated with a flowing substance. Typically, the flowing

substance is much thicker than a liquid (like concrete). A rheometer along with the flowing fluids, also measures the effects of flow at different pressures-especially key characteristics of the flow like shear (how difficult it is to change the flow) or how the flow of a substance tends to drag surrounding materials. The output of a rheometer is typically a set of curves that depict these forces as the pressure on the flowing material changes. Rheometers are almost as varied as the substances and forces that they measure.

Types of Rheometer:

Rotational or Shear rhoemeters: In rotational or shear rheometers, the applied shear force or shear strain can be controlled effectively. Shear rheometers are broadly classified into three types. They are pipe or capillary rheometer, rotational cylinder rheometer and cone and plate rheometer.

Pipe or capillary rheometer: In this type, liquid is forced through a tube having a constant cross-section and known diameter having a laminar flow condition. The flow rate or pressure drop is fixed and one of the other parameter is measured for a constant value of the first parameter. Then the flow rate is controlled to shear rate and the pressure drop into shear strain. Finally varying the pressure or flow rate is found out.

Rotational rheometer: In rotational cylindrical type, the liquid is to be measured, placed in a ring shaped object of any one of two cylinder. Then one cylinder is rotated at constant speed. In this way, the shear rate inside the ring is measured and then the liquid is dragged into another cylinder. Finally the force of this liquid exerted on the cylinder is found out which can be converted to shear strain.

Cone and plate rheometer: The cone and plate rheometer, the liquid for which viscosity is to be measured is placed on the horizontal plate and hollow cone placed into it. The angle between the surface of the cone and the plate is very small, nearly about 1^{o}. Then the plate is rotated and force on the cone is measured to find out the shear stress by finding the degree of twist and the rotation speed determines the shear rate.

5.3 Alumina NPs size and concentration effect on the viscosity of nanofluids

Viscosity measurement of neat diesel and Al_2O_3 NPs dispersed Nanofluids:

The viscosity of Al_2O_3 NPs dispersed Jatropha biodiesel based nanofluids was measured using a rotational Rheometer (Physica, MCR-301, Anton Paar). It consists of two parallel cylindrical plates having a gap of 0.5mm between which the fluid whose viscosity were supposed to be measured, has to be placed; One of these two parallel plate is rotated at a controlled rotation rate in order to shear the sample contained in the gap. The shear rate is kept at a constantof 50/s. Shear stress is determined by measuring the torque on one of these two parallel plates. Measurements of the viscosity of the samples were considered in a temperature range of 20^{o}C to 75^{o}C for different concentrations of alumina nanofluids, neat Jatropha biodiesel and neat diesel. And dynamic viscosity of the nanofluid can be obtained from the relation:

For Newtonain Fluids

$$\tau = \mu\gamma$$

For Non-Newtonian Fluids

$$\tau = K\gamma^n$$

Where τ is the shear stress in Pa,

μ is the viscosity and

γ is the shear rate s^{-1},

n is the flow behavior index and

K is the flow consistency index in $Pa.s^n$.

The output data obtained from these settings were viscosity, shear stress, speed and torque corresponding to the temperature. The viscosity of the neat diesel fuel measured in our laboratory was found to be 2.704cst at 40^{o}C which is matching the range of values given in the literature [86]. Similar way, the viscosity of Al_2O_3 NPs dispersed Jatropha biodiesel based nanofluids was measured for different concentrations and also for different storage time and the results were plotted for viscosity versus shear stress as shown in the Fig.5.3 to 5.6.

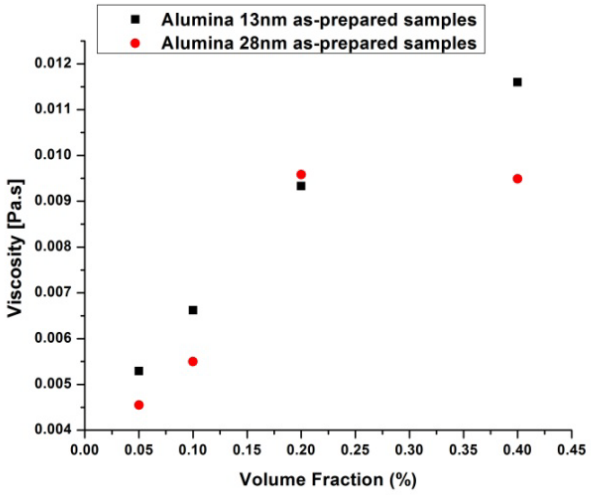

Fig.5.3: Plot of Viscosity Vs Volume Fractions of the Alumina nanofluids having two sizes (~13nm and 28nm) of as-prepared samples at room temp.

Fig.5.3 shows the plot between the viscosity and different volume fractions at room temperature for two different sizes (~13nm and ~28nm) of alumina NPs based nanofluids. The concentrations prepared were 0.05% VF, 0.1%VF, 0.2%VF and 0.4%VF for both the sizes of ~13nm and ~28nm respectively. From Fig 5.3, it is concluded that alumina nanofluids having ~13nm sizes is possessing higher viscosity than that of 28nm sizes nanofluids which may be due to the fact that in the case of ~28nm sizes alumina nanofluids, Al_2O_3 NPs (~28nm size) are settled down at a faster rate than that of their counter particle sizes (~13nm). Also the rate of settling down of the alumina nanoparticles (~28nm size) of 0.4% volume fractions is more rapid and having clusters of bigger size particles, as compared with that of 0.05% and 0.1% volume fractions. Hence, increasing the volume fractions, both the sizes of alumina NPs (~13nm and 28nm) dispersed nanofluids are showing higher viscosity. The rate of settling down for 0.1% volume fractions (~28nm size) is more faster than that of 0.05% volume fractions. It is also observed that for the case of 0.2% volume fractions of alumina nanoparticles (~28nm size) based nanofluids is showing entirely different phenomenon. The viscosity of 0.2% volume fraction for both the alumina nanoparticles (~13nm and ~28nm sizes) based nanofluids are almost the same with ~28nm size alumina nanoparticles having slightly higher viscosity than that of their counter ones ~13nm size alumina nanoparticles based nanofluids. This shows that the viscosity of both the sizes (~13nm and ~28nm) of alumina nanoparticles based nanofluids having similar flow

properties when the volume fraction is close to 0.2% and further investigations in this regard is still required to fully understand this unique phenomenon. However, one of the reason is that at 0.2% vf, both are showing the stability. Fig 5.4 and 5.5 shows the plot between the viscosity versus shear stress of alumina nanoparticles dispersed jatropha biodiesel based nanofluids for as-prepared samples for both the sizes of alumina nanofluids by varying the percentage volume fraction. It also shows the comparison of viscosity versus Shear Stress of alumina nanofluids with respect to synthesized jatropha biodiesel (without any nanoparticles dispersions) and also with that of neat diesel fuel.

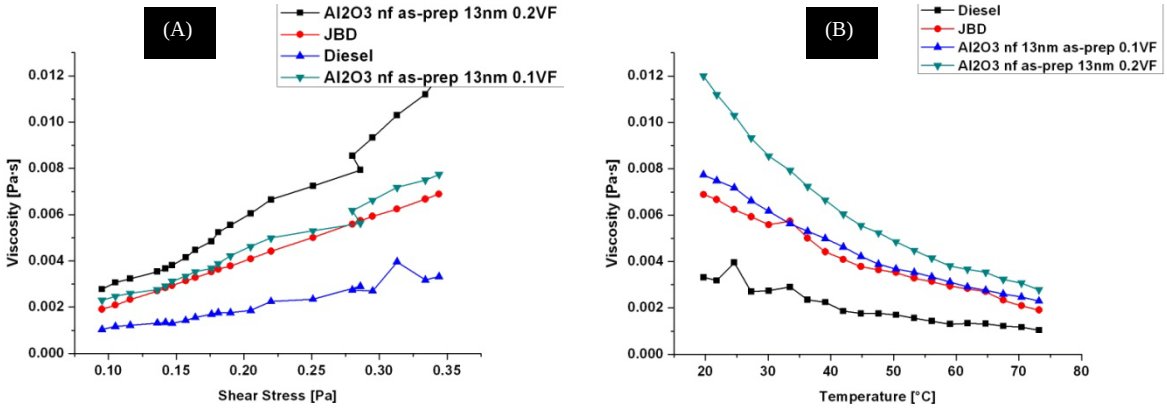

Fig.5.4: Plots of Al_2O_3 Nanofluids (~13nm size) for as-prepared samples having varying concentrations of 0.05, 0.1, 0.2 and 0.4%VF (A) Viscosity and Shear Stress (B) Viscosity and Temperature

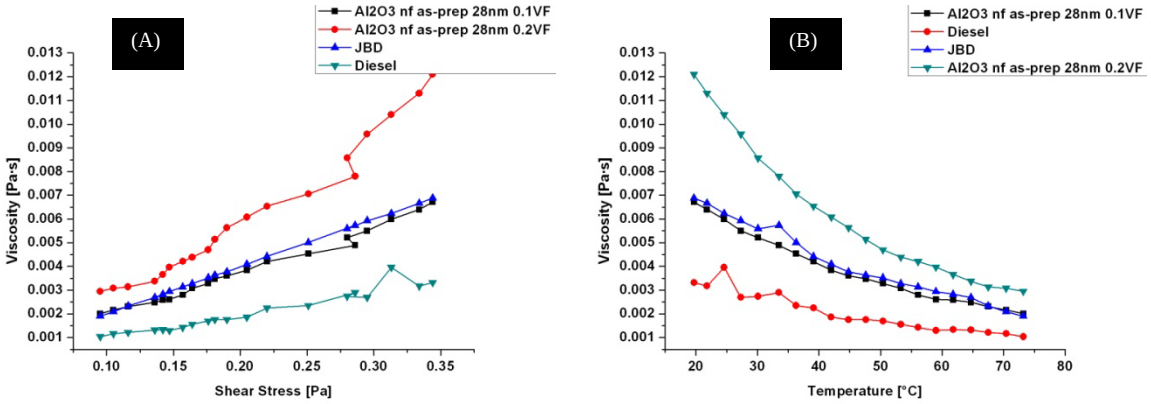

Fig.5.5: Plots of Al_2O_3 Nanofluids (~28nm size) for as-prepared samples having varying concentrations of 0.05, 0.1, 0.2 and 0.4%VF (A) Viscosity and Shear Stress (B) Viscosity and Temperature

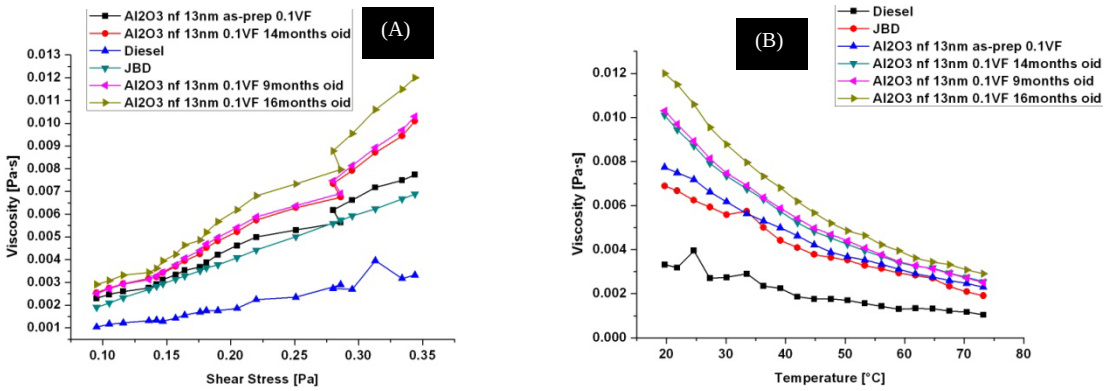

Fig.5.6: Plots of Al_2O_3 Nanofluids (~13nm size) for different storage samples having 0.1%VF (A) Viscosity and Shear Stress (B) Viscosity and Temperature

Fig.5.4(a)-(b) show that the viscosity of diesel is the lowest for all the values of shear stress, followed by 0.05%VF and 0.1%VF of 13nm size alumina nanofluids, and synthesized Jatropha biodiesel which may be due to the fact that the alumina nanoparticles contribute the catalytic properties when used as a fuel and the optimal quantity may be in the range of 0.05%VF to 0.1%VF. While viscosity of alumina nanofluids having concentrations 0.2%VF and 0.4%VF always remained higher than that of neat synthesized jatropha biodiesel at all the values of shear stress since the quantity may be more than the threshold value for the catalytic properties to be imparted to the jatropha biodiesel.

Fig.5.6 show viscosity versus Shear Stress of alumina nanoparticles (~13nm) dispersed jatropha biodiesel based nanofluids for different sedimentation time of 0.1%. It also shows the comparison of the same with respect to synthesized jatropha biodiesel (without any nanoparticles dispersion) and also with respect to neat diesel fuel. It is clear from the Fig.(5.4 and 5.5) that the viscosity of as-prepared samples of 13nm size alumina nanofluids having 0.1%VF at higher temperature may possess the fuel properties nearer to that of diesel fuel when compared with that of all other sedimentation times which may be due to the reason that as the sedimentation time increases, more and more of the alumina nanoparticles gets agglomerated and settles down at the bottom of the sample test tube when compared to that of the as-prepared samples. Due to this agglomeration and settling down of the alumina nanoparticles with respect to sedimentation time, more and more of synthesized jatropha biodiesel may be present whose viscosity was definitely much higher than that of alumina nanofluids of 0.05%VF and also higher than that of neat diesel fuel.

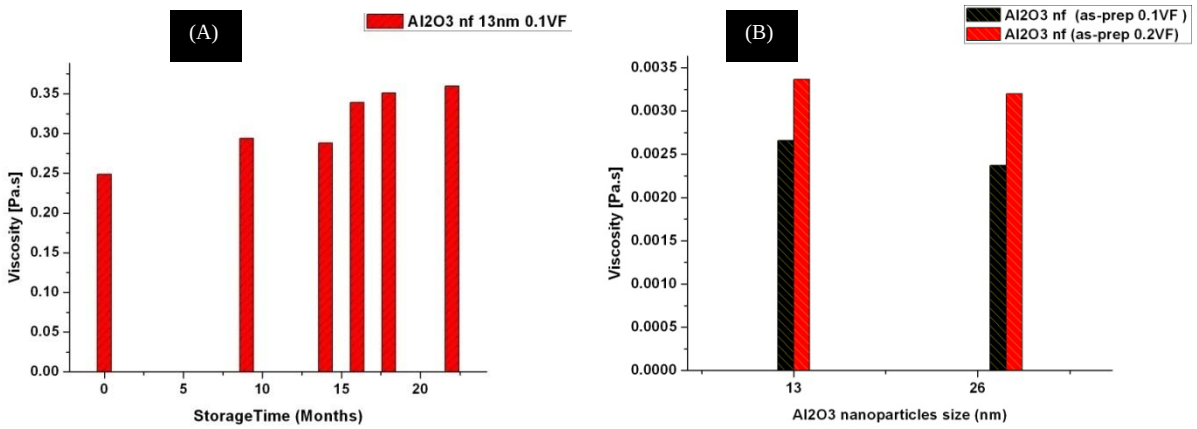

Fig5.7 (A)Viscosity vs storage time of Al_2O_3 nanofluids (~13nm, 0.1VF) **Fig.5.7(B)Viscoisty vs Al_2O_3 NPs size for as-prepared samples**

5.4 MWCNTs effect on the viscosity of the nanofluids

Fig.5.8 show the plot of viscosity with varying shear stress MWCNTs dispersed Jatropha biodiesel based nanofluids for different concentrations upto a stability durations of 10 days along with the viscosity measurements of neat diesel and also neat Jatropha biodiesel. From the Fig.5.8, it is clear that MWCNTs dispersed nanofluids of as-prepared having a percentage volume fraction of 0.001 and 0.005 are showing lower viscosity as compared to that of neat Jatropha biodiesel. Hence, on adding nanomaterials to the jatropha biodiesel, its viscosity can be reduced which helps in improving the combustible properties of diesel engines.

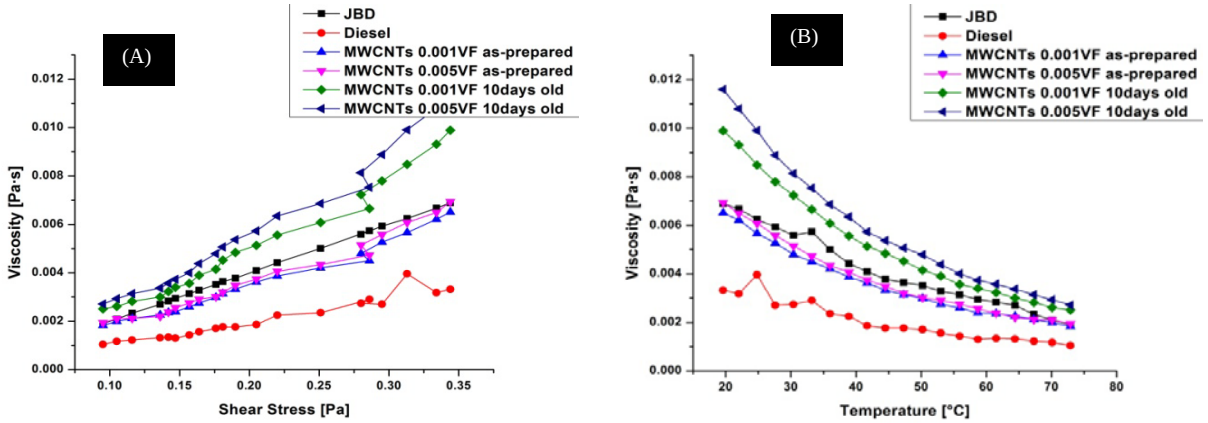

Fig.5.8: Plots of MWCNTs Nanofluids for as-prepared samples having 0.001, 0.005 %VF as-prepared and 10days old samples showing (A) Viscosity and Shear Stress (B) Viscosity and Temperature

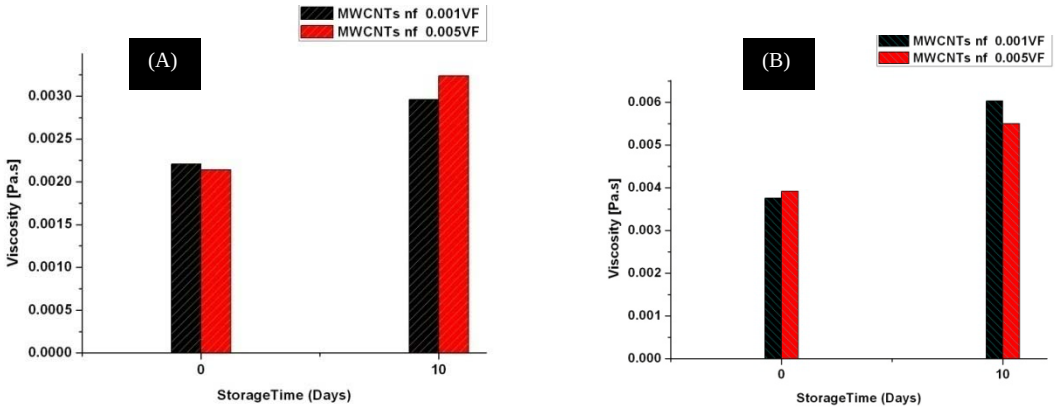

Fig5.9 Viscosity vs storage time of MWCNTs at (A) Shear stress of 0.125Pa. (B) 40^{o}C

However, as the percentage volume fraction increases, viscosity is also increasing as can be seen for as-prepared samples of 0.005 when compared with 0.001%VF. But, for the 10days storage time of nanofluids, viscosity is higher than that of Jatropha biodiesel and also higher than the as-prepared samples. As the temperature of the nanofluids increases, viscosity of the nanofluids decreases.

5.5 Material Effect (Alumina and MWCNTs) on the Viscosity of the nanofluids:

Fig 5.10 shows the Viscosity with Temperature of as-prepared sample and longest stable samples of alumina nanofluids of (~13nm) and MWCNTs dispersed nanofluids respectively. It is found that MWCNTs of as-prepared sample having a volume fraction of 0.001 has the lowest viscosity than that of Al_2O_3 NPs dispersed nanofluids. But on comparing the storage time of the both the materials, Al_2O_3 nanofluids having a storage durations of 14months has lesser viscosity than that of MWCNTs nanofluids having a storage duration of 10days.

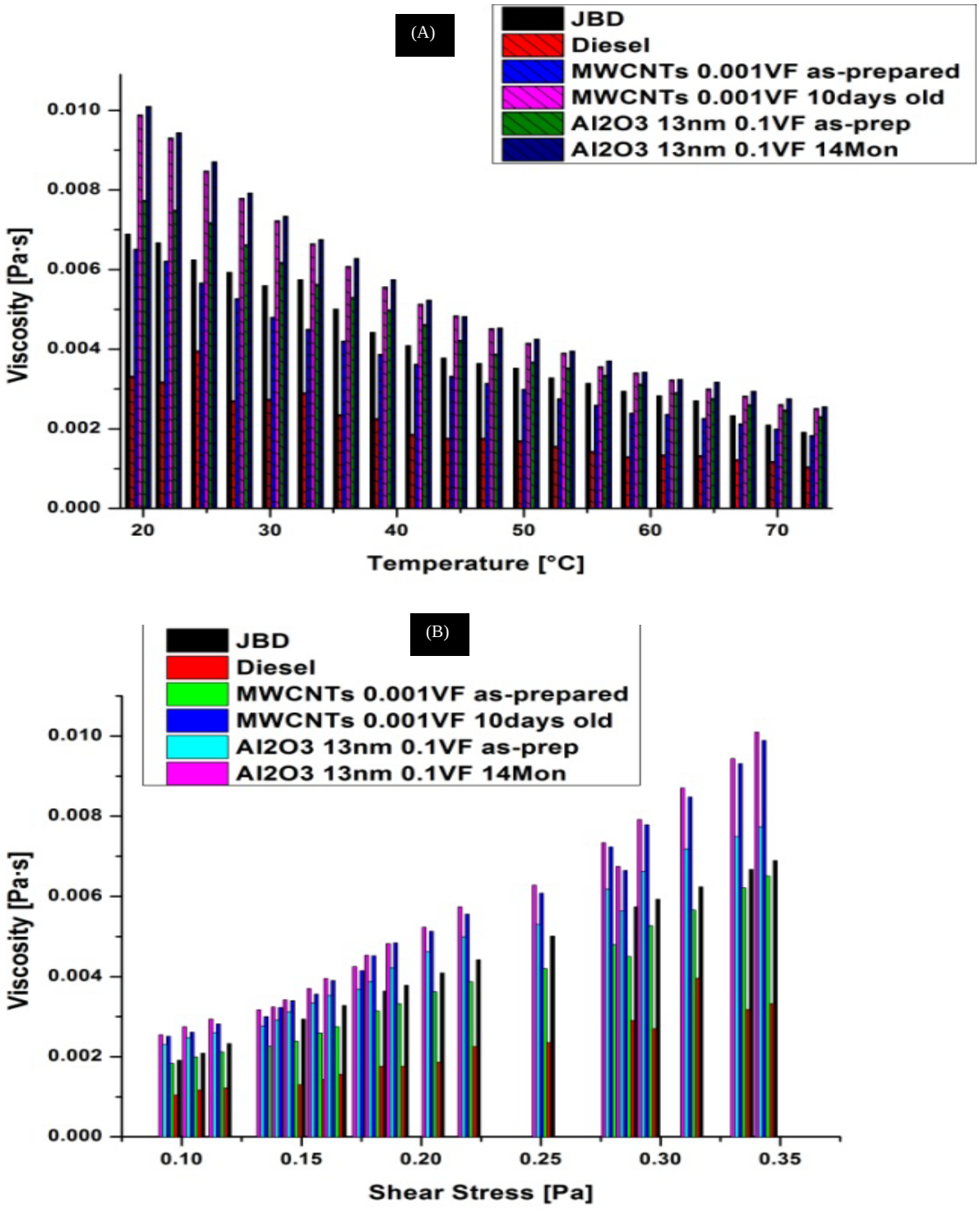

Fig.5.10 Plots of Al_2O_3 (~13nm) and MWCNTs with as-prepared and longer stability time samples (A)Viscosity Vs Temperature (B) Viscosity Vs Shear Stress

5.6 Conclusions:

The size and materials effect on the viscosity of alumina nanoparticles (~13nm and ~28nm) and MWCNTs dispersed jatropha biodiesel based nanofluids has been investigated. The influence of alumina nanoparticles sizes, the storage time periods of both the nanomaterials / nanoparticles on the viscosity of the biodiesel based nanofluids are reported in this chapter. Since alumina nanoparticles having ~28nm size is not showing dispersion stability for longer durations, investigations were carried out for alumina nanofluids having average size of ~13nm having 0.1%VF for a storage time of more than 22months, while investigations were limited to as-prepared samples for ~28nm size alumina nanofluids. It was observed that as-prepared samples having 0.05%VF and 0.1%VF of both the sizes of alumina nanofluids (~13nm and ~28nm), were showing viscosity lesser than that of neat jatropha biodiesel.

It is concluded that as the Al_2O_3 NPs sizes decreases, viscosity of the nanofluids increases for all the different nanoparticles loading (0.1, 0.2 and 0.4%VF). Also as the Al_2O_3 NPs loading increases, the viscosity is directly proportional and is higher for higher loading in both the ~13nm and ~28nm sizes Al_2O_3 NPs dispersed biodiesel nanofluids. However, increasing the temperature of the nanofluids, viscosity is decreasing sharply for all the loading for both ~13nm and ~28nm Al_2O_3 NPs based nanofluids. Second conclusion is that as the storage time of the nanofluids increases, the viscosity also increases for all the particle loading. However, with increasing the temperature, viscosity of all the different storage time samples sharply decreases. This results support the fact that alumina nanoparticles could be used as catalytic materials to enhance the combustion properties of the diesel engines when used as an alternate fuels.

Chapter 6

Nanomaterial and Their Size Effect on Thermal Conductivity of the nanofluids nanofluids

6.1 Introduction

Thermal Conductivity is a property of the materials to conduct heat and several different types of materials conduct heat by different phenomenon. For example, high energy generations rates within electronics or turbines require the use of materials with very high thermal conductivity such as copper, aluminium and silver. On the other hand, materials with low thermal conductance such as polysterene and polymers are used inbuilding construction or in furnaces in an effort to slow the flow of heat, i.e. for insulation purposes.

Nanofluids are new class of engineered fluids whose thermal conductivities are different than that of basefluids or the nanparticles or nanomaterials dispersed in the basefluids. Therefore, to measure accurately the thermal conductivity of the nanofluids several methods or approaches are existing such as Transient Plane Source, Steady-State Parallel-Plate, Cylindrical Cell method,

Temperature Oscillation, 3w and Transient hot-wire (THM) methods. These are briefly outlined in the following section.

Transient Plane Source (TPS) method

The Fourier law of heat conduction forms the basis for the TPS method. The components of the setup consist of a container, a constant temperature bath, a thermometer and a thermal constants analyzer whose probe is vertically immersed in the container with the nanofluid. The temperature of the probe rises when it is supplied with a constant electric power. This rise can be derived from measuring the change in resistance of the probe, from which the thermal conductivity of the nanofluid is ultimately calculated.

In the case of the onset of natural convection, the thermal constants analyzer is designed to automatically give a notification. This way, the result can be proved to be more reliable. As a preventive measure of the occurrence of natural convection, necessary control of the analyzer parameters are often carried out.

The TPS method offers certain advantages which have been mentioned in literature and are listed here point-wise:

- Measurements are carried out in a very short interval of time.
- This method can be utilized on samples that have a wide range of thermal conductivity (From 0.02 to 200 W/mK)
- The size of the sample can be flexible.

Steady-state parallel-plate method

This method is based on the transfer of heat predominantly in a single direction. This is often carried out using parallel-plate or concentric cylindrical designed equipment. Challoner and Powell came up with a design in which a small amount of fluid is placed in between two parallel copper plates [84]. A heater is used to supply heat to the fluid in between the plates, due to which the entire setup including the plates gets heated up resulting in a temperature rise. The one dimensional heat equation, coupled with the values of the cross sectional areas and the overall geometry of the setup, is then used to calculate the overall thermal conductivity value across the plates.

Cylindrical cell method

The cylindrical cell method follows a steady state approach. In the year 2009, Kurt et al. measured the thermal conductivity of ethylene glycol – water solutions and compared the experimental results with those obtained by using Artificial Neural Networks (ANN). In this method, the nanofluid is placed in the annular space of two coaxial cylinders. An electric heater placed inside the inner cylinder provides heat that flows in the radial direction. The temperature gradient caused by the flow of this heat is measured by two thermocouples. The thermal conductivity of the nanofluid is then calculated by using the Fourier's law in cylindrical coordinates [88].

Two thermocouples are utilized to measure temperature difference after applying power and heat transform caused by heater. Using Fourier's law in coaxial cylinders, thermal conductivity of sample in the gap could be computed.

Temperature Oscillation method

In this method, a temperature oscillation is imposed on the nanofluid and the resulting temperature response is then measured. Roetzel et al. [91] first proposed the oscillation method based on which the Temperature Oscillation method was developed.

The experimental setup consists of a test cell with both the sides surrounded by cooling water supplied by a thermostatic bath. Electric power is supplied to the Peltier element and the resulting temperature responses are measured by thermocouples. These measurements are then fed to an amplifier. A data logger is used to store the measurements in a computer that is installed with the required software prior to performing the experiment [91].

3w method

This method is similar to the THW method in the sense that a single element acts both as the source of heat and a temperature probe. The concept of temperature oscillation is used here, wherein a heat wave is generated by passing a sinusoidal current of *w* frequency. This heat wave has a frequency of 2*w*. Cahill [92] gives the exact solution of the temperature oscillations which are related to the amplitude of the power generated and the frequency of the line source of heat.

This method is mostly used for the measurement of temperature dependent thermal conductivity of nanofluids. Oh et al. [94] used this method to measure the thermal conductivity of Al_2O_3 dispersed in DI and ethylene glycol at room temperature

Transient hot-wire (THW) method

Transient hot-wire method is used for many research applications. In this method, the thermal conductivity of an unknown nanofluid is determined by considering it as an unknown resistor whose resistance can be determined with the help of wheat-stone bridge circuit. Initially, the wheat-stone bridge circuit is balanced at no-load conditions and when connected to the data logger with constant current source, electric power is supplied for a very brief period of time to a thin metallic wire immersed in a fluid. This period usually is confined to an interval of 0-2 seconds. The power that is applied causes the temperature of the wire to rise owing to the Joule effect of heating. This rise in temperature with time depends on the properties [such as thermal conductivity] of the fluid medium surrounding the wire. a series of readings having a very small variations in voltage can be obtained and when these reading are plotted on a graph, the slope of the graph gives the rate of heat transfer from which the thermal conductivity can be calculated. Thus this method avoids the onset of heat transfer by natural convection, the effects of which gradually increase with time as the temperature gradients increase since, thermal conductivity is carried out within a very short period of time, usually less than 2 seconds.

This method has a limitation in that it cannot be applied to electrically conducting fluids owing to the leakage of current that can happen from the wire. Nagasaka and Nagashima [96] found a way around this limitation in the year 1981 by coating the wire with a thin insulation wire, which prevents the current from leaking into the surrounding fluid.

6.2 Experimental set-up of the thermal conductivity of the nanolfuids

Theory of the THW principle

Assumptions in the Transient Hot Wire Method:

1) The wire is of infinite length
2) The medium whose thermal conductivity is to be measured surrounds the wire and is also infinite.
3) The thermal conductivity of the wire is assumed to be infinite, so that the temperature distribution within the wire is considered to be uniform.
4) Heat transfer from the wire to the surrounding medium is assumed to take place only by the process of conduction.

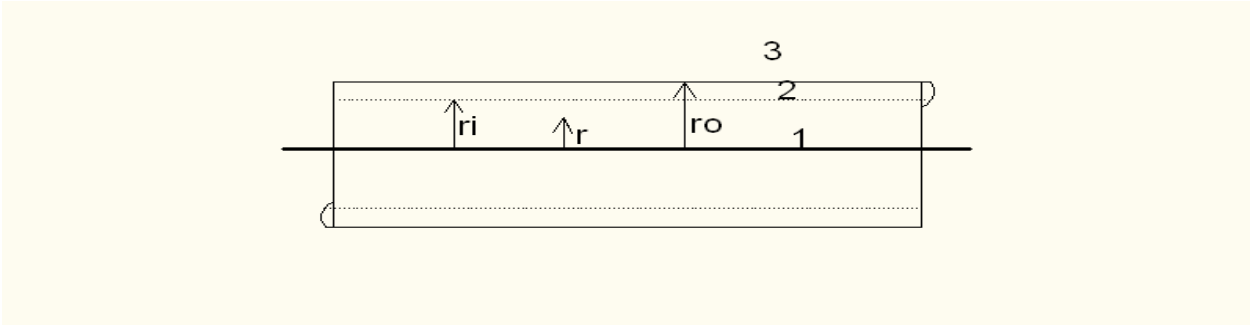

Fig.6.1: Regions in an insulated hotwire immersed in a fluid

The regions of heat transfer from the hotwire to the fluid around it are three in number. Region (1) is the inner bare wire. Region (2) is the insulation coating around the wire and Region (3) is the surrounding fluid. Fourier's law of heat conduction, when applied to these three regions, in the cylindrical coordinates gives:

$$\frac{\partial^2 \Delta T_1}{\partial r^2} + \frac{1}{r}\frac{\partial \Delta T_1}{\partial r} - \frac{1}{k_1}\frac{\partial \Delta T_1}{\partial r} = -\frac{q}{\pi r {r_1}^2 \lambda_1} \quad ; \quad 0<=r<=r_1 \qquad ---- \quad (6.1)$$

$$\frac{\partial^2 \Delta T_2}{\partial r r^2} + \frac{1}{r}\frac{\partial \Delta T_2}{\partial r} - \frac{1}{k_2}\frac{\partial \Delta T_2}{\partial r} = 0 \quad ; \quad r_1<=r<=r_0 \quad ---- \quad (6.2)$$

$$\frac{\partial^2 \Delta T_3}{\partial r r^2} + \frac{1}{r}\frac{\partial \Delta T_3}{\partial r} - \frac{1}{k_3}\frac{\partial \Delta T_3}{\partial r} = 0 \quad ; \quad r_0<=r \qquad ---- \quad (6.3)$$

Following initial and boundary conditions apply to the above equations:

$\Delta T_1 = \Delta T_2 = \Delta T_3 = 0$ ---- (6.4)

$$\lambda_1 \frac{\partial \Delta T_1}{\partial r} = \lambda_2 \frac{\partial \Delta T_2}{\partial r}$$

$\Delta T_1 = \Delta T_2$---- (6.5)

$$\lambda_2 \frac{\partial \Delta T_2}{\partial r} = \lambda_3 \frac{\partial \Delta T_3}{\partial r}$$

$\Delta T_2 = \Delta T_3$ ----- (6.6)

$\Delta T_3 = 0$ ---- (6.7)

$$\frac{\partial \Delta T_1}{\partial r} = 0$$

Based on the above initial and boundary conditions, a solution to the temperature profile in region 1 was derived by Nagasaka et al. [38] which is:

$$\Delta T_1(t) = \int_0^i \Delta T_1(r,t)\frac{2\pi r dr}{\pi {r_1}^2} = \frac{q}{4\pi\lambda 3}\left(\ln t + A + \frac{1}{t}(Blnt + C)\right) \quad ---- \quad (6.8)$$

ΔT_1 is the temperature profile; A, B and C are constants pertaining to the geometry of the hotwire;

For wires of low diameter, the second term in the above equation has a value that is much lesser than the constant term A. Thus, if $\frac{1}{t}(Blnt + C)$ is much greater than A, it can be neglected and the aboveequation essentially reduces to a linear relationship between the temperature gradient and ln t.

$\Delta T_1 = \frac{q}{4\pi\lambda 3} \ln t$ ---- (6.9)

Slope, $m = \frac{q}{4\pi\lambda 3} = \frac{i^2 R_4}{4\pi l \lambda_3} \lambda_3 = \frac{i^2 R_4}{4\pi l}$ ----- (6.10)

Where, l = length of the platinum wire, R_4 = Resistance of the hotwire cell, i = input current supplied.

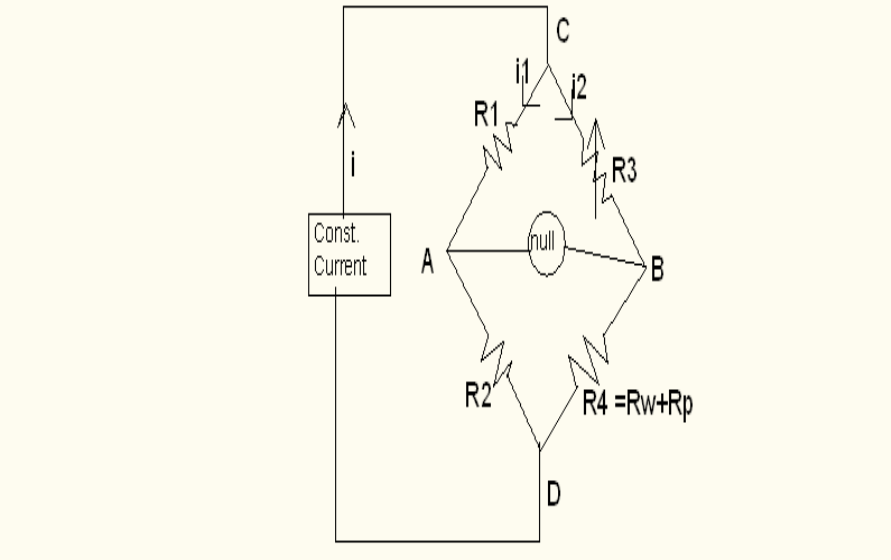

Fig.6.2: Wheatstone bridge circuit for THW experimental set-up

The Wheatstone bridge shown in Fig 6.2 is often employed to compare the value of an unknown resistance with a known resistance. Table 6.1 gives values of resistances used in this experiment.

Table:6.1 Resistances used in the experiment

Symbol	Meaning	Value(Ω)
$R_1 = R_2 = R$	Fixed Resistor	10.047
R_3	Resistance of the potentiometer	2.855
$R_4 = R_w + R_p$	Resistance of the hot wire cell	2.115

Here, R1 and R2 are the fixed resistors, thus leading to a fixed ratio of R1/R2.

One of the other arms of the Wheatstone bridge, R3, is a 100 Ω potentiometer.

In the final arm, the resistance of the hotwire is taken as R_w, and an additional R_p is used to denote the parasitic resistance associated with the hotwire cell.

The bridge output voltage is the difference between voltage at point A and point B.

$V_{out} = V_A - V_B$

Using the voltage divider relation, V_{out} can be written as

$$V_{out} = V_{in}\left[\frac{R_w+R_p}{R_3+R_w+R_p} - \frac{R_2}{R_1+R_2}\right] \text{----} \quad (6.11)$$

Applying Kirchhoff's current law at point C gives,

$i_T = i_1 + i_2$---- (6.12)

$$= \frac{V_{in}}{R_1+R_2} + \frac{Vin}{R_3+R_4}$$

$$= V_{in}\left\{\frac{R1+R2+R3+R4}{(R1+R2)(R3+R4)}\right\}$$

Substituting the value of Vin eq (6.11),

$$V_{out} = i\left\{\frac{(R1+R2)(R3+R4)}{R1+R2+R3+R4}\right\}\left\{\frac{R4R1-R2R3}{(R1+R2)(R3+R4)R}\right\}$$

$$= i\left\{\frac{R4R1-R2R3}{R1+R2+R3+R4}\right\}$$

$$Vin = i\left\{\frac{(Rw+Rp)R1-R2R3}{R1+R2+R3+Rw+Rp}\right\} \quad \text{----} \quad (6.13)$$

If R_w changes by ΔR_w

$$V_{out} + \Delta V_{out} = i\left\{\frac{(Rw+\Delta Rw+Rp)R1-R2R3}{R1+R2+R3+Rw+\Delta Rw+Rp}\right\}$$

According to the initial balanced state condition, $V_{out} = 0$. Also taking R_1=R_2=R, we get:

$$\Delta V_{out} = i\left\{\frac{(Rw+\Delta Rw+Rp)R-R R3}{R+R+R3+Rw+\Delta Rw+Rp}\right\}$$

$$\Delta V_{out} = i\left\{\frac{(Rw+Rp-R3)R+\Delta RwR}{2R+R3+Rw+\Delta Rw+Rp}\right\}$$

ΔRw can be written in terms of the other parameters, as follows:

$$\Delta R_w = \left\{\frac{(Rw+Rp-R3)R-(2R+R3+Rw+Rp)\frac{\Delta Vout}{i}}{\frac{\Delta Voit}{i}-R}\right\} \quad \text{----} \quad (6.14)$$

The change in resistance, coupled with the measured value of the temperature coefficient of resistance, can be used to calculate the correction to the thermal conductivity.

$$\Delta T_w = \frac{\Delta R_w}{R_w(\alpha)} \quad \text{----} \quad (6.15)$$

From the equation (9),

$$\Delta T_w = \frac{q}{4\pi\lambda_3} \ln t$$

Therefore, on equation the ΔT_w value from eq (6.9) and (6.15), we get

$$\frac{q}{4\pi\lambda_3} \ln t = \Delta T_w = \frac{\Delta R_w}{R_w(\alpha)}$$

$$\frac{q}{4\pi\lambda 3} \ln t = \Delta T_w = \frac{\left\{\frac{(Rw+Rp-R3)R-(2R+R3+Rw+Rp)\frac{\Delta Vout}{i}}{\frac{\Delta Vout}{i}-R}\right\}}{Rw(\alpha)} \quad \text{----} \quad (6.16)$$

Plotting ΔT_w (a function of ΔV) against ln (t) results in a straight line, where the slope can be used in calculating thermal conductivity.

Where, $q = V*I / (l*t)$; $V = I*R$; $Q = I^2R$; $\lambda = i^2*R_w / (slope*(4*\prod*l)$

(ΔT) = Temperature difference,

λ = Thermal Conductivity, watts/m/^{o}k

t = Time in sec.

q = Rate of Heat Transfer, watts

V = Voltage, volts,

I = Current, ampere

R = Resistance, ohm

l = length of the Platinum wire, m

t = time the current flows through the platinum wire, sec

Block Diagram for the experimental setup

Fig 6.3 shows the schematic of an electrical circuit for measuring the thermal conductivity of fluids. A Wheatstone bridge is employed for measuring the change in temperature of the hotwire. Two of the Wheatstone bridge arms are fixed resistors of value 10.047Ω. The hotwire cell and a potentiometer of range 100 Ω form the other two arms of the bridge. A data logger is employed

to record the unbalanced voltage across the bridge as a function of time in a computer. A power supply is used as a constant current source.

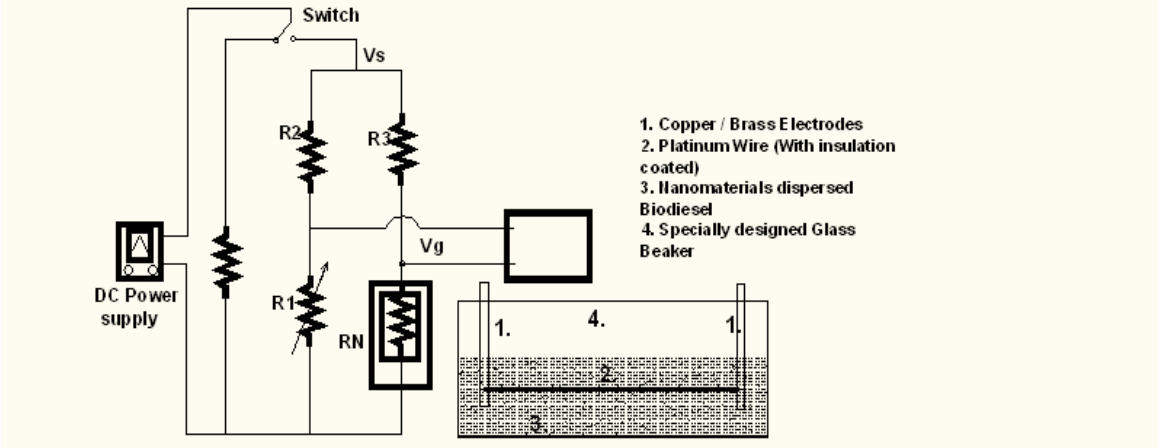

Fig.6.3 Block diagram of a THW method set-up

Experimental Apparatus of the thermal conductivity measurement

The core portion of the setup constitutes a platinum wire of ~25 μm diameter and 3.5 cm length. The ends of the wire are soldered to two stainless steel screws which act as clamps to keep the wire straight. The wire is suspended in a hot wire cell filled with the nanofluids whose thermal conductivity is to be measured. The leakage current from the supports to the surrounding fluid is ensured to be eliminated by coating them with two layers of epoxy that is an electric insulator.

An Agilent source meter which acts as a current source is employed to supply current to the Wheatstone bridge. An Agilent digital multimeter is used to measure the voltage output and other resistances. This instrument is connected to a personal computer, and the data logging software is downloaded from Agilent website that records the readings. Fig 6.4 is an image of the entire thermal conductivity setup which clearly depicts all the individual components.

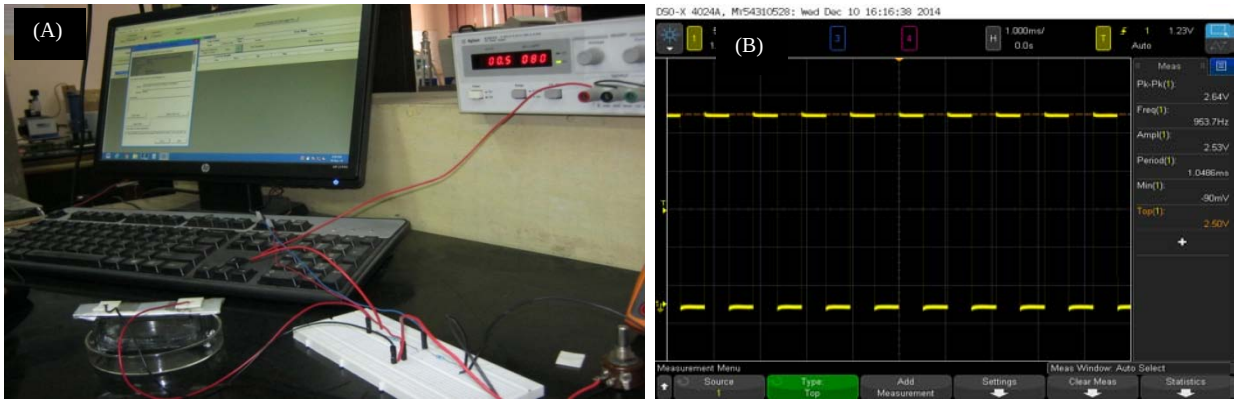

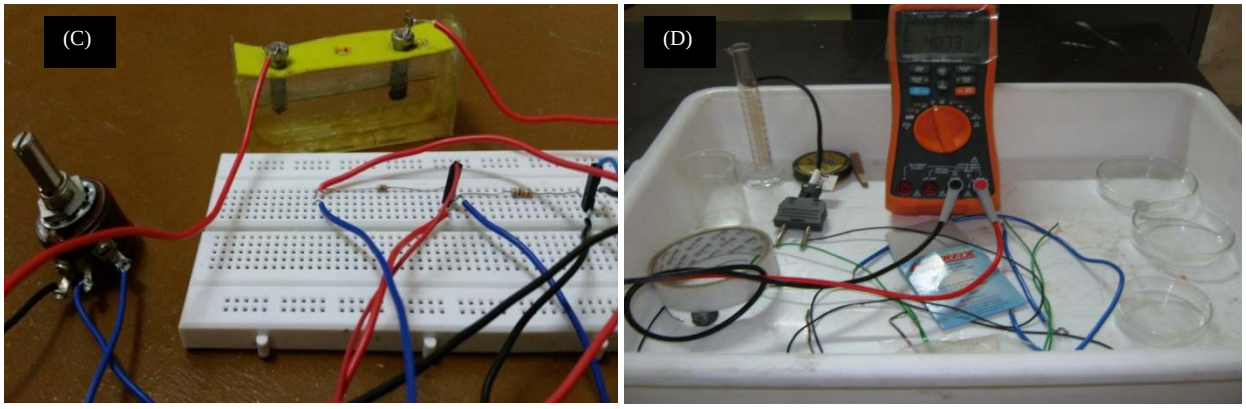

Fig 6.4 (A) Experimental set-up (B) Data logger Readings (C) Wheat-stone bridge circuit (D) Multi-meter connections to circuit

Experimental Data:

$R_4 = (R_w + R_p) = 3.57$ ohms

$R = R_1 = R_2 = 5.6$ ohms

R_3 (Resistance of potentiometer) = 3.5 ohms

$\alpha = 0.0039$ /k

R_o = Resistance of platinum wire (0.25mm thick) = 3.41 ohms

Experimental procedure

- Calculate the temperature coefficient of resistance of the platinum wire
- Calculate the thermal conductivity of distilled water for calibration purpose

Procedure for measuring the resistance of the platinum wire

Two-wire method is used for calculating the resistance. $R_1$is the platinum wire of length 3.5cm and is connected to two points in a breadboard.R_2 is a fixed resistance of known value (R_2= 3.331 Ω) and is connected in series with the wire. This overall series connection is then connected to a constant current supply, as shown in Fig 2.6. For each value of input current, ohms law V=IR holds for both R_1 and R_2. As the resistances are in series, the same value of current flows through both of them.

Thus, $V_1 = IR_1$, and

$V_2 = IR_2$.

$$\frac{V1}{R1} = \frac{V2}{R2}$$

$$R_2 = \frac{V_2}{V_1} X R_1$$

The voltages V_1 and V_2 across the resistances are measured using a multimeter, and the above equation is then solved for R_2 which gives the resistance of the platinum wire. This experiment is repeated for different values of input current, and the average of the calculated resistances is taken.

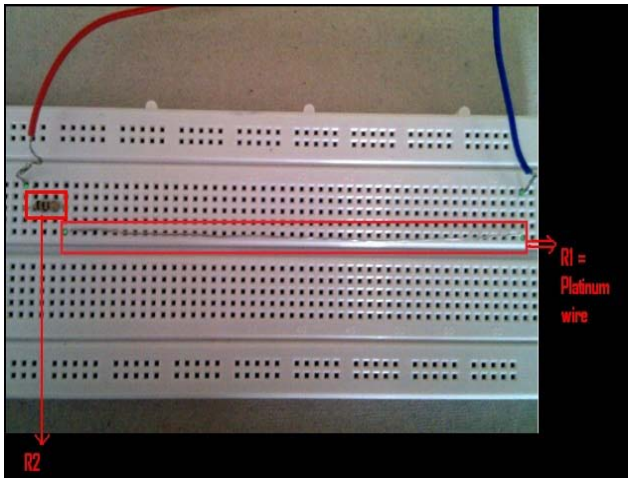

Fig.6.5: Series connection of resistors (R1 = Platinum wire and R2 = 3.331Ω)

Measurement of Temperature Coefficient of Resistance of the platinum wire (α)

α of a material is defined as the change in resistance per degree change in temperature. For a given platinum wire of a definite purity, it is a constant value. The equation for α is as follows:$\alpha = \frac{1}{Ro}\frac{\Delta R}{\Delta T}$, where R_o is the resistance of the platinum wire at the reference temperature To.The process of measuring α value involves measuring the resistance of the wire at different temperature values using the two-wire approach, and plotting the data. The graph between the resistance and temperature was plotted. The slope dR/dT is then divided by R_o to calculate α = 0.0039 /K. which is same as that of the published value.

$$\alpha = \frac{Slope}{Ro} = 0.0039\ /K$$

Measurement of the thermal conductivity for Distilled water:

The experimental setup was calibrated by using the DI water of known thermal conductivity (0.6009 W/m-K [45]) at a temperature of 22^{o}C and the values were taken 3-4 times using the same parameters.

Balancing of the Wheatstone bridge: Initially, a small value of current (2 mA) was supplied to the Wheatstone bridge circuit, and the potentiometer was slowly varied until the output voltage reaches approximately 10μV till the bridge was balanced (ratio R_1/R_2 is equal to R_3/R_4). The constant, low value of input current minimizes heating of the platinum wire during initial bridge balancing.

Once the bridge was balanced, the resistances of the potentiometer and the hotwire cell were measured and noted down, a constant current (75mA) was then supplied to the bridge at start time t=0, which created a voltage imbalance, ΔV, in the wheatstone bridge circuit due to a change in the resistance of the hotwire. The output voltage across the Wheatstone bridge was measured using a DATA LOGGER (A/D converter). These readings were recorded on the computer at the rate of 1reading/200milli-sec, by connecting the DATA Logger (A/D Converter) to a computer using a PC-Connectivity cable. The thermal conductivity is then calculated by using equation 6.16 by plotting the ln(t) vs ΔTw. The entire experiment was conducted at an optimum time period of 3-5 seconds to eliminate the thermal convection occurring during thermal conductivity of nanofluids measurements. For calibration purpose, standard DI Water was considered and by using our transient hot-wire method (THW), the thermal conductivity of DI Water was measured.

Fig 6.6 ((A) – (B)) plots the ΔT values against the ln(time) values for DI water at a temperature of 28^{o}C and an input constant current of 75mA and the value of thermal conductivity is obtained from the slope of the graph. The thermal conductivity of the DI Water by using eq.6.16 is 0.57 W/mk at 28^{o}C. The standard value is 0.607 W/mk at room temperature. The percentage of error is 5%. The thermal conductivity measurement of Jatropha biodiesel was also carried out using the same process. Fig 6.6(B) shows the plot of ln(t) vs ΔT for Jatropha biodiesel and thermal conductivity was calculated by eq. 6.16 and was found to be 0.25 W/mk.

Table 6.2 Thermal conductivity of DI water

Name of Fluid	Thermal Conductivity, W/mK (Literature value)	Thermal Conductivity, W/mK (Experimental value)	Error (%)
DI Water	0.607	0.57	5

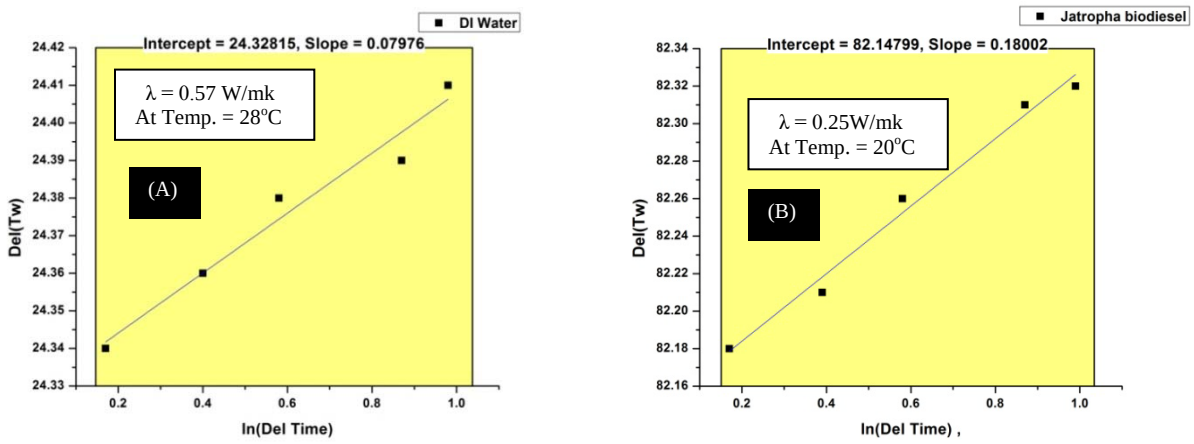

Fig 6.6 Plots of Del(Tw) vs ln(Del Time) to obtain slope of the graphs for thermal conductivity calculations (A) DI Water (B) Neat Jatropha biodiesel.

6.3Alumina NPs size effect on the Thermal Conductivity of nanofluids

Fig. 6.7(A - F) shows the plots of Del(Tw) and ln(Del Time) from which the thermal conductivity of average size ~13nm and ~28nm is calculated for a volume fraction of 0.1%. It is found from Fig 6.7(A – F) that the thermal conductivity of alumina nanofluids having a storage time of 27 months has the highest value when compared with that of as-prepared samples of both the sizes (~13nm and ~28nm). On comparing for different storage time durations also, it is found that the alumina nanofluids of ~13nm size with 0.1%VF, longest storage time duration has the highest thermal conductivity (which is for 27months). This may be due to the changes in the morphological effect from spherical to cubicles and also due to the increase in size of the nanoparticles.

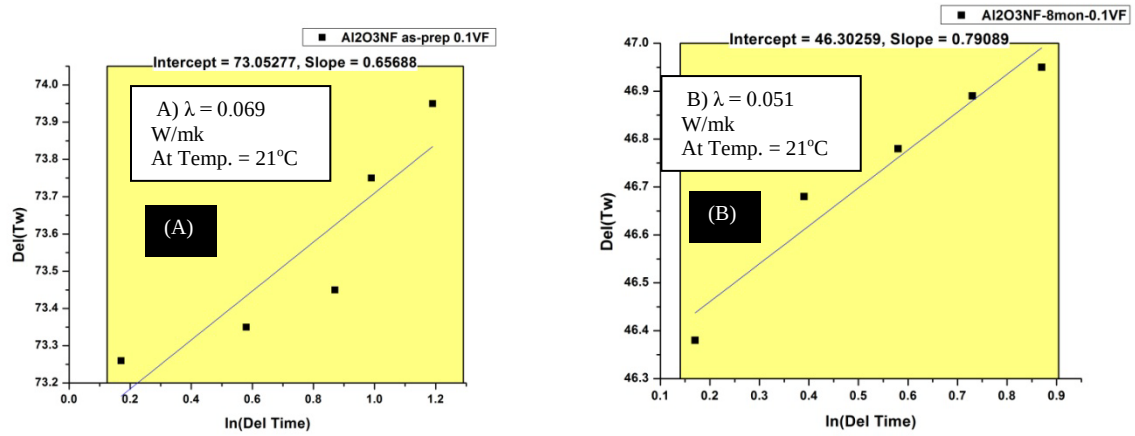

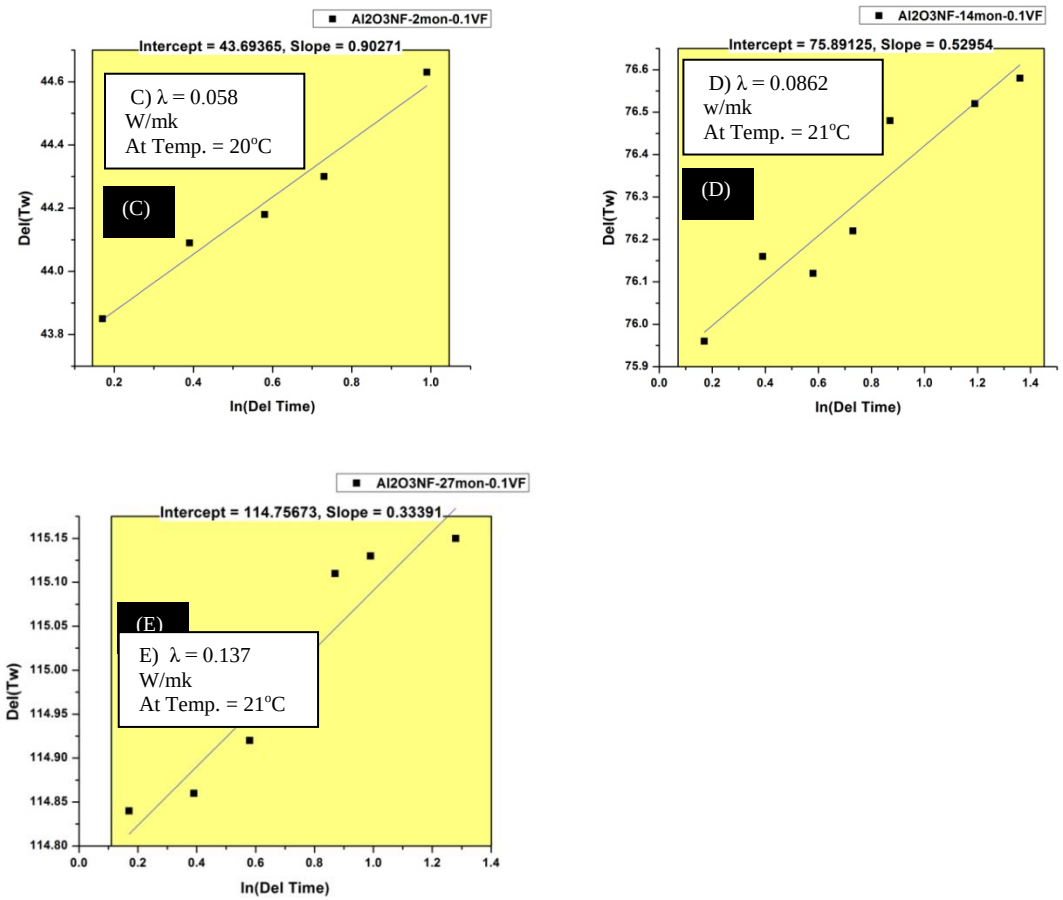

Fig 6.7 Plots of Del(Tw) vs ln(Del Time) to obtain slope of the graphs for thermal conductivity calculations of Al_2O_3 NF 0.1%VF (A) ~13nm as-prepared (B) ~13nm 2Months old (C) ~13nm 8Months old (D) ~13nm 14Months old (E) ~13nm 27 Months old (F) ~28nm as-prep sample respectively.

Fig 6.8(a and b) shows the plot of Thermal conductivity versus stability time duration of alumina nanofluids having 0.1%vf respectively. From Fig. 6.9(a), it is seen that Thermal Conductivity (TC) is initially high for as-prepared samples because for larger number alumina nanoparticles are being dispersed in the Jatropha biodiesel. Then, there is decrease in TC of alumina nanofluids which is due to the reason that some of the alumina nanoparticles being larger in size gets agglomerated and settles down at the bottom of the sample tubes, thus, not contributing to the dispersion state of the nanofluids. This effect is seen is in the Fig. 6.8 upto to the stability time of 2months for 0.1%VF. After 2 months of storage time, there would be increase in the size of the alumina nanoparticles due to which there is again an increase in the thermal conductivity of alumina nanofluids. This trend is observed upto a storage time of 27months as seen in Fig 6.8.

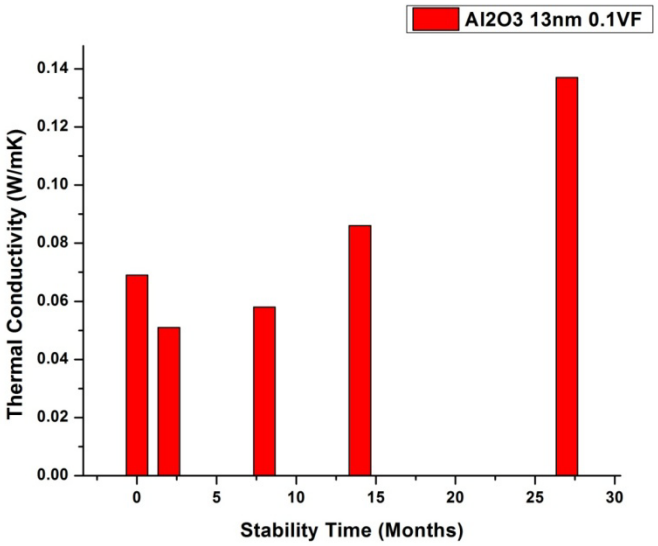

Fig 6.8: Thermal Conductivity versus Stability Time of alumina nanofluids (~13nm) 0.1%VF for different stability time.

6.4MWCNTs effect on Thermal Conductivity of nanofluids:

Fig 6.9 (A – D) shows the plots of ΔT values against the ln(time) values for as-prepared and 10days older samples of MWCNTs dispersed Jatropha biodiesel based nanofluids having 2 different percentage volume fractions namely 0.001 and 0.005 respectively and using the Eq. 6.16, the thermal conductivity is calculated. It is found that the as-prepared sample having 0.0005%VF of MWCNTs is having the highest thermal conductivity of 0.127 W/mk, while the as-prepared sample with 0.001%VF of MWCNTs was having 0.035W/mk. This may be due to the variations in the concentrations of 0.001%VF as compared to the sample with 0.005%VF. The thermal conductivity of sample with 10days older is comparatively less than the as-prepared samples since the MWCNTs during the 10days of storage time must have got agglomerated due to very high density and hence, the MWCNTs must have got settled down at the bottom of the sampling tube

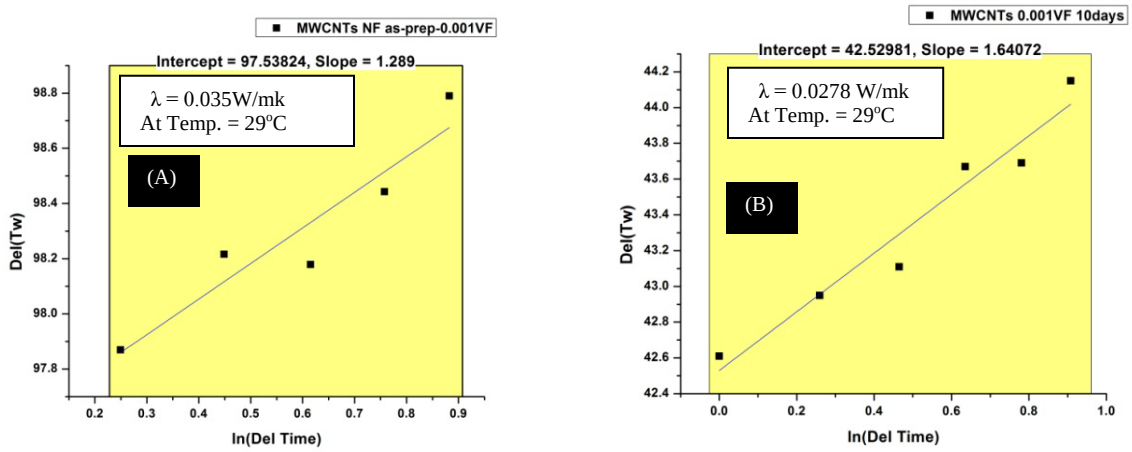

Fig 6.9 Plots of Del(Tw) vs ln(Del Time) to obtain slope of the graphs for thermal conductivity calculations of MWCNTs nanofluids : (A) 0.001%VF as-prepared (B) 0.001%VF 10days old (C) 0.005%VF as-prepared (D) 0.005%VF 10days old samples respectively

6.5 Material Effects (alumina and MWCNTs) on the Thermal conductivity of nanofluids

Table 6.2 compares the thermal conductivity of Al_2O_3 NPs and MWCNTs dispersed Jatropha biodiesel based nanofluids for as-prepared and older storage samples having different volume fractions. It is seen that thermal conductivity of MWCNTs having 0.005%VF has higher thermal conductivity than that of Al_2O_3 nanofluids of 0.1%VF. From this result it is concluded that the thermal conductivity of MWCNTs is higher than alumina nanoparticles.

Table 6.3 : Experimental measurement of Thermal Conductivity of different fluids

Name of the fluid	Nanoparticles sizes	% Volume Fractions of nanomaterials dispersions	Storage Time of nanofluids	Thermal Conductivity W/mk
DI Water		-	-	0.57
Jatropha Biodiesel		-	-	0.25
Al_2O_3 NF	13nm	0.1	As-prepared	0.069
Al_2O_3 NF	13nm	0.1	2Months	0.051
Al_2O_3 NF	13nm	0.1	8Months	0.058
Al_2O_3 NF	13nm	0.1	14Months	0.086
Al_2O_3 NF	13nm	0.1	27Months	0.137

MWCNTs NF		0.001	As-prepared	0.035
MWCNTs NF		0.001	10days	0.0278

6.6 Conclusions:

In this chapter, thermal conductivity of alumina nanofluids and MWCNTs dispersed nanofluids was investigated. The set-up for the same was in-house designed and the validity of the set-up was confirmed by conducting the thermal conductivity experiments for known fluids such as DI-Water. After confirming the percentage of error to be within 5%, thermal conductivity of alumina and MWCNTs dispersed Jatropha biodiesel based nanofluids were carried out for 0.1%VF(in the case of alumina nanofluids) and 0.001 and 0.005%VF (in the case of MWCNTs) having different storage time to find out the optimum value.

Table 6.2 shows that Al_2O_3 nanofluids of 0.1%VF having a storage time of 27 months has the highest thermal conductivity of 0.137W/mK compared to all other samples of ~13nm size and also as-prepared samples of ~28nm. This effect can be related to the changes that take place in the size and morphology of alumina nanofluids as shown in the TEM image of Fig.4.6.
In the case of MWCNTs, as-prepared sample of 0.005%VF has higher thermal conductivity of 0.127W/mK when compared to 10 days older sample of the same concentration. Since during the storage time of 10 days, some of the MWCNTs might have formed clusters and would have got settled down in the sample tube and the remaining MWCNTs which are in suspensions state even after 10days remained as active participants for the thermal conductivity properties of the nanofluids.

On comparing the material effect of alumina nanoparticles and MWCNTs, it is seen from the Table 6.2 that the thermal conductivity for as-prepared samples of MWCNTs having 0.005%VF is very much higher even for a small percentage of volume fractions as compared to that of Al_2O_3 nanofluids having 0.1%VF. This may be due to the fact that MWCNTs has larger surface area of contact when compared to the alumina nanoparticles.

Chapter 7

Nanomaterials and Their Size Effect on Hot-Plate Evaporation Rate Testing of Nanofluids

7.1 Introduction

This chapter deals with the evaporation rate study of both the materials that is, alumina and MWCNTs based biodiesel based nanofluids. Since 0.1%VF alumina NPs based nanofluids are showing better stability, all the tests were performed only for 0.1%VF having an ~13nm and ~28nm nanofluids only. Also the evaporation rate for longer storage time nanofluids for both alumina and MWCNTs are discussed.

7.2 Experimental set-up of the hot-plate evaporation rate test:

The experimental set-up for evaporation rate measurement consists of a hot-plate of 100mm x 100mm x 4mm which was placed on the electric heater with a curvature of 2mm depth and 5mm diameter machined at its centre. At a distance of 25mm from the hot-plate, the burette filled with alumina nanoparticles dispersed biodiesel based nanofluids of the required percentage volume fraction was fixed with the help of retort stand. Also a K-Type thermocouple was fixed on the

curvature of the hot plate with one end while the other end of K-Type thermocouple was fixed to the multimeter to measure the temperature of the hot plate during the evaporation of the fuel droplets. Fig 7.1 show the schematic of the experimental set-up for the evaporation rate measurements wherein the droplets of respective nanofluids were made to fall on the curvature of the hot-plate, and the time taken to evaporate the droptlets of the nanofluids were noted down. Fig 7.2 show the experimental set-up for the evaporation rate measurement. This procedure was done for the different samples and plots of temperature vs. evaporation time was plotted accordingly.

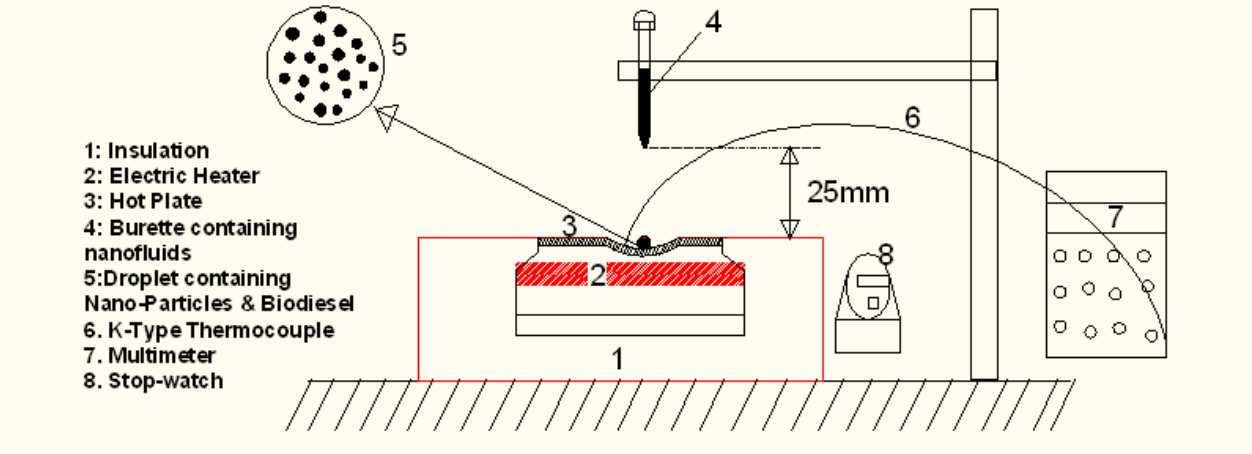

Fig.7.1: Schematic of the experimental set-up for evaporation rate test

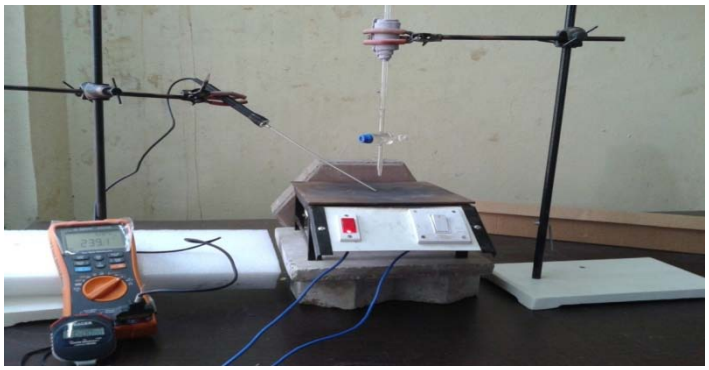

Fig.7.2: Experimental set-up for the evaporation rate test of the nanofluids

7.3 Alumina NPs size effect on Hot-Plate Evaporation Rate of nanofluids

The experimental tests were conducted for a set of ~13nm sizes 0.1%VF and ~28nm sizes 0.1%VF nanofluids and also for different storage time nanofluids for a temperature range of 300^{o}C to 900^{o}C for every 20^{o}C rise in temperature. This difference of temperature was given so

that when the first droplet hits the surface of the hot-plate, it was observed that the temperature of the hot-plate instantly cools down by ~20^{o}C. So some time was to be considered for maintaining uniformity in rise of hot-plate temperature before the testing of the subsequent fuel droplets on the hot-plate. In this way the hot-plate evaporation rate test was conducted for 5 different samples, namely, pure diesel oil, pure Jatropha biodiesel, alumina nanofluids of 0.1%volume fractions (~13nm) of as-prepared samples, 1month old samples and 1Year old samples.

Droplet Size Calculations:

73 droplets of alumina nanofluids = 2ml

Therfore, 1 droplet = 2/73 ml = 0.0274ml

Therefore, 0.0274ml = $(4/3) * \pi * (r_{Avg})^3$

Therefore, r_{Avg} = 0.187cm

Therefore **average diameter, d_{Avg} of the droplet size** = $(2*r_{Avg})$ = **0.374cm**

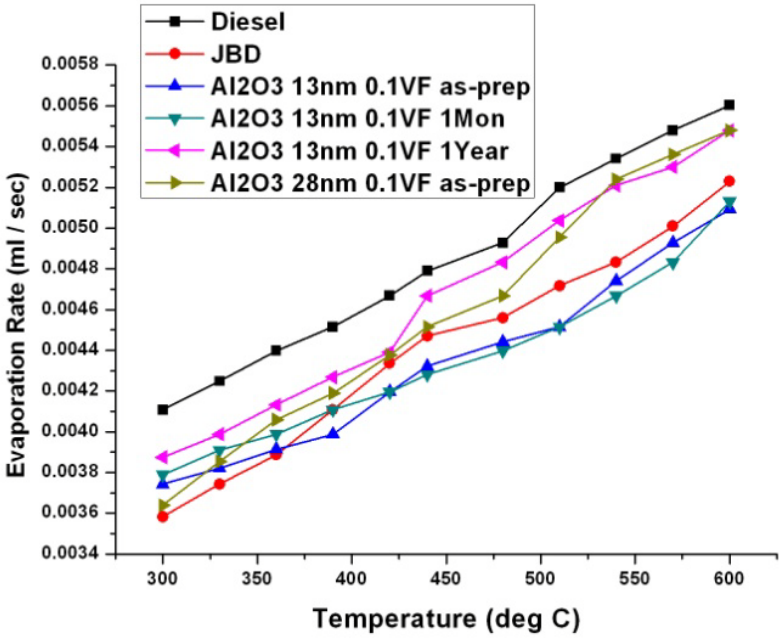

Fig.7.3: Plots of evaporation rate vs temp for as-prepared ~13nm and 28nm alumina nanofluid and different storage time ~13nm alumina nanofluids for temperature range of 300^{o}C to 600^{o}C.

Fig.7.3 shows the evaporation rate with alumina nanofluids of ~13nm size with 0.1%volume fractions at different temperatures of 300^{o}C to 600^{o}C for the as-prepared samples of ~28nm having 0.1%VF and with different storage time of ~13nm alumina nanofluids samples. These are

compared with the evaporation rate results of pure diesel and also with pure Jatropha biodiesel over a temperature range of 300°C to 900°C maitaining a temperature difference of 20°C. The evaporation rate test experiments were conducted for alumina nanofluids of ~13nm having 0.1% volume fraction for three different stability times namely, as-prepared samples, 1 month old sample and 1 year old samples and also for 0.1%VF of average size ~28nm Al_2O_3 nanofluids as-prepared samples. These results were compared with evaporation rate results of pure diesel and pure Jatropha biodiesel. From Fig 7.3, it is clear that ~28nm as-prepared Al_2O_3 nanofluids evaporation rate is always higher than ~13nm as-prepared Al_2O_3 nanofluids. Hence increasing the size of the alumina nanoparticles, the biodiesel evaporation rate can be improved. However it is also observed from Fig 7.3 that for ~13nm 1year stored time sample, evaporation rate is very comparable to neat diesel at higher temperatures beyond 450°C. Same improvements in evaporation rate is seen for ~28nm Al2O3 sample beyond 550°C. From Tem analysis (Fig 4.7), it is confirmed that one year older ~13nm Al2O3 nanofluids, size and morphology changes to ~40nm and cubical shapes. This may be the reason that for one year stored time~13nm Al_2O_3 nanofluids, evaporation rate is improved as compared to as-prepared and 1months stored time ~13nm Al_2O_3 nanofluids.

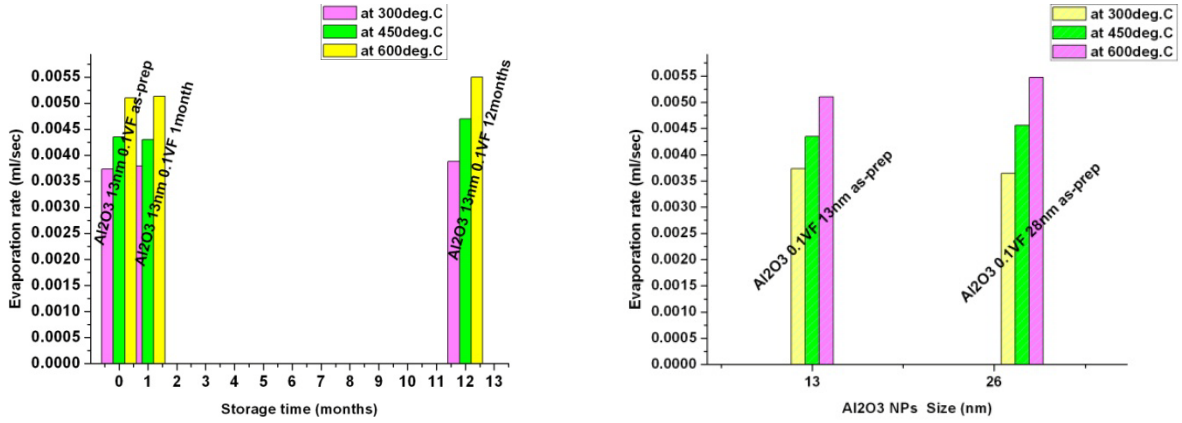

Fig 7.4 (A).Evaporation rate vs storage time of Al_2O_3 NF ~13nm size at 300, 450 and 600°C

Fig(B)Evaporation rate of both sizes of Al_2O_3 NPs (~13 and ~28nm) at 300, 450 and 600°C

Fig7.4(A) compares the evaporation rate of the stored samples of Al_2O_3 ~13nm size nanofluids at 3 different temperatures 300°C, 450°C and 600°C for as-prepared, 1month old and 12months older samples respectively. From Fig 7.4(A), it is confirmed that the enhancement in evaporation

rate is higher for 12months older Al_2O_3 nanofluids when compared with 1 month and as-prepared Al_2O_3 nanofluids. Fig 7.4(B) compares the size effect of evaporation rate for both the Al_2O_3 nanofluids at 3 different temperatures 300^{o}C, 450^{o}C and 600^{o}C respectively. It is confirmed that the evaporation rate of as-prepared samples of Al_2O_3 nanofluids for ~28nm size is marginally higher than that of as-prepared samples of ~13nm size Al_2O_3 for temperatrures higher than 450^{o}C. While at lower temperature (300^{o}C) evaporation rate of smaller size (~13nm) Al_2O_3 nanofluids is showing higher evaporation rate than that of larger size (~28nm) Al_2O_3 nanofluids. This effect may be due to the reason that in larger size Al_2O_3 nanofluids, more quantity of JBD may be seeped inside the alumina nanoparticles ahd hence better enhancement if evaporation rate is occuring as compared to its counter one of ~13nm size alumina nanofluids.

7.4 MWCNTs effect on evaporation rate of nanofluids

In this test, multi-walled carbon nanotubes dispersed jatropha biodiesel based nanofluids (0.001 and 0.005%VF) as-prepared and 10days older samples were tested for the evaporation rate and the results were plotted for different temperatures. In this experiment of hot-plate evaporation rate of MWCNTs nanofluids, the droplets of test samples (i.e, MWCNT's dispersed nanofluids) were made to fall on the middle portion of the curvature of the hot-plate, and the time taken to evaporate the droptlets completely were noted down. Same procedure was done for all the different MWCNT's dispersed nanofluids and also with pure jaropha biodiesel and pure diesel oil. Fig.7.5 shows the evaporation rate of the 0.001%VF MWCNTs nanofluids for as-prepared and also for 10days older samples along the evaporation rate of diesel and JBD.

From Fig 7.5, it is clear that at higher temperatures, the evaporation rate of 0.001%VF of 10 days storage MWCNTs nanofluids is higher than that of 0.001%VF MWCNTs dispersed as-prepared nanofluids samples. Therefore, longer term stored MWCNTs nanofluids are showing better evaporation rate as compared to the as-prepared samples at higher temperatures. Also by comparing 0.001%VF with the diesel and Jatropha bio-diesel (basefluid), 0.001%VF at higher temperature is showing enhancement in the evaporation rate beyond 525^{o}C. At this temperature 0.001%VF is showing better evaporation rate when compared to the of commercial diesel also.

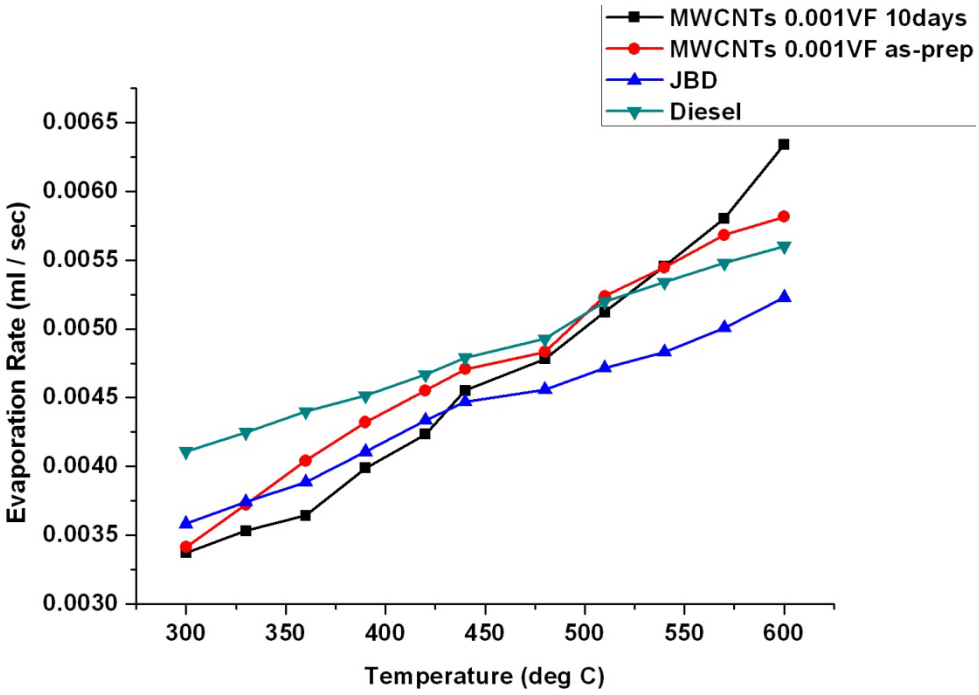

Fig.7.5: Evaporation rate of MWCNTs nanofluids for as-prepared and their longer storage time samples with neat JBD and Diesel fuel.

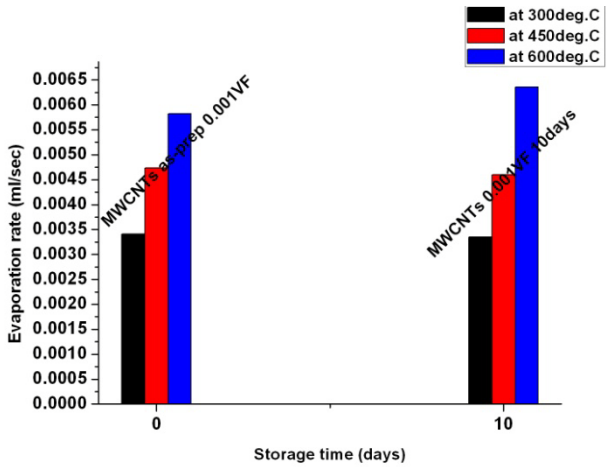

Fig7.6 Evaporation rate vs storage time of MWCNTs at 300, 450 and 600^{o}C

Fig7.6 shows the evaporation rate of MWCNTs nanofluids having 0.001%VF for as-prepared and 10days older samples at three different temperature 300^{o}C, 450^{o}C and 600^{o}C respectively. From the Fig 7.6, it is clear that at all the temperature, as the temperature incereases evaporation rate of the MWCNTs nanofluids increases for both as-prepared and 10days older samples, but the rate increase of evaporation rate is higher for 10days oder samples at 600^{o}C.This may be due

to the reason that during the 10 days of storage time, some quantity of JBD (basefluids) may have got accumulated inside the hollow tubes of MWCNTs and hence the combined effect of JBD and MWCNTs is improving the evaporation rate of MWCNTs nanofluids.

7.5 Material Effect (Alumina and MWCNTs) of nanofluids:

In this section, the best samples evaporation rate of Al_2O_3 nanofluids (~13nm) and MWCNTs nanofluids of as-prepared samples and their longer storage samples are compared with their evaporation rate versus temperature. From Fig 7.5, it is observed that at lower temperature ~13nm Al_2O_3 nanofluids having 0.01%VF of 1year storage sample is showing higher evaporation rate as compared to MWCNTs based nanofluids having 0.001%VF. However at higher temperature (beyond 500^{o}C) MWCNts based nanofluids are showing better evaporation rate even higher than the commercial diesel.

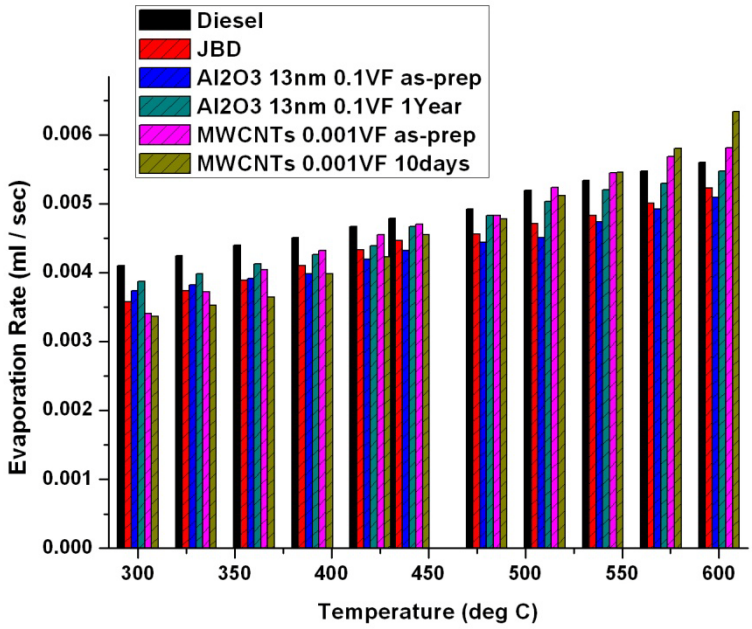

Fig.7.5: Evaporation Rate Vs Temperature of as-prepared and longer stability time samples of Al_2O_3 (~13nm) and MWCNTs along with neat Jatropha biodiesel and commercial diesel.

7.6 Conclusions:

The hot-plate evaporation rate test is conducted for stable alumina nanoparticles (~13nm size) and also for MWCNTs dispersed jatropha biodiesel based nanofluids for different percentage volume fractions and also for their higher stable storage time samples for a temperature range of 300^{o}C to 600^{o}C. From these experimental results, it is concluded that alumina nanofluids of

1year duration of stability time is showing higher evaporation rate and is comparable to that of diesel fuel at a temperature range of 525^{o}C to 600^{o}C while the MWCNT's dispersed nanofluids was having an evaporation rate of 0.001% volume fractions of as-prepared samples and also with that of 10 days older samples, the evaporation rate is much closer to that of pure diesel at a temperature range of 420^{o}C to 600^{o}C.

Chapter-8

CONCLUSIONS

In this research work, investigations were carried out to study the effect of nanomaterials on their size and nature of the nanomaterials for the improvement in the energy applications of the diesel engine so that the few of the important long term issues of the alternate fuels such as stability of the nanofluids, viscosity of the nanofluids, burning rate of the nanofluids and thermal conductivity of the nanofluids, for improvement in efficiency of the diesel engines can be obtained. In this regard, alumina nanomaterials of two different sizes and MWCNTs were considered to investigate the size effect and material effect of the nanofluids on the important properties such as stability of the nanofluids, viscosity of the nanofluids, evaporation rate of the nanofluids and thermal conductivity of the nanofluids.

Nanofluids were prepared for two different sizes of alumina NPs and also for MWCNTs. Results showed that alumina nanofluids having ~13nm of 0.1%VF showed a stability of more than 14months with changes in its morphology. The size of the alumina nanomaterials has changed from ~13nm to ~40nm and their shape also changed from spherical to cubical which were confirmed from TEM images of Fig.4.7. While the alumina nanofluids of ~28nm did not show any of the long term stability properties. Due to this reason, further investigation on properties such as viscosity, thermal conductivity and evaporation rate were confined to alumina nanofluids of ~13nm only.

MWCNTs nanofluids, were also prepared for various percentage volume fractions out of which only 0.001%VF showed a stability duration of 10 days and hence, further investigations of MWCNTs nanofluids such as viscosity, thermal conductivity and evaporation rate were limited only to 0.001%VF.

Investigations carried out on the viscosity of the alumina nanofluids revealed that the alumina nanofluids of ~13nm having 0.1%VF of as-prepared sample and also 14months older samples are less viscous than that of neat biodiesel. This effect may be due to the interaction of the particle to particles and also due to the Brownian motion of the jatropha biodiesel and the

alumina NPs of ~13nm size. Due to the smaller size, these nanomparticles undergo changes in their size and shape and hence induce the charge effect with the jatropha biodiesel thus reducing in the viscosity of the nanofluids. In the case of MWCNTs dispersed jatropha biodiesel based nanofluids, investigations was done only for 0.001%VF of as-prepared samples since, stability of 10 days was achieved only for 0.001%VF. The results of viscosity of MWCNTs nanofluids also showed the similar trend. That is, viscosity of MWCNTs dispersed nanofluids was comparatively less than that of neat jatropha biodiesel.

Studies on thermal conductivity of alumina nanofluids was carried out for ~13nm size having different stability time durations such as as-prepared, 2Months, 8Month, 14Months and 27Months older samples respectively and it was found that the alumina nanofluids of ~13nm size having 0.1%VF stored for 27months has the highest thermal conductivity of 0.137W/mK than the rest of the stored samples. The alumina nanofluids of 0.1%VF with 27 months of stored duration improves the heat conducting capacity of the nanofluids due to the changes of sizes of the nanoparticles from ~13nm to ~40nm. In the case of MWCNTs, the thermal conductivity was carried out only for as-prepared sample of 0.001%VF and it was found to be 0.035W/mK.

Hot-Plate evaporation rate test of alumina nanofluids and MWCNTs nanofluids were carried out for alumina nanofluids of ~13nm and ~28nm sizes and the results were compared with that of neat jatropha biodiesel and also with commercially available diesel. From the results of hot-plate evaporation rate, it was concluded that the alumina nanofluids of 14months old sample has the higher evaporation rate at higher temperatures of 525^{o}C. Also it was found that at higher temperature, alumina nanofluids of ~13nm size (14months old sample) possess higher evaporation rate than that of neat jatropha biodiesel. In the case of MWCNTs, the hot-plate evaporation rate was carried out for 0.001%VF. The results showed that the evaporation rate of 0.001%VF MWCNTs nanofluids was even more higher than the alumina nanofluids of all the samples and it is almost the same as that of commercial diesel at a temperature of 450^{o}C and above.

- **LIMITATIONS and SCOPE FOR FUTURE WORK:**

In this work there were many limitations due to which compromises has to be made some of which were mentioned below. One of the most important limitations was the characterization of

the stability of nanofluids. To investigate the long term stability of the nanofluids, one needs to characterize the nanofluids on regular basis on different characterizing tools such as FESEM and TEM. But due to the busy schedule of the FESEM or TEM instruments, characterizing on regular basis of one year was not possible. Also, this research project requires more exhaustive work which could not be completed due to the time constraint. Hence the future work requires some of the following investigations listed below:

- More intensive work on long term stability of MWCNTs dispersed nanofluids which needs novel surface functionalization or modification of MWCNTs for longer term stability.
- Advanced tools for carrying out the Thermal Conductivity and Ignition Probability tests of nanofluids.
- Advanced machinery equipment for the testing of efficiency and emissions of the nanofluids on the diesel engine test rig.
- Investigations of many other oxide nanomaterials on the stability of the nanofluids.

***

REFERENCES:

1. A. Brito, M. E. Borges, and N. Otero "Zeolite Y as a Heterogeneous Catalyst in Biodiesel Fuel Production from Used Vegetable Oil" Energy & Fuels2007,21,3280–3283 doi: 10.1021/ef700455r
2. Kafuku, G., and M. Mbarawa. "Alkaline CatalyzedBiodiesel Production fromMoringaoleiferaOil with Optimized Production Parameters".Applied Energy 87 (8):2561–2565 (2010)
3. Amish P. Vyas, N. Subrahmanyam, Payal A. Patel, "Production of biodiesel through transesterification of Jatropha oil using KNO3/Al2O3solid catalyst", Fuel 88 (2009) 625–628doi:10.1016/j.fuel.2008.10.033
4. Olamide A. Oshodi, Chikaodili E. Chukwuneke and Okoro Linus *"The viscometric analysis of biodiesel from mustard and coconut Oil" Eur. Chem. Bull.,* 2014, *3(9),* 946-948
5. Macor A, Avella F, Faedo D. Effects of 30% v/v biodiesel/diesel fuel blend on regulated and unregulated pollutant emissions from diesel engines. Appl Energy 2011; 88:4989–5001
6. Sidibé SS, Blin J, Vaitilingom G, Azoumah Y. Use of crude filtered vegetable oil as a fuel in diesel engines state of the art: literature review. Renew Sust Energy Rev 2010;14:2748–59
7. Lacey P, Gail S, Kientz JM, Milovanovic N, Gris C, Jahirul MI. Internal fuel injector deposits. JSAE 20119075, SAE 2011-01-1925; 2011.
8. Ali Y. Beef tallow as a biodiesel fuel: the graduate college in the University of Nebraska; 1995.
9. Qi DH, Chen H, Geng LM, Bian YZ, Ren XC. Performance and combustion characteristics of biodiesel–diesel–methanol blend fuelled engine. Appl Energy 2010;87:1679–86
10. Pehan S, Jerman MS, Kegl M, Kegl B. Biodiesel influence on tribology characteristics of a diesel engine. Fuel 2009;88:970–9
11. Celik I, Aydin O. Effects of B100 biodiesel on injector and pump piston. Tribol T 2011;54:424–31
12. Caprotti R, Breakspear A, Klaua T, Weiland P, Graupner O, Bittner M. RME behavior in current and future diesel fuel FIE's. SAE Ppaer No. 2007-01 3982; 2007.
13. Sinha S, Agarwal AK. Experimental investigation of the effect of biodiesel utilization on lubricating oil degradation and wear of a transportation CIDI engine. J Eng Gas Turb Power 2010;132:42801–11
14. Reksowardojo IK, Bui HN, Sok R, Kilgour AJ, Brodjonegoro TP, Soerawidjaja TH, et al. The effect of biodiesel fuel rubber (hevea brasiliensis) seed oil on a direct injection (DI) diesel engine. Asean Eng J 2011;1:65–81
15. Agarwal AK. Biofuels (alcohols and biodiesel) applications as fuels for internal combustion engines. Prog Energy Combust 2007;33:233–71
16. Haseeb ASMA, Fazal MA, Jahirul MI, Masjuki HH. Compatibility of automotive materials in biodiesel: a review. Fuel 2011;90:922–31

17. Basinger M, Reding T, Rodriguez-Sanchez FS, Lackner KS, Modi V. Durability testing modified compression ignition engines fueled with straight plant oil.Energy 2010;35:3204–20
18. Leung DYC, Wu X, Leung MKH. A review on biodiesel production using catalyzed transesterification. Appl Energy 2010;87:1083–95
19. Shu G, Dong L, Liang X. A review of experimental studies on deposits in thecombustion chambers of internal combus. Int J Eng Res 2012
20. Leedham A, Caprotti R, Graupner O, Klaua T. Impact of fuel additives on diesel injector deposits. SAE Paper No. 2004-01-2935; 2004.
21. S.Karthikeyan, A.Elango, and A.Prathima "Performance and Emission Study on Zinc Oxide Nanoparticles addition with Promolion Stearin Wax Biodiesel of C I Engine" Journal of Scientific and Industrial Research, Vol. 73 March 2014 , pp187 – 190
22. A. Eyssartier, B. Cuenot, L.Y.M. Gicquel and T.Poinsot CERFACS "Using LES to predict ignition sequences and ignition probability of turbulent two-phase flames" Preprint submitted to Comb. and Flame, June 10, 2011
23. A. Mishra , L. Kundan & S. S. Mallick "Modeling Thermal Conductivity for Alumina-Water Nanofluids" , Particulate Science and Technology: An International Journal, 32:3, 319-326, (2014) DOI: 10.1080/02726351.2013.835599
24. Ali Alahmer "Reduction a Particulate Matter of Diesel Emission by the Use of Several Oxygenated Diesel Blend Fuels" Int. J. of Thermal & Environmental Engineering Volume 7, No. 1 (2014) 45-50 DOI: 10.5383/ijtee.07.01.006
25. Anurag S.Hatwar, V.M.Kriplani "A review on Heat Transfer Enhancement with Nanofluids" International Journal of Advance Research In Science And Engineering , IJARSE, Vol. No.3, Issue No.3, March 2014
26. B. Akbari, M. Pirhadi Tavandashti and M. Zandrahimi "Particle Size Characterization of Nanoparticles – A Practical approach" Iranian Journal of Materials Science & Engineering Vol. 8, Number 2, Spring 2011
27. P.Keblinski, S.R.Phillpot, S.U.S.Choi and J.A.Eastman, "Mechanisms of heat flow in suspensions of nano-sized particles (nanofluids)International Journal of Heat and Mass Transfer 45 (2002) 855-863.
28. B. Kerschgens, T. Lackmann, H. Pitsch, A. Janssen, M. Jakob and S. Pischinger " Tailored surrogate fuels for the simulation of diesel engine combustion of novel biofuels" THIESEL 2012 Conference on Thermo- and Fluid Dynamic Processes in Direct Injection Engines.
29. Bruno Lamas , Bruno Abreu, Alexandra Fonseca, Nelson Martins, Mónica Oliveira "Assessing colloidal stability of long term MWCNTs based nanofluids" Journal of Colloid and Interface Science 381 (2012) 17–23 doi.org/10.1016/j.jcis.2012.05.014
30. Bui Hung Thang, Phan Hong Khoi, and Phan Ngoc Minh "Simulation of Heat Dissipation for High Power Electronic Component using Carbon Nanotube Nanofluids" International Journal of Scientific and Research Publications, Volume 4, Issue 10, October 2014

31. C. Yang, W.Li, A. Nakayama "Convective heat transfer of nanofluids in a concentric annulus" International Journal of Thermal Sciences 71 (2013) 249 - 257 doi.org/10.1016/j.ijthermalsci.2013.04.007
32. Calin D. Iclodean, Florin Mariasiu "Possibility to Increase Biofuels Energy Efficiency used for Compression Ignition Engines Fueling" TEM Journal – Volume 3 / Number 1 /2014
33. D. Madhesh and S. Kalaiselvam "Preparation and Characterization of MWCNT -Water Nanofluids for Heat Transfer Applications" International Journal of Advanced Mechanical Engineering. Volume 4, Number 2 (2014), pp. 193-198.
34. D. Subramaniam , A. Murugesan , A. Avinash & V. Arivadivan "A characteristic evaluation of alumina–zirconia-coated engine fuelled with punnai methyl ester" International Journal of Ambient Energy, (2013) DOI: 10.1080/01430750.2012.759152
35. Dongsheng Zhu, Xinfang Li, Nan Wang, Xianju Wang, Jinwei Gao, Hua Li "Dispersion behavior and thermal conductivity characteristics of Al2O3–H2O nanofluids" Current Applied Physics 9 (2009) 131–139 doi:10.1016/j.cap.2007.12.008
36. Douglas Hector Fontes, Enio Pedone Bandarra Filho "Theoretical analysis of alumina-water Nanofluids flowing in Horizontal tubes" 22nd International Congress of Mechanical Engineering (COBEM 2013) November 3-7, 2013, Ribeirão Preto, SP, Brazil
37. Dr Paul Holdstock "Does charge transfer correlate with ignition probability?" Journal of Physics: Conference Series142(2008) 012009 doi:10.1088/1742-6596/142/1/012009
38. Dr. V. Ravi, Mabusabu "A Study on Heat Transfer Characteristics Of Ethylene Glycol based nanofluid And Carbon Nanotube (CNT) Mixture In Nucleate Pool Boiling." International Journal of Mechanical Engineering Research & Applications (IJMERA) Vol. 1 Issue 4, September – 2013
39. E. Ekramian, S. Gh. Etemad, M. Haghshenasfard "Numerical Investigations of Heat Transfer Performance of Nanofluids in a Flat Plate Solar Collector" International Journal of Theoretical and Applied Nanotechnology Volume 2, Year 2014 DOI: 10.11159/ijtan.2014.005
40. E. Sukjit, J.M. Herreros, K.D. Dearn, A. Tsolakis, K. Theinnoi" Effect of hydrogen on butanolebiodiesel blends in compression ignition engines" international journal of hydrogen energy 38 (2013) 1624e1635 doi.org/10.1016/j.ijhydene.2012.11.061
41. Fabiana C. Hamilton, Rogério N. Carvalho, Marcelo J. Colaço, and Albino J. K. Leiroz "Heat Transfer Coefficient Estimation of an InternalCombustion Engine using Particle Filters" EngOpt 2012 – 3rd International Conference on Engineering Optimization Rio de Janeiro, Brazil, 01 - 05 July 2012.
42. Faris Mohammed Ali, W. Mahmood Mat Yunus and Zainal Abidin Talib "Study of the effect of particles size and volume fraction concentration on the thermal conductivity and thermal diffusivity of Al2O3 nanofluids" International Journal of Physical Sciences Vol . 8(28), pp. 1442-1457, 30 July, 2013 DOI: 10.5897/IJPS10.544
43. Fei Duan "Thermal Property Measurement of Al2O3-Water Nanofluids" School of Mechanical and Aerospace Engineering, Nanyang Technological University Singapore (2012)

44. Feng-Chen Li, Juan-Cheng Yang, Wen-Wu Zhou, Yu-Rong He, Yi-Min Huang, Bao-Cheng Jiang "Experimental study on the characteristics of thermal conductivity and shear viscosity of viscoelastic-fluid-based nanofluids containing multiwalled carbon nanotubes" Thermochimica Acta 556 (2013) 47– 53 doi.org/10.1016/j.tca.2013.01.023
45. George Okeke, Sanjeeva Witharana, Joseph Antony, Yulong Ding "Computational Analysis of Factors Influencing Enhancement of Thermal Conductivity of Nanofluids" Institute of Particle Science and Engineering, University of Leeds, Leeds, LS2 9JT, UK
46. Haifeng Jiang, Hui Li, Qianghui Xu, Lin Shi "Effective thermal conductivity of nanofluids considering interfacial nano-shells" Materials Chemistry and Physics 148 (2014) 195e200 doi.org/10.1016/j.matchemphys.2014.07.031
47. Harish Kumar Patel ,Dr. V.N.Bartaria "Review and Experimental Comparison of Al_2O_3 and Water Mixture Based NanofluidThermal Conductivity as Heat Transfer Fluid" IPASJ International Journal of Mechanical Engineering (IIJME) Volume 2, Issue 9, September 2014
48. Heydar Maddah, Mahdokht Rezazadeh, Mojtaba Maghsoudi and Syamak NasiriKokhdan "The effect of silver and aluminum oxide nanoparticles on thermophysical properties of nanofluids" Journal Of Nanostructure in Chemistry2013,3:28
49. How-Ran Chao, Ta-Chang Lin, Mu-Rong Chao, Feng-Hsiang Chang, Chao-I Huang, Chung-Bang Chen "Effect of methanol-containing additive on the emission of carbonyl compounds from a heavy-duty diesel engine" Journal of Hazardous Materials B73 2000 39–54
50. J. L. Jiménez-Pérez , J. F. Sánchez-Ramírez, Z. N. Correa-Pacheco, A. Cruz-Orea·E. Chigo Anota, F. Sánchez-Sinencio "Thermal Characterization of Solutions Containing Gold Nanoparticles at Different pH Values" Int J Thermophys (2013) 34:955–961 DOI 10.1007/s10765-012-1372-0
51. J. Sadhik Basha & R. B. Anand "An Experimental Study in a CI Engine Using Nanoadditive Blended Water–Diesel Emulsion Fuel" International Journal of Green Energy, 8:3, 332-348, (2011) DOI: 10.1080/15435075.2011.557844
52. Ji-Hwan Lee, Seung-Hyun Lee, and Seok Pil Jang "Do temperature and nanoparticle size affect the thermal conductivity of alumina nanofluids?" Applied Physics Letters 104, 161908 (2014); doi: 10.1063/1.4872164
53. Joohyun Lee , Yong-Jin Yoon , John K. Eaton, Kenneth E. Goodson, andSeoung Jai Bai "Analysis of Oxide (Al_2O_3, CuO, and ZnO) and CNT Nanoparticles Disaggregation Effect on the Thermal Conductivity and the Viscosity of Nanofluids" International Journal of Precision Engineering and Manufacturing Vol. 15, No. 4, pp. 703-710 April 2014 DOI: 10.1007/s12541-014-0390-1
54. Joshua Folaranmi "Production of biodiesel (B100) from Jatropha oil using sodium hydroxide as catalyst" Journal of petroleum engineering, Volume 2013, Article ID 956479, 6 pages doi : 10.1155/2013/956479
55. Juan A. Melero, L. Fernando Bautista, G. Morales, J. Iglesias, and D. Briones "Biodiesel Production with Heterogeneous Sulfonic Acid-Functionalized Mesostructured Catalysts" Energy & Fuels2009,23,539–547 doi: 10.1021/ef8005756

56. K.B. Anoop, Sarit K. Das, S. Kabelac "Experimental convective heat transfer studies in a turbulent flow regime using alumina-water nanofluids" QScience Connect2013:39 doi.org/10.5339/connect.2013.39
57. Kamaldeep Singh, Sumeet Sharma, D. Gangacharyulu "Experimental Study of Thermophysical Properties of Al_2O_3/Water Nanofluid "IJRMET Vo l. 3, Is s uE2, Ma y-ocT2013
58. Kazi Mostafijur Rahman, Mohammad Mashud, Md. Roknuzzaman and Asadullah Al Galib "Biodiesel from Jatropha oil as Alternative fuel for Diesel Engine" International Journal of Mechanical & Mechatronics IJMME-IJENS Vol: 10 No: 03
59. L. Syam Sundar , Manoj K. Singh , E. Venkata Ramana , Budhendra Singh , Jose ´Gra´cio & Antonio C. M. Sousa "Enhanced Thermal Conductivity and Viscosity of Nanodiamond-Nickel Nanocomposite Nanofluids" SCIENTIFICREPORTS 4 : 4039 DOI: 10.1038/srep04039
60. Leyuan Yu, Dong Liu, Frank Botz "Laminar convective heat transfer of alumina-polyalphaolefin nanofluids containing spherical and non-spherical nanoparticles" Experimental Thermal and Fluid Science 37 (2012) 72–83 doi:10.1016/j.expthermflusci.2011.10.005
61. M. Tajik Jamal-Abadi, A. H. Zamzamian "Optimization of Thermal Conductivity of Al2O3 Nanofluid by Using ANN and GRG Methods" Int. J. Nanosci. Nanotechnol., Vol. 9, No. 4, Dec. 2013, pp. 177-184
62. M.J. Pastoriza-Gallegoa , C. Casanova , J.L. Legido , M.M. Pineiro "CuO in water nanofluid: Influence of particle size and polydispersity on volumetric behaviour and viscosity" Fluid Phase Equilibria 300 (2011) 188–196 doi:10.1016/j.fluid.2010.10.015
63. Mahesh Juneja and D. Gangacharyulu "Experimental Analysis on Influence of Temperature and Volume Fraction of Nanofluids on Thermophysical Properties" International Journal of Emerging Technologies in Computational and Applied Sciences (IJETCAS) IJETCAS 13-345 (2013)
64. Manila Chieruzzi, Gian F Cerritelli, Adio Miliozzi and José M Kenny "Effect of nanoparticles on heat capacity of nanofluids based on molten salts as PCM for thermal energy storage" Nanoscale Research Letters2013,8:448
65. Indranil Manna "Synthesis, Characterization and Application of Nanofluid —An Overview" Journal of the Indian Institute of Science VOL 89:1 Jan–Mar 2009
66. Mark A. Kedzierski "Viscosity and density of CuO nanolubricant" International Journal of Refrigeration 35 (2012) 1997 – 2002 doi.org/10.1016/j.ijrefrig.2012.06.012
67. Nezahat Bozi, MirayKara, Oylum Sunal, Ertan Alptekin, NebahatDeg˙ Irmenbasi "Investigation of the fuel properties of biodiesel produced over an alumina-based solid catalyst" Turk J Chem 33 (2009) , 433 – 442 doi:10.3906/kim-0809-28
68. Nubia M. Ribeiro, Angelo C. Pinto, Cristina M. Quintella, Gisele O. da Rocha,|,O Leonardo S. G. Teixeira, Lı´lian L. N. Guarieiro, Maria do Carmo Rangel, Ma´rcia C. C. Veloso, Michelle J. C. Rezende, Rosenira Serpa da Cruz, Ana Maria de Oliveira, Ednildo A. Torres, and Jailson B. de Andrade "The Role of Additives for Diesel and Diesel Blended (Ethanol or Biodiesel) Fuels: A Review" Energy & Fuels2007,21,2433-2445 doi : 10.1021/ef070060r

69. O. Deriabina, N. Lebovka, L. Bulavin, A. Goncharukn "Regulation of dispersion of carbon nanotubes in binary water+1-Cyclohexyl-2-pyrrolidone mixtures" Physica E 59 (2014) 150–157 doi.org/10.1016/j.physe.2014.01.017
70. Pradeep Prabhakar, Dr.Chanpreet Singh, Dr..D. GangaCharayulu "Synthesis and Experimental details of Thermophysical Properties of Nanofluids" International Journal of Enterprise Computing and Business Systems, Volume 2 Issue 1 January 2013,
71. Prof. V. S. Swaminathan "Study Estimation of Thermal Conductivity in Oxide Nanoparticles" ELK ASIA PACIFIC Journal of Applied Thermal Engineering Volume 1 Issue 1, September (2014)
72. R.K. Sahu , Somashekhar S.H., Manivannan P.V. "Investigation on Copper Nanofluid obtained through Micro Electrical Discharge Machining for Dispersion Stability and Thermal Conductivity" Procedia Engineering 64 (2013)946 – 955 doi: 10.1016/j.proeng.2013.09.171
73. Ravi Sankar.B , Nageswara Rao. D, Srinivasa Rao.Ch. "Nanofluid Thermal Conductivity – A Review" International Journal of Advances in Engineering & Technology, Nov. 2012 Vol. 5, Issue 1, pp. 13-28
74. Ritu Pasrija and Sunita Srivastava "The interfacial layer effect on thermal conductivity of CNT nanofluids" CURRENT SCIENCE, VOL. 107, NO.6,25 SEPTEMBER 2014
75. S K Sharma, R K Das, R Kumar "Performance ParameterAnalysis of Diesel Enginebu using a Mixture of Diesel, Jatropha oil, Mno – Nanomaterialand a suitable Antioxidant– a review" International Journal of Mechanical and Production Engineering, Volume- 1, Issue- 6, Dec-2013
76. S. A. Angayarkanni and John Philip "Role of Adsorbing Moieties on Thermal Conductivity and Associated Properties of Nanofluids" J. Phys. Chem. C2013, 117, 9009−9019 doi.org/10.1021/jp401792b
77. S.C.Vijayakumaar , R. Lakshmi Shankar, Dr.K.Babu "Effect ofCNT-H20 Nanofluid on the Performance of Solar Flat Plate Collector-An Experimental Investigation" Proceedings of the "International Conference on Advanced Nanomaterials & Emerging Engineering Technologies" (ICANMEET-20 13) organized by Sathyabama University, Chennai, India in association with DRDO, New Delhi, India, 24'h _26'" July, 2013.
78. Choi, S. U. S., and Eastman, J. A. ,"Enhancing thermal conductivity of fluids with nanoparticles" International mechanical engineering congress and exhibition, San Francisco, CA, 1995.
79. Laura Fedele, Laura Colla, Sergio Bobbo, Simona Barison and Filippo Agresti "Experimental stability analysis of different water based nanofluids" Nanoscale Research Letters 2011, 6:300
80. Ji-Hwan Lee, Seung-Hyun Lee, and Seok Pil Jang "Do temperature and nanoparticle size affect the thermal conductivity of alumina nanofluids?" Applied Physics Letters 104, 161908 (2014); doi: 10.1063/1.4872164
81. Sandeep Pal , Tikamchand Soni, Akriti Agrawala and Deepak Sharma" Review on Enhanced ThermalConductivity of Colloidal Suspension of Nanosized Particles (Nanofluids)" International Journal of Advanced Mechanical Engineering Volume 4, Number 2 (2014), pp. 199-214

82. Seung-IL Choi, Hafizur-Rehman, Yoon-Sub Eom, Myoung-Kuk Ji, Jun-Hyo Kim, Han-Shik Chung and Hyo-Min Jeong "Investigation of Thermal Conductivity and Convective Heat Transfer of Alumina Nanofluids under Laminar Flow" Journal of the Korean Society for Power System Engineering KSPSE Vol. 17, No. 2, pp. 78-86, 2013
83. Ta-Chang Lin, Mu-Rong Chao "Assessing the influence of methanol-containing additive on biological characteristics of diesel exhaust emissions using microtox and mutatox assays" The Science of the Total Environment 284 2002 61 – 74 PII: S 0 0 4 8 - 9 6 9 7 0 1 00866-X
84. Tony John, T. S. Krishnakumar "Experimental studies of Thermal Conductivity, Viscosity and Stability of Ethylene Glycol Nanofluids" International Journal of Innovative Research in Science, Engineering and Technology Volume 2, Special Issue 1, December 2013
85. V. Sajith, C. B. Sobhan, and G.P.Peterson "Experimental Investigations on the Effects of Cerium Oxide Nanoparticle Fuel Additives on Biodiesel "Advances in Mechanical Engineering Volume 2010, Article ID 581407,6pages doi:10.1155/2010/581407
86. Topi Rönkkö, Liisa Pirjola, Leonidas Ntziachristos, Juha Heikkilä , Panu Karjalainen, Risto Hillamo, and Jorma Keskinen "Vehicle Engines Produce Exhaust Nanoparticles Even When Not Fueled" Environ. Sci. Technol. 2014, 48, 2043 dx.doi.org/10.1021/es405687m
87. Matthew Jones, Calvin H Li, Abdollah Afjeh, GP Peterson "Experimental study of combustion characteristics of nanoscale metal and metal oxide additives in biofuel (ethanol)" Nanoscale Research Letters2011,6:246
88. V. Kumaresan, R. Velraj "Experimental investigation of the thermo-physical properties of water–ethylene glycol mixture based CNT nanofluids" Thermochimica Acta 545 (2012) 180– 186 doi.org/10.1016/j.tca.2012.07.017
89. V. Kumaresan , R. Velraj , Sarit K. Das "Convective heat transfer characteristics of secondary refrigerant based CNT nanofluids in a tubular heat exchanger" International Journal of Refrigeration 35 (2012) 2087 – 2096 doi.org/10.1016/j.ijrefrig.2012.08.009
90. Ali M.A. Attia, Ahmed I. El-Seesy, Hesham M. El-Batsh and Mohamed S. Shehata "Effects of Alumina nanoparticles additives into Jojoba Methyl Ester-Diesel mixture on Diesel Engine Performance" ASME 2014 International Mechanical Engineering Congress & Exposition , IMECE 2014 November 14-20, 2014, Montreal, Canada
91. W. Rashmi, M. Khalid, A.F. Ismail, R. Saidur & A.K. Rashid "Experimental and numerical investigation of heat transfer in CNT nanofluids", Journal of Experimental Nanoscience, (2013) DOI: 10.1080/17458080.2013.848296
92. Xin Deng, Zhen Fang, Yun-hu Liu, Chang-Liu Yu "Production of biodiesel fromJatropha oil catalyzed by nanosized solid basic catalyst" Energy xxx (2011) 1e8 doi:10.1016/j.energy.2010.12.043
93. Yanan Gan, Yi Syuen Lim, Li Qiao "Combustion of nanofluid fuels with the addition of boron and iron particles at dilute and dense concentrations" Combustion and Flame 159 (2012) 1732–1740 doi:10.1016/j.combustflame.2011.12.008

94. Xuejun Liu, Xianglan Piao, Yujun Wang, and Shenlin Zhu "Calcium Ethoxide as a Solid Base Catalyst for the Transesterification of Soybean Oil to Biodiesel" Energy & Fuels2008,22,1313–1317 doi : 10.1021/ef700518h
95. J. Sadhik Basha, R.B. Anand "Performance, emission and combustion characteristics of a diesel engine using Carbon Nanotubes blended Jatropha Methyl Ester Emulsions" Alexandria Engineering Journal (2014)53, 259–273 doi.org/10.1016/j.aej.2014.04.001
96. Xuejun Liu, Huayang He, Yujun Wang, Shenlin Zhu, Xianglan Piao "Transesterification of soybean oil to biodiesel using CaO as a solid base catalyst" Fuel 87 (2008) 216–221 doi:10.1016/j.fuel.2007.04.013
97. Himanshu Tyagi, Patrick E. Phelan, Ravi Prasher, Robert Peck, Taewoo Lee, Jose R. Pacheco, and Paul Arentzen "Increased Hot-Plate Ignition Probability for Nanoparticle-Laden Diesel Fuel" NANO LETTERS XXXX Vol. xx, No. x doi : 10.1021/nl080277d
98. Yanan Gan and Li Qiao "Optical Properties and Radiation-Enhanced Evaporation of Nanofluid Fuels Containing Carbon-Based Nanostructures" Energy Fuels2012, 26, 4224−4230 doi.org/10.1021/ef300493m
99. Yanan Gan, Yi Syuen Lim, Li Qiao "Combustion of nanofluid fuels with the addition of boron and iron particles at dilute and dense concentrations" Combustion and Flame 159 (2012) 1732–1740 doi:10.1016/j.combustflame.2011.12.008
100. Apichai Jomphoak, Thitima Maturos, Tawee Pogfay, Chanpen Karuwan, Adisorn Tuantranont, and Thawatchai Onjun "Enhancement of Thermal Conductivity with Al2O3for Nanofluids". National Electronics and ComputerTechnology Center (NECTEC), 112 Thailand Science Park, Pathumthami 12120.
101. Y Rozita , R Brydson and A J Scott " An investigation of commercial gamma-Al2O3 nanoparticles" Journal of Physics: Conference Series241(2010) 012096 doi:10.1088/1742-6596/241/1/012096
102. Y. Hwang, J.K. Lee, C.H. Lee, Y.M. Jung, S.I. Cheong, C.G. Lee, B.C. Ku, S.P. Jang "Stability and thermal conductivity characteristics of nanofluids" Thermochimica Acta 455 (2007) 70–74 doi:10.1016/j.tca.2006.11.036
103. Y.V.Hanumantha Rao, Ram Sudheer Voleti, A.V.Sitarama Raju and P.Nageswara Reddy "Experimental investigations on jatropha biodiesel and additive in diesel engine" Indian Journal of Science and Technology Vol.2 No 4 (Apr. 2009)
104. Yanan Gan, Li Qiao "Evaporation characteristics of fuel droplets with the addition of nanoparticles under natural and forced convections" International Journal of Heat and Mass Transfer 54 (2011) 4913–4922 doi:10.1016/j.ijheatmasstransfer.2011.07.003
105. Yi-Hsuan Hung and Wen-Chieh Chou "Chitosan for Suspension Performance and Viscosity of MWCNTs" International Journal of Chemical Engineering and Applications, Vol. 3, No. 5, October 2012 DOI: 10.7763/IJCEA.2012.V3.215
106. Yuan-Chung Lin, Shou-Heng Liu, Yan-Min Chen, Tzi-Yi Wu "A new alternative paraffinic–palmbiodiesel fuel for reducing polychlorinated dibenzo-p-dioxin/dibenzofuran emissions from heavy-duty diesel engines "Journal of Hazardous Materials185 (2011) 1–7 doi:10.1016/j.jhazmat.2010.07.071

107. Yulong Ding, Haisheng Chen, Liang Wang, Chane-Yuan Yang, Yurong He, Wei Yang, Wai Peng Lee, Lingling Zhang and Ran Huo "Heat Transfer Intensification Using Nanofluids" KONA No.25 (2007)
108. Neetu Jha and S. Ramaprabhu, "Thermal and Electrical Conductivity Studies of Metal Oxide-Multiwalled Carbon Nanotubes Nanocomposite Based Nanofluids" Journal of Nanofluids Vol. 1, pp. 63–70, 2012, doi:10.1166/jon.2012.1004
109. Haghshenas Fard M, Talaie M and Nasr S "Numerical and experimental investigation of heat transfer of ZnO/water nanofluid in the concentric tube and plate heat exchanger" 2011 Thermal Sci. 15 183–94
110. Kumar K D and Gowd B U M " Convective heat transfer characteristics of graphene dispersed nanofluids Int. J. Mech. Eng. Robot. Res. 2 250–60, 2012.
111. Neetu Jha and S. Ramaprabhu, "Thermal and Electrical Conductivity Studies of Metal Oxide-Multiwalled Carbon Nanotubes Nanocomposite Based Nanofluids" Journal of Nanofluids Vol. 1, pp. 63–70, 2012, doi:10.1166/jon.2012.1004
112. Mare T, Halelfadl S, Sow O, Estelle P, Duret S and Bazantay F " Comparison of the thermal performances of two nanofluids at low temperature in a plate heat exchanger" 2011 Exp. Thermal Fluid Sci. 351535–43
113. Kin Yuen Leong, Nurfadhillah MOHD Hanafi, Risby MOHD Sohaimi, Noor Hafizah Amer "The effect of surfactant on Stability and Thermal Conductivity of Carbon Nanotube based Nanofluids" Department of Mechanical Engineering Universiti Pertahanan Nasional Malaysia Kem Sungai Besi 57000 Kuala Lumpur, Malaysia
114. S. M. H. Jayhooni, M. H. Nowzari, K. Jafarpur , numerical simulation of l aminar forced convection heat transfer of t wo square prisms inside nanofluids, 2012.
115. Yurong Hea, Yi Jinb, Haisheng Chenc, Yulong Dinga , Daqiang Cangb, Huilin Lud, Heat transfer and flow behaviour of aqueous suspensions of TiO2nanoparticles (nanofluids) flowing upward through a vertical pipe , 2012.
116. Joohyun Lee , Yong-Jin Yoon , John K. Eaton, Kenneth E. Goodson, andSeoung Jai Bai "Analysis of Oxide (Al_2O_3, CuO, and ZnO) and CNT Nanoparticles Disaggregation Effect on the Thermal Conductivity and the Viscosity of Nanofluids" International Journal of Precision Engineering and Manufacturing Vol. 15, No. 4, pp. 703-710 April 2014 DOI: 10.1007/s12541-014-0390-1
117. Rad Sadri, Goodarz Ahmadi, Hussein Togun, Mahidzal Dahari, Salim Newaz Kazi, Emad Sadeghinezhad and Nashrul Zubir "An experimental study on thermal conductivity and viscosity of nanofluids containing carbonnanotubes" Nanoscale Research Letters2014,9:151
118. T.T. Baby, S. Ramaprabhu, Investigation of thermal and electrical conductivity of graphene based nanofluids, J. Appl. Phys. 108 (2010) 1–6.
119. T.T. Baby, S. Ramaprabhu, Enhanced convective heat transfer using graphene Dispersed nanofluids, Nanoscale Res. Lett. 6 (2011) 289–297
120. Nasrin Sabet Sarvestany, Abdulali Farzad , Ehsan Ebrahimnia-Bajestan & Massoud Mir "Effects of Magnetic Nanofluid Fuel Combustion on the Performance and Emission Characteristics" , Journal of Dispersion Science and Technology, 35:12, 1745-1750, (2014) DOI: 10.1080/01932691.2013.874296
121. W. Yu, H. Xie, ―A Review on Nanofluids: Preparation, Stability Mechanisms, and

Applications, Journal of Nanomaterials,vol2012, pp.1-17, 2012.

122. S.Karthikeyan, A.Elango, and A.Prathima "Performance and Emission Study on Zinc Oxide Nanoparticles addition with Promolion Stearin Wax Biodiesel of C I Engine" Journal of Scientific and Industrial Research, Vol. 73 March 2014 , pp187 – 190
123. X. Yang and Z. H. Liu, ―A kind of nanofluid consisting of surface - functionalized nanoparticles, ―Nanoscale Research Letters, vol. 5, no. 8, pp. 1324–1328, 2010.
124. L. Chen and H. Xie, ―Surfactant -free nanofluids containing double- and single-walled carbon nanotubes functionalized by a wet mechanochemical reaction,‖ Thermochimica Acta, vol. 497, no. 1-2, pp. 67–71, 2010.
125. M. B. Shafii, F. Daneshvar, N. Jahani, and K. Mobini "Effect of Ferrofluid on the Performance and Emission Patterns of a Four-Stroke Diesel Engine" Advances in Mechanical Engineering Volume 2011, Article ID 529049,5pages doi:10.1155/2011/529049
126. Lee, J.H., Lee, S.H., Choi, C.J., Jang, S.P., Choi, S.U.S., 2010, A review of thermal conductivity data, mechanisms and models for nanofluids, *Int. J. Micro-Nano Scale Transport.*, vol. 1: p. 269-322.
127. Nubia M. Ribeiro, Angelo C. Pinto, Cristina M. Quintella, Gisele O. da Rocha,|,O Leonardo S. G. Teixeira, Lı´lian L. N. Guarieiro, Maria do Carmo Rangel, Ma´rcia C. C. Veloso, Michelle J. C. Rezende, Rosenira Serpa da Cruz, Ana Maria de Oliveira, Ednildo A. Torres, and Jailson B. de Andrade "The Role of Additives for Diesel and Diesel Blended (Ethanol or Biodiesel) Fuels: A Review" Energy & Fuels2007,21,2433-2445 doi : 10.1021/ef070060r
128. Lee, J.W., Jung, J.Y., Lee, S.G., Kang, Y.T., 2011, CO_2 bubble absorption enhancement in methanol-based nanofluids, *Int. J. Refrig.*, vol. 34: p. 1727-1733.